University of Salerno

Department of Industrial Engineering

Ph. D. Thesis in

MECHANICAL ENGINEERING

XI CYCLE (2009–2012)

Receptivity in transition prediction

Donato de Rosa

Supervisor
Ch.mo Prof.
Paolo Luchini
Ch.mo Prof.
Flavio Giannetti

Coordinator
Ch.mo Prof.
Vincenzo Sergi

To Whom I Love

Vae victis.

Dedica

Il mio grazie al Prof. Paolo Luchini, tutor del mio Dottorato di Ricerca, per aver contribuito alla mia crescita professionale.

Ringrazio il carissimo Prof. Flavio Giannetti per il supporto scientifico e morale durante lo svolgimento del Dottorato, unitamente a Serena e Vincenzo.

Ringrazio Raffaele Donelli che mi ha seguito e sostenuto nelle attività di ricerca fin dall'Università.

Un ringraziamento al CIRA per avermi offerto l'opportunità di svolgere il Dottorato e ai partecipanti del progetto RECEPT per la disponibilità al confronto e alla discussione.

Desidero ringraziare, non ultime, le persone che mi sono state vicino nei momenti di sconforto incontrati durante questo percorso. È grazie a loro se non ho mai mollato e ho capito che ce la potevo fare: la mia famiglia e Rossella. Grazie di esserci.

D. de Rosa

Nomenclature

$\tilde{\mathscr{S}}$	Adjoint stress
α	Streamwise wavenumber
β	Spanwise wavenumber
δ	Boundary layer height
δ^*	Boundary layer displacement thickness
δ_r	Characteristic length
$\tilde{\epsilon}$	Parameter for multiple–scale method
γ	Specific heat ratio
λ_k	Eigenvalue
$\tilde{\mathbf{v}}_k$	Left eigenvector
$\mathbf{A}$	Coefficient matrix of zero–order problem
$\mathbf{u}_k$	Right eigenvector
$\boldsymbol{C}$	Coefficient matrix of first–order problem
$\boldsymbol{G}$	Coefficient matrix of first–order problem
$\boldsymbol{H}$	Coefficient matrix of first–order problem
μ	Dynamic viscosity
ν	Kinematic viscosity
ω	Frequency

ρ	Density
$\hat{S}$	Source terms in Navier–Stokes equations
θ	Boundary layer momentum thickness
θ	Eikonal function
$\mathbf{r}$	Receptivity vector
$\mathbf{y}$	Source Vector
A	Wave amplitude
A_0	Wave amplitude in the first neutral point
c	Phase velocity
c_k	Coefficients of the eigenvalue problem
h	Wall shape function
k	Roughness height
M	Mach number
N	N factor
P	Mean component of pressure
p	Variable component of pressure
r	Thermal recovery factor
r_h	Sensitivity
R_n	Nose radius
Re	Reynolds number
T	Temperature
t	Time
Tu	Turbulence
U	Mean component of streamwise velocity
u	Variable component of streamwise velocity

V Mean component of normal velocity

v Variable component of normal velocity

W Mean component of spanwise velocity

w Variable component of spanwise velocity

x Streamwise coordinate

y Normal coordinate

z Spanwise coordinate

Subscripts

0 Initial value

∞ Free–stream value

aw Adiabatic wall

cr Critical value

e External value

i Imaginary part of complex number

ip Inflection point

r Real part of complex number

tr Value at transition

w Value at wall

x Chordwise value

Acronyms

ALTTA Application of hybrid Laminar flow Technology on Transport Aircraft

CF Crossflow

CFD Computational Fluid Dynamics

CIRA Italian Aerospace Research Center

DNS Direct Numerical Simulation

ELFIN European Laminar Flow INvestigation

ETW European Transonic Wind Tunnel

EUROLIFT EUROpean high LIFT programme

EUROTRANS EUROpean program for TRANsition prediction

FOI Swedish Defence Research Agency

HLFC Hybrid Laminar Flow Control

LES Large Eddy Simulation

LFC Laminar Flow Technology

LST Linear Stability Theory

NLF Natural Laminar Flow

OSE Orr–Sommerfeld Equation

PANT PAssive NoseTip program

PSE Parabolic Stability Equations

PSJ Plasma Synthetic Jet

RANS Reynolds-Averaged Navier-Stokes

RECEPT RECEPTivity and amplitude-based transition prediction

SDBD Single–Dielectric Barrier Discharge

SUPERTRAC SUPERsonic TRAnsition Control

TELFONA TEsting for Laminar Flow On New Aircraft

TS Tollmien–Schlichting

UAV Unmanned Aerial Vehicle

Contents

List of Figures

Chapter 1

Introduction

The topic of laminar turbulent transition constitutes one of the most important research fields for aerodynamic teams. As a matter of fact, the laminar-turbulent transition is a complex phenomenon, which has many multidisciplinary applications such as skin friction drag reduction, anti-icing and de-icing system performance prediction (civilian aircraft), air intake performance (UAV, missile) and heat transfer rates prediction (reentry vehicles). These applications need an accurate prediction of the boundary layer state and the control of its thickness by active or passive systems. Providing pertinent and realizable technological solutions, encompassing all Mach number flight regimes from subsonic up to hypersonic vehicles (civil or military), will become a strategic task for industry.

The state of the boundary layer is of high importance since skin friction drag and heat transfer rates in a turbulent boundary layer can be several times higher than those in laminar one. Last but not least, predicting the state of the boundary layer in wind tunnels and ensuring the same state during the real flight by taking into account disturbances resulting from the experimental set up leads to the design of transition triggering devices.

In order to reduce development costs, experiments are iteratively compared to numerical simulations mainly based on LST and/or CFD to predict the natural and triggered transition. The extension of CFD into application areas such as transition prediction is still in the start-up phase and is only made possible by increasing computer resources. The most commonly applied Reynolds-Averaged Navier-Stokes (RANS) methods are not able to simulate flow features occurring in the boundary layer, but some semi-empirical criteria based on stability theory and the e^N method [1] are implemented in CFD solvers for subsonic and supersonic flow regimes.

Several projects had the objective to investigate the laminar to turbulent transition and an overview of them is described below. ELFIN (European Laminar Flow INvestigation), 1989-1992, was an European funded programs

on laminar flow technology. In the framework of ELFIN, natural laminar flow experiments were conducted on a glove bonded to the wing surface of a Fokker 100 aircraft. In the following project ELFIN II, 1993-1995, a series of analyses by using local stability methods were performed based on flight tests data, followed by wind tunnel experiments. In the EUROTRANS project (EUROpean program for TRANsition prediction), 1996-1998, non-local stability methods were applied to test cases from ELFIN I and II, while ALTTA (Application of hybrid Laminar flow Technology on Transport Aircraft), 2000-2003, was intended to apply hybrid laminar flow technology with the aim of reducing the aerodynamic drag of an aircraft by delaying the laminar/turbulent transition. EUROLIFT I (EUROpean high LIFT programme), 2000-2003, had the objectives to perform experiments in order to create an experimental data base and to assess and improve available numerical tools. The experiments were carried out in the cryogenic very high Reynolds number test facility ETW to bridge the gap between sub-scale testing and flight conditions to understand and incorporate scaling effects. In the framework of EUROLIFT II, 2004-2007, the objective was to provide specific physical understanding of the various vortex dominated flow effects at the cut-outs of a high lift system including the scale effects up to flight conditions. The major objective of the TELFONA project (TEsting for Laminar Flow On New Aircraft), 2005-2009, was the development of the capability to predict the in-flight performance of a future laminar flow aircraft using a combination of wind tunnel tests and CFD calculations. During the project, two wings aimed to pro-green aircraft configuration were designed and manufactured for wind tunnel experiments, the Pathfinder and Performance, namely. The research responded to an opportunity to design a wing with a significantly higher aspect ratio and lower sweep than today's standard. The objective of the SUPERTRAC project (SUPERsonic TRAnsition Control), 2005-2007, was to explore the possibilities of viscous drag reduction on supersonic aircraft wings.

The last project relative to laminar to turbulent transition topic is the RECEPT program (RECEPTivity and amplitude-based transition prediction), 2011-on going, whose major objective is the development of the capability to predict the in-flight performance of a future laminar flow aircraft through development of more accurate transition prediction tools. The idea is to develop a transition prediction method which includes the effects of the initial disturbance amplitude. The main issue for such method is the information about the process of how the external disturbances interact with the boundary layer, e.g. the receptivity process.

The main subject of the present research relates to the objectives of the

RECEPT project through the study of the boundary layer instabilities and their receptivity to disturbances. The goals of the present work therefore are:

- to develop a fast tool that can be integrated in an industrial code for transition prediction
- to introduce corrections for non–parallel flow in order to assess their importance in real wing designs and more general and complex boundary layers.

Fluid dynamic instabilities leading to transition from laminar to turbulent flow in an incompressible boundary layer are considered, paying attention to the receptivity process.

The problem of boundary-layer receptivity is solved by introducing the multiple-scale technique and applying it to the linearized Navier-Stokes equations reducing it to an Orr-Sommerfeld non–homogeneous formulation case. The resulting algorithm is not computationally expensive and can be efficiently included in industrial codes for transition prediction.

The route to transition, in boundary layer flows, can be divided into different stages. First, the external disturbances are internalized in the boundary layer through the receptivity process. Then a wave, due to the external perturbations, originates inside the boundary layer, growing and leading to a linear amplification or decay as described by the linearized Navier-Stokes equations. If the amplitude of the excited wave is greater than a certain threshold, a further instability called secondary instability can occur, provoking a non-linear breakdown and causing transition from laminar to turbulent flow. It can happen that this transition scenario, related to the exponential growth of Tollmien–Schlichting waves (modal disturbances), is bypassed by another strongly amplifying mechanism due to linear phenomena but caused by other than exponential instabilities. In fact, the linear theory for the instability analysis sometimes fails predicting a stable behavior for flows which experiments show to be unstable. This is called bypass transition and basically regards algebraic instabilities and transient growth.

Since transition turns out to have a quite heavy economic impact, transition prediction criteria are usually applied in order to estimate the location of transition during the aerodynamic design of aircraft wings. The most used and apparently most reliable criterion is the e^N method. It was introduced only for the exponentially growing disturbances like Tollmien–Schlichting waves and is based on the idea that when the amplitude of the unstable

wave is e^N times (where N is between 9 and 11) the amplitude of the wave at the first neutral point, transition occurs. Clearly, the external environment and its influence on the boundary layer stability is not accounted for by this technique. On the contrary, the goal of a receptivity study is to improve transition prediction methods extending transition criteria to include the free–stream disturbance environment. In other words, receptivity allows us to relate the amplitude of the instability wave produced inside the boundary layer (Tollmien–Schlichting wave) to the physical amplitude of the external exciting disturbance. The main excitation sources are usually acoustic waves, vorticity waves and wall vibrations. However, their temporal frequency and spatial wavelength are not in the same range as those of the Tollmien–Schlichting waves, so that resonance can be reached only via an "adaptation mechanism", for instance produced by wall roughness.

In the present thesis, following the approach presented by Zuccher [2], multiple scales are introduced in a non–homogeneous form in order to investigate the interaction between different disturbances. This technique is not usually used in fluid dynamic problems, but can be preferable to other methods for the study of boundary layer receptivity, because it offers the possibility to account for nonparallel effects due to boundary layer growth, it does not have numerical stability problems, it is not computationally expensive, and therefore can be included in industrial codes for transition prediction.

The second chapter of this thesis is devoted to stability and transition in order to briefly introduce an overview on boundary layer theory, instability and transition prediction and control. In the third chapter, the multiple scale method is described for homogeneous and non-homogeneous cases, while in the fourth one, the receptivity problem is considered using multiple scales, identifying a receptivity function. In the fifth chapter an application is shown in order to validate the code for stability analysis and report the results on receptivity function. The last chapter is relative to the receptivity to free-stream disturbances and some results are shown relative to the interaction between roughness–acoustic wave and roughness–vortical wave.

Chapter 2

Boundary layer stability and transition

The classical example relative to the flow regimes called *laminar* and *turbulent* one is the smoke flowing from a cigarette while standing in a vertical position. In the proximity of the burning region, it is possible to observe a "regular" path in the smoke which remains detached from the air, while at a certain distance the pattern becomes irregular and the smoke is completely mixed with the air. The former region is characterized by the *laminar* regime, while the latter is the *turbulent* regime. The passage from the first to the second is called *transition*.

The example of the smoke is just intended to introduce the concept of flow instability. The laminar flow is defined stable if it returns to its original state after a perturbation is applied. It is unstable if the disturbance generated by the perturbation does not decay but grows triggering the turbulent flow.

The boundary layer on a body interacting with a fluid in motion can be laminar or turbulent, as the flow near a cigarette. The study of laminar–turbulent transition phenomena in a boundary layer is of vital importance to the design of modern commercial aircraft. Laminar flow over selected parts of the wings and fuselage is highly desired in order to achieve low skin–friction drag and low surface heating. A low skin–friction drag is essential for the optimisation of the fuel consumption and can lead to a drastic reduction in the actual cost of a commercial airplane. The heating rates generated inside a turbulent boundary layer may be several times higher than those of a laminar boundary layer, so a detailed knowledge of the transition point is crucial during the design stage, determining the choice of materials required in the structure of the wings and the fuselage, especially for re-entry vehicles.

2.1 Boundary layer

Prandtl [3] introduced the concept of "boundary layer" as a thin fluid layer on the surface of a body in a flow (see figure 2.1). Prandtl assumed that on the body the fluid velocity is zero (no slip, no suction or blowing condition), increasing to the free stream value across a very thin layer. Thus, the wall–normal component of the derivative of the velocity $\frac{du}{dy}$ becomes large inside the boundary layer and the shear stress is relevant even in fluid with low viscosity.

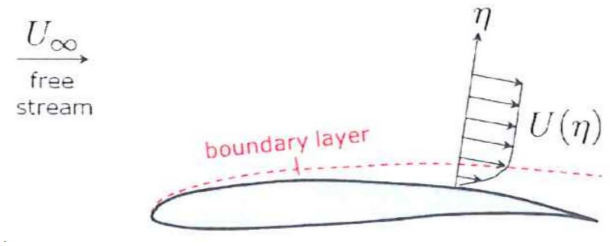

Figure 2.1: Boundary layer

As described above, the flow regime can be divided into three different regions, when the fluid is regularly moving the flow is called laminar, when the motion is irregular it is called turbulent and the passage from the former to the latter is called transition. The laminar flow is unstable if the disturbance generated by a perturbation does not disappear but grows changing the laminar state to the turbulent one. A common feature under which the flow becomes unstable seems to be the dependence on the Reynolds number, which represents the relative importance of the convective and inertial mechanisms to the dissipative ones. Experiments show that in very high Reynolds–number flows, turbulence eventually develops. The first experimental evidence of this dependence was demonstrated by Reynolds [4]: he observed that transition from laminar to turbulent flow can occur if Reynolds number Re is larger than a certain characteristic value, called critical Reynolds number Re_{cr}. It is important to remark that Re_{cr} is a threshold from which the laminar flow can evolve to turbulent state but does not necessarily mean that the flow will develop towards turbulence, since damping effects could occur. Re_{tr} is instead the transitional Reynolds number defined as the value at which the flow begins to be fully turbulent.

2.2 Boundary layer instabilities

The equations governing the motion of a fluid are the Navier–Stokes equations, a set of nonlinear partial differential equations. A practical approach for this kind of equations is to study the local stability, i.e. the stability of a particular flow field to infinitesimal small disturbances. This can be accomplished by performing a linearization of the governing equations and studying the resulting system according to the theory of linear differential equations.

The concept of stability can be *temporal* or *spatial*. In the temporal analysis, a perturbation is applied at a certain initial time and its evolution is observed as a function of time. On the contrary, for the spatial analysis, the perturbation is applied at a certain location and is followed, observing the spatial evolution. Another classification relative to spatial theory is if the perturbation is applied everywhere or locally. Moreover, in the second case, it is possible to introduce the concepts of *convective* or *absolute* instability if the disturbance grows everywhere but in the application point or it grows also in the point where it is applied, respectively. Such definitions will be briefly described in §2.3.1.

As we are interested in spatial stability analysis, it is necessary to describe the different zones that can be identified in figure 2.2. Close to the

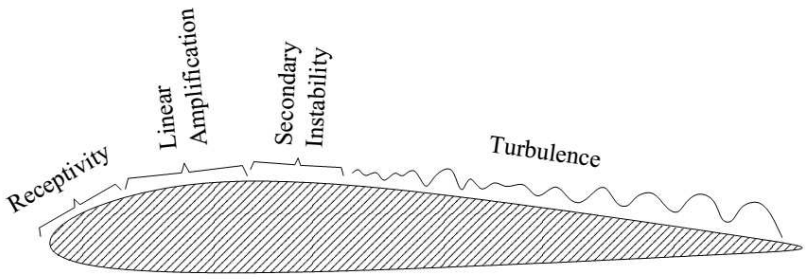

Figure 2.2: Transition scenario

leading edge, the external disturbances are introduced in the boundary layer in the so–called receptivity zone, where waves are excited by some perturbations coming from the environment. Downstream the linear amplification zone is found, where the disturbances grow (amplified) or decay (dumped) determined by the linearized Navier–Stokes equations, then the secondary instability zone follows and eventually nonlinear breakdown leading to turbulence. Transition can be delayed controlling any of these stages, but

receptivity seems to be one of the most important because it is related to the origin of the instability. On the other hand, if the external perturbation is sufficiently strong, the transition can occur because of the *bypass* mechanism instead of the receptivity mechanism.

Although linear theory can only give a good description of the instability process in the linear amplification region of the transitional process, it represents one of the most powerful tool used nowadays by the industry for the design of commercial components.

2.2.1 Historical review

The first major theoretical contributions to the study of hydrodynamic stability were made by Helmholtz [5], Kelvin [6, 7], Rayleigh [8, 9] and Reynolds [4] between 1868 and 1883. Rayleigh derived for the first time the linearized equation describing the evolution of the disturbances in a parallel, inviscid incompressible flow. The systems described by this equation show the peculiar characteristic to be at most marginally stable but never asymptotically stable. The main result derived from the Rayleigh equation is the inflectional point criterion according to which basic velocity profiles without inflectional points are (marginally) stable with respect to two–dimensional disturbances. Viscous effects were for the first time taken into account by Orr[10] and Sommerfeld [11] who, separately, developed an ordinary differential equation (the Orr–Sommerfeld equation or OSE) to study the linear stability of two dimensional disturbances in an incompressible parallel flow. In 1928, Tollmien [12] was able to find approximate analytical solutions for the OSE. In 1933, Schlichting [13] obtained a first estimate for the critical Reynolds number at which instability first arises and calculated approximated amplification rates for a two–dimensional disturbance. Later, Squire [14] accounted for three–dimensional disturbances using his transformation: his analysis shows that, according to linear theory, the critical Reynolds number in an incompressible boundary layer is always attained by two-dimensional waves. A first experimental proof showing the validity of linear theory was given by Taylor in 1923 [15] in his experiment on the stability of flows between two rotating cylinders. Further analytical progresses were made by Lees & Lin [16] in 1946 while Schubauer & Skramstadt [17] in 1947 performed an experiment which unequivocally showed the existence of Tollmien–Schlichting (TS) waves in the boundary layer and confirmed their role in the transition process. In 1953, Thomas [18] gave a numerical method to evaluate the stability of the Poiseuille flow and in 1964 Kaplan[19] obtained for the first time the neutral curve in the

Frequency–Reynolds number plane for a boundary layer flow. Van Ingen [1] and Smith & Gamberoni [20] in 1956 developed a semi-empirical method for the transition prediction based exclusively on linear theory: this is termed the e^N method. Although the e^N method neglects most of the physical processes in the transition phenomena (like the receptivity, nonlinear mechanisms, resonances, real spatio–temporal evolution of the perturbation), it has been applied successfully in many practical cases and it is still the preferred tool used by the industry. Together with the development of new spectral techniques (Orszag [21]) for the solution of eigenvalue problems in a finite domain, other numerical methods for the determination of higher modes of the stability equations become available. Mack [22] in 1969 reported the existence of a second unstable mode which can be found for free-stream Mach numbers larger than 2.2. He investigated the effects of suction and heat transfer on the stability of the boundary layer showing that the first mode is stabilised if the wall is cooled while the second mode is simultaneously destabilised. These conclusions were also verified experimentally by Lysenko & Maslov [23]. Mack [24] studied the behavior of the spectrum of the Orr–Sommerfeld equation for different kinds of mean flow profiles. He observed that for unbounded flows only a discrete number of modes exists, suggesting the existence of a continuous spectrum. Grosch & Salwen [25, 26] showed the validity of this hypothesis in both the temporal and the spatial problem and built biorthogonality relations which allow to use the spectrum as a filter. Further progress on the stability of boundary layers were made by Saric & Nayfeh [27], who derived the OSE through a multiple–scale expansion of the Navier–Stokes equations. After the experiments conducted by Klebanoff [28], a renewed interest in the effects of three–dimensional disturbances in a two–dimensional boundary layer led to a new series of theoretical investigations. In fact, although Squire's theorem asserts that for incompressible flows the critical Reynolds number is first reached by two-dimensional waves, Stuart [29] showed that the maximum amplification rate happens for three-dimensional disturbances. Simultaneously to the development of linear theory, new researches were conducted to study the effects of nonlinear mechanisms. The linear theory is in fact an accurate tool for the description of the fluid dynamics instabilities in the early stages of transition, but it cannot give reliable information when the disturbance reaches a finite amplitude. After a linear amplification stage, well predicted by the OSE, the disturbance enters a region where nonlinear phenomena give rise to violent high frequency motions via a secondary instability mechanism: nonlinear effects and parametric excitation play here a major role, as first realized by C. L. Maseev [30]. Asymptotic methods,

essentially based on the triple–deck theory of Stewartson [31], Neiland [32] and Messiter [33], and new powerful computational techniques have been developed in order to shed light on the later stages of the transitional process. The fast growing power of modern digital computer has enabled the study of secondary instability mechanisms, nonlinear modes interaction and effects of mean flow distortion using direct numerical simulations (DNS) of the whole Navier–Stokes equations (Kleiser & Zang [34]). Fasel, Meitz & Bachman [35] discussed the use of "Large Eddy Simulation" (LES) to investigate the final breakdown stage. These methods, anyway, require a considerable computational effort. The Parabolic Stability equations (PSE) (Bertolotti, Herbert & Spalart [36]) offers a more economic method to investigate the stability properties of a boundary layer. These equations are derived from the Navier–Stokes equations with a multiple scale expansion similar to the one used to obtain the OSE: the main difference here is that some of the streamwise derivatives are retained in the process, leading to a system of partial differential equations instead of an ODE. Under some constraints, the PSE can be shown to be parabolic and can be solved with a simple marching procedure. Grea [37] applied the ray theory to the analysis and control of flow instability in boundary layers.

2.3 Linear stability theory

The classical approach to the boundary layer stability theory [38, 39, 40] is based on the linearization of the Navier–Stokes equations about a given base flow, obtaining the equations for the disturbance. The behavior of the disturbance is then determined: if it grows, the base flow is unstable; if it decays, the base flow is stable. Supposing that the base flow is two–dimensional (only the streamwise component U and wall–normal component V of the velocity are present) and parallel ($V = 0$ and U depends only on the wall–normal coordinate, $U = U(y)$ so that $U_x = 0$), and considering a two–dimensional perturbation, the linearized Navier–Stokes equations are

$$u_x + v_y = 0 \tag{2.1}$$

$$u_t + Uu_x + vU_y = -p_x + \frac{1}{Re}\nabla^2 u \tag{2.2}$$

$$v_t + Uv_x = -p_y + \frac{1}{Re}\nabla^2 v \tag{2.3}$$

where the subscript stands for the derivation variable and the perturbation is expressed as a traveling wave:

$$(u, v, p) = (u(y), v(y), p(y))e^{i(\alpha x - \omega t)} \tag{2.4}$$

so that, simplifying the previous system, the classical equation for the velocity v can be derived [41]:

$$i\left[(\alpha U-\omega)\left(v_{yy}-\alpha^2\right)-\alpha U_{yy}v\right]=\frac{1}{Re}\left(v_{yyyy}-2\alpha^2 v_{yy}+\alpha^4 v\right) \tag{2.5}$$

It is a fourth–order linear homogeneous ordinary differential equation, called Orr–Sommerfeld equation, derived independently by Orr [10] and Sommerfeld [11]. The boundary conditions require the perturbation to vanish at the borders of the domain

$$v(0) = v_y(0)=0 \tag{2.6}$$
$$v(\infty) = v_y(\infty)=0 \tag{2.7}$$

Since both the equation and boundary conditions are homogeneous, an eigenvalue problem is derived which furnishes the dispersion relation:

$$D(\alpha,\omega,Re)=0 \tag{2.8}$$

The dispersion represents the dependence of wave speed upon wavelenght [42], i.e. waves of different wavelengths travel at different phase speeds. Recalling that stability can be temporal or spatial, when the temporal stability is considered, α and Re are fixed and real while ω is complex and its imaginary part gives the temporal growth rate; for the spatial stability ω and Re are fixed and real, and the imaginary part of α furnishes the spatial growth rate. The solution $v(y)$ is called eigenfunction. From this analysis, the neutral stability curve can be obtained: it represents the locus of points for which the growth rate (spatial or temporal) is zero, identifying regions of stability or instability in the $\alpha - Re$ or $\omega - Re$ plane respectively.

2.3.1 Type of instabilities

Fluid dynamic instabilities [41] can be classified as inviscid, viscous and algebraic. Not only the nature of the instability is important in determining the transition location but also its spatio–temporal evolution which differs between convective and absolute instabilities.

Inviscid instability

Inviscid instabilities are relative to large Reynolds-numbers flows, in the limit $Re \to \infty$. This instability can be divided into non–local and local one. Non–local instabilities are characterised by a low frequency and a

fast growth and a classical example is given by the centrifugal instabilities like Görtler vortices. Local instabilities, instead, are typical of jets, wakes and boundary layer with inflectional mean flow profiles and are essentially characterised by high frequencies and fast growth.

Neglecting the viscous terms in the Orr–Sommerfeld equation, i.e. the ones containing Re^{-1}, the Rayleigh equation is found:

$$v_{yy} - \left(\frac{U_{yy}}{U - c} + \alpha^2 \right) v = 0 \tag{2.9}$$

where $c = \omega/\alpha$ is the phase velocity.

The most important conclusions regarding inviscid stability are summarized in the following theorems [39]:

Theorem 1 (Rayleigh (1880)) *For the inviscid instability it is necessary for the velocity profile $U(y)$ to have an inflection point: $U_{yy}(y_{ip}) = 0$ where y_{ip} is the y location of the inflection point*

Theorem 2 (Fjørtof (1950)) *For the inviscid instability it is necessary for the shear $\|U_y\|$ to be maximum at the inflection point y_{ip}*

Theorem 3 (Fjørtof (1950)) *If an inflection point exists, for the inviscid instability it is further necessary $U_{yy}(U - U(y_{ip})) = 0$ somewhere on the profile*

Theorem 4 (Lin (1945)) *Let y_c be the position at which $U - c = 0$: if $U(y)$ has an inflection point at $y = y_c$, a neutral disturbance ($c_i = 0$) may exists whose phase velocity $c_r = U(y_c)$*

Theorem 5 (Rayleigh (1880)) *The phase velocity c_r of an amplified disturbance must always lie between the minimum and maximum value of $U(y)$*

The most important consequence of these theorems is that velocity profiles with an inflection point are unstable in real life at high Reynolds number. On the other hand, for many years it was believed that viscous profiles without a point of inflection would be stable. Indeed the viscosity can be destabilizing in certain cases: Poiseuille flow is stable in the inviscid case, unstable in the viscous one.

Viscous instability

Viscous instability can be identified by the eigenvalues of the Orr–Sommerfeld equation. Considering as base flow a parallel one (Poiseuille, Couette or Blasius profile) the unstable perturbation wave is called Tollmien–Schlichting wave which is characterized by high frequency and low growth. From the Orr–Sommerfeld equation the neutral stability curve can be obtained. In the spatial stability framework, it represents the locus of points, in $\omega - Re$ plane, for which $\alpha_i = 0$.

For Blasius profile on a flat plate the following results are obtained [39]: the minimal critical Reynolds number, which represents the first neutral point, is $R_{cr} = 520$ or $Re_x = 91000$ where $Re_x = U_e x/\nu$ and $R = \sqrt{Re_x}$. In the first neutral point, the wave parameters are: $\alpha\delta^* = 0.3012$, $\omega/\alpha_r = 0.3961U_e$ and $\omega\nu/U_e^2 = 2.29\ 10^{-4}$ where δ^* is the displacement thickness. The maximum wavenumber for the instability is $\alpha\delta^* = 0.35$.

Convective instability

Convective instabilities are characterised by the fact that the disturbance is convected away by the mean flow. The flow can then remain laminar until the disturbance has traveled a considerable distance over which it grows according to the specific amplification rate of the instability, eventually leading to transition. The typical example is represented by the TS waves.

Absolute instability

Absolute instabilities are characterised by the fact that a disturbance grows in time at a fixed location until nonlinear effects become important and secondary instabilities lead to transition. They are present in flows like near wake flows, over compliant surfaces or rotating disk.

2.3.2 Algebraic instability

During the 1980s and 1990s, attention was paid to a physical mechanism called *lift-up*. The name derives from the fact that low-velocity fluid is lifted up and high-velocity fluid pushed down so that a streak-like spanwise non-uniformity originates in the velocity field close to wall [2]. From the theoretical point of view, this mechanism can be explained by transient growth due to algebraic instability. This kind of instability is not related to the eigenvalues of Orr–Sommerfeld equations and can manifest both in inviscid and viscous flows. Their study can explain the *bypass* mechanism which is

observed in some transition processes, a phenomenon quite common in high freestream turbulence environments. The evolution of the disturbance inside the boundary layer does not involve a linear amplification stage like that one predicted by the OSE, but transition is promoted by fast amplification of low frequency three–dimensional streaks.

2.4 Transition prediction

Since transition can occur by means of different processes a globally valid method for the prediction does not exist. Direct numerical simulation (DNS) or large eddy simulation (LES) could be applied, but the computation effort is still too high for engineering applications. Simpler approaches, based on empirical correlations, require less resources but provide only the transition location and do not model any physical process.

2.4.1 Correlation methods

In the following sections, an overview relative to several empirical and semi-empirical criteria is reported.

Database method

The general principle is to compute the disturbance growth rate from tabulated values or from analytical relationships which have been established from exact stability computations performed, in general, for self-similar mean velocity profiles (Falkner-Skan profiles in 2D, incompressible flows). For this reason, these methods are often referred to as "database" methods. As soon as the growth rate is known, the N factor can be estimated in a classical way. Such methods have been proposed by Gaster and Jiang (1994), van Ingen (1996), Stock (1996).

Empirical criteria

Many empirical correlations have been proposed for 2D, incompressible flows. They were deduced from experimental data collected in low turbulence wind tunnel; they take the pressure gradient effects into account, for low values of turbulence Tu (which does not appear explicitly in the correlations). Michel, for example (1952) correlated the values of two Reynolds numbers at transition, Re_θ and Re_x. Granville (1953) developed a correlation which takes two important parameters into account, namely the stability properties and the flow history. The stability is characterized by

the difference $Re_{\theta_T} - Re_{\theta_{cr}}$ in momentum thickness Reynolds number from the neutral stability point to the transition location. The flow history is characterized by an averaged Pohlhausen parameter.

As far as crossflow instability is concerned, some specific criteria have been developed. As an example, the so-called C1 criterion, proposed by Arnal et al, 1984, is an empirical correlation between the crossflow Reynolds number $Re_{\delta 2}$ and the streamwise shape factor at transition. For incompressible flows: $\delta_2 = -\int_0^\delta \frac{W}{U_e} dy$.

Semi-empirical criteria

Anderson and Bowcutt [43] proposed a correlation based on experimental data on cones:

$$\log_{10} \mathrm{Re}_{tr} = 6.421 \exp\left(1.209\ 10^{-4} M_e^{2.641}\right) \tag{2.10}$$

The correlation links Reynolds number based on transition abscissa to the Mach number at the edge of boundary layer M_e. However, the relation is limited to slender and axisymmetric geometries (such as cones) [44] and the effect of roughness is not considered. The transition point is located where Re_s, i.e. Reynolds number based on curvilinear abscissa, intersects Re_{tr}.

PANT criterion is based on classical supersonic and hypersonic wind tunnel tests conducted during the "PAssive NoseTip Program" [45, 46, 47]. The criterion, developed by Anderson in 1975, finds out the transition point when the parameter

$$\Psi_1 = \mathrm{Re}_{\theta_{tr}} \left(\frac{kT_e}{\theta T_w}\right)^n \tag{2.11}$$

is equal to 215 for $n = 0.7$. $\mathrm{Re}_{\theta_{tr}}$ is the transition parameter, while $\frac{kT_e}{\theta T_w}$ is the disturbance parameter [48]. The criterion is suitable for hypersonic fields with no reactions as experimental data were obtained in supersonic and hypersonic low enthalpy wind tunnels while coefficients were calculated for perfect gas. The correlation fails for sharp bodies and too blunt bodies and it should be modified with a parameter based on the radius of the nose [49], [50], [51]. Reda [50] suggested different parameter values corresponding to $\Psi_1 = 574$ and $n = 1.3$.

Batt & Legner criterion was defined based on the PANT data and smooth wall transition data, intending to model both natural and roughness induced transition. The correlation includes a curvature correction on the disturbance parameter [48, 47].

$$\mathrm{Re}_{\theta_{tr}} = 500 \left(\frac{\frac{kT_e}{\theta T_w}}{1 + 350\frac{k}{R_n}}\right)^{-1.5} \tag{2.12}$$

so that the stabilizing effects of favorable pressure gradient due to the convexity of the vehicle shape are included via the parameter R_n [48, 50].

Van Driest & Blumer criterion, developed for isolated spherical roughness elements placed over cones, is written in a general form:

$$\mathrm{Re}_{\delta^*} = \left(\frac{k}{\delta^*}\right)^p A.B.C. \tag{2.13}$$

where $p \approx -1$, $A = \left(1 + \frac{\gamma-1}{2}M_e^2\right)$ is the compressibility correction, $B = f\left(\frac{\tilde{T}}{T_e}\right)$ is the temperature correction and C is the pressure gradient correction i.e. curvature correction [47].
The correlation is:

$$k = \frac{33.4}{\mathrm{Re}_\theta}\theta\left(1 + \frac{\gamma-1}{2}M_e^2 - 0.81\frac{T_{aw}-T_w}{T_e}\right)\mathrm{Re}_s^{0.25} \tag{2.14}$$

where $T_{aw} = T_e\left(1 + r\frac{\gamma-1}{2}M_e^2\right)$ and $r = 0.85$. This is one of the most complex criteria as it takes curvature into account, compressibility and thermal effects. A modified version of the previous correlation ignores the temperature correction term simplifying the criterion (VDB/NASA):

$$k = 147.7\delta^*\left(\frac{1 + \frac{\gamma-1}{2}M_e^2}{\mathrm{Re}_{\delta^*}}\right)^{0.91} \tag{2.15}$$

Reshotko and Tumin criterion is still based on the PANT database and it was developed considering the role of transient growth in roughness–induced transition [51, 52]. They performed several spatial transient growth calculations for boundary layers developed on flat plates or cones and in case of stagnation point flows. The main hypothesis that they introduced is the assumption that the roughness–induced disturbance velocities are assumed proportional to the roughness height k. They presented the following summary relation for the PANT [53] data:

$$k = 180\frac{\theta}{\mathrm{Re}\,\theta}\left(\frac{2T_w}{T_e}\right)^{1.27} \tag{2.16}$$

Dirling criterion is based on the properties of the flow field at the height parameter k for distributed roughness, as it is the effective disturbance parameter.

$$\mathrm{Re}_{kk} = \frac{\rho_k k U_k}{\mu_w} \qquad 200 < \mathrm{Re}_{kk} < 400 \tag{2.17}$$

The large interval for Re_{kk} may represent the variation from distributed (200) to large isolated (400) roughness [50].

2.4.2 The e^N method

One of the main drawbacks of the previous methods is that the stability equations are not taken into account. Instead, the e^N method is based on the linear behavior of instability waves as described by the Orr–Sommerfeld equation. This method was developed independently by van Ingen [1] and Smith & Gamberoni [20] who proposed a correlation between the amplification of linear waves with the onset of transition. Such method, anyway, does not take account of non–linear instability.

Transition is assumed to occur when the wave amplitude A is e^N times the wave amplitude at the beginning of amplification A_0, corresponding to the first neutral point of the neutral stability curve in the $\omega - Re$ plane. The first neutral point represents the point where the imaginary part of the eigenvalue equals zero, $\alpha_i = 0$, for the first time. The factor N is defined as

$$N = -\int_{x_0}^{x} \alpha_i(x')dx' \tag{2.18}$$

where x_0 is the streamwise location corresponding to the first neutral point and α_i is the imaginary part of the wavenumber $\alpha = \alpha_r + i\alpha_i$. At the neutral point $\alpha_i = 0$. In a low disturbance environment, transition is experimentally observed when the factor N is between 9 and 11.

This method neglects the receptivity mechanism as the amplitude of the initial disturbance is not considered. In order to consider somehow the disturbance, Mack [54] suggested a dependence of N from the free–stream turbulent intensity level Tu

$$N = -8.43 - 2.4\ln(Tu)$$

valid for $Tu < 3\%$. Transition location is found at the location x where $N(x)$ is equal to the given threshold.

2.5 Transition control

Delaying transition from laminar to turbulent flow provides many obvious advantages. Flow control aims not only at transition delay but also at separation delay, lift increase, drag reduction, turbulence control, relaminarization and noise suppression.

Control strategies can be classified in different ways. One possibility is to consider the energy or power required in order to control the flow field, obtaining a first main division in passive or active control. In the former case no energy is needed (see the successful development of NACA 6–series

airfoils for which transition was delayed just by shaping the wall in a specific way), in the latter energy is required. Active control can be further divided into open–loop or reactive. Open–loop control consists in the application of steady or unsteady energy input without regard to the particular state of the flow. For this reason, no sensors are required. On the other hand, when a variable characterizing the flow field is measured and used in order to change the flow itself, reactive control is applied. Therefore, reactive control is a special class of active control where the control input is continuously adjusted based on measurements of some kind.

Another possible classification can be based on whether the control technique directly modifies the shape of the base flow, making it more stable, or directly influences the perturbation generated inside the boundary layer, avoiding its amplification. Suction at the wall, shaping, wall heating/cooling, wall motion, streamwise or spanwise pressure gradient can be grouped in the former class of techniques, whereas wave cancellation belong to the techniques that directly act on the disturbance.

2.5.1 Laminar flow control

"Laminar Flow Control" technology (LFC) is an active boundary layer control technique employed to maintain the laminar state. LFC can be achieved using devices such as synthetic jets or plasma actuators, but the major drawback of this technology is the energy consumption which could be higher than the resulted savings.

Synthetic jet

Synthetic jet is an active control technique that seems to be particularly interesting for efficient low–cost applications. A deforming membrane oscillates inside a close cavity, producing periodic suction/blowing with a zero–net mass flux across its small exit orifice, so momentum is added into the external boundary layer. The interaction of synthetic jets with an incoming boundary layer results in an apparent modification of the surface shape and enables significant global modification of the embedding flow [55].

Plasma actuator

A scheme of a single–dielectric barrier discharge (SDBD) plasma actuator [56] is reported in figure 2.3. The device consists of thin electrodes separated by dielectric material. One of the electrode is exposed to air and

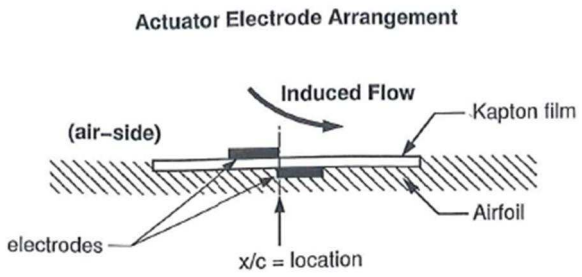

Figure 2.3: Schematic drawing of a single–dielectric barrier discharge actuator

the other is fully covered by the dielectric material. A high voltage alternating current (a. c.) is supplied to the electrodes. When the a. c. amplitude is large enough, the air ionizes in the region of the largest electric potential. The ionized air under the action of a gradient of the electric field produces a body force on the ambient air. This induces a virtual aerodynamic shape and a change in the pressure distribution over the body on which the actuator is placed. The air near the electrodes is weakly ionized and the heating of the air is limited.

Plasma synthetic jet

Another type of actuator is the plasma synthetic jet (PSJ) . A PSJ is made of a plasma arc positioned inside a cavity containing a small orifice adjacent to the surface where the actuation has to be applied. The heating of the gas inside the cavity increases the pressure and the gas exits the orifice with a velocity that can reach $500 - 600\ m/s$ with pulsations frequencies up to 5000 Hz. The device provides a zero–net mass flux jet and can be operated for flow control or thrust generation.

2.5.2 Natural laminar flow control

An alternative concept of drag reduction which does not require a supply of energy is referred to as "Natural Laminar Flow" (NLF). NLF employs a favorable pressure gradient to delay the transition process. Proper wall shaping has been employed to design laminar flow wings which have shown good performances especially when used in a low sweep configuration. The stabilization of a boundary layer over an airplane wing by pushing the longitudinal location of the pressure minimum as far as possible downstream

dates 1930s and led to the successful development of NACA 6–series airfoils. Factors that limit the utility of this technique include performance degradation at angles of attack different from the one for which the shape was optimized, insect impact, dirty particulates, ice formation.

In most of the high speed aircraft, anyway, a strong sweep is usually required in order to achieve better aerodynamic performances. Application of common NLF techniques in these cases proved to be unsuccessful because the flow field becomes vulnerable to a boundary layer instability termed "cross–flow vortex instability" (CF). An active system is usually required to prevent the appearance of CF from causing the laminar flow to become turbulent.

2.5.3 Hybrid laminar flow control

A significant advance made in the development of laminar flow techniques is the concept of "Hybrid Laminar Flow Control" (HLFC). HLFC integrates the concepts of NLF and LFC to reduce suction or heat transfer requirements and reduce the system complexity. The key features of HLFC are:

1. Suction is required only in the leading edge region ahead of the front spar
2. NLF is maintained through proper tailoring of the geometry
3. The HFLC wing design shows good performances in the turbulent regime

The application of wall suction was the first method historically introduced in order to delay boundary–layer transition. It was used by Prandtl in 1904 to prevent flow separation from the surface of a cylinder.

The main effect of suction at the wall is the modification of the velocity profile in the neighborhood of the surface, implying the change of the stability characteristics of the flow. Additionally, suction inhibits the growth of boundary layer and thus the critical Reynolds number based on boundary–layer thickness may never be reached.

Although laminar flow can be maintained to extremely high Reynolds numbers, provided that enough fluid is sucked away, the goal is to reach the delay of transition with the minimum suction flow rate, since this will reduce the power necessary and the momentum loss due to suction.

Assuming continuous and uniform suction (for instance through a porous wall) and that the flow outside the boundary layer is not affected by the

loss of mass at the wall, the asymptotic velocity profile inside the boundary layer is an exact solution of the Navier–Stokes equations and is expressed as

$$U(y) = U_\infty \left[1 - \exp\left(-\frac{|v_w|y}{\nu}\right)\right] \tag{2.19}$$

where v_w is a negative constant representing the value of the uniform suction velocity at the wall [38].

A problem arising from the application of this technique is that structure is negatively affected by the presence of holes in it and also manufacturing matters arise. Another problem is related to the protection of the surface of an aircraft wing from insect impacts, ice formations or other small particles.

2.5.4 Wave cancellation

An alternative approach to the previously proposed methods is wave cancellation. This technique is not based on the modification of the boundary layer profile, but aims at acting directly on the perturbation. If the frequency, orientation and phase angle of the dominant element of the spectrum of a linear growing disturbance is detected, a control system and appropriate located disturbance generators may then be used to produce a desired cancellation or suppression of the detected disturbance. Wave cancellation is feasible only when the disturbances are still relatively small, their growth is governed by linear equations and the principle of superimposition is still valid.

2.6 Receptivity

The transition point is strongly affected by the amount of "noise" present in the external environment. Increased free–stream disturbance level enhances the amplitude of the instability wave, hastening transition. The typical external disturbances can be acoustic waves, free stream vorticity waves or wall vibrations. For all of them, even if the frequency is the same as the TS waves, the typical wavelength is much greater than the TS one. It means that this kind of disturbances cannot create any coupling with the boundary layer instability waves, i. e. disturbances are not resonant with the TS waves.

A "mechanism" is therefore needed in order to allow the adaptation of the exciting wavelength to the TS one and Morkovin [57] introduced the term "receptivity" in order to indicate qualitatively the physical process by which free–stream external disturbances enter the boundary layer and excite

instability waves. This effect can be obtained by the boundary layer growing near the leading edge or by a fast surface variation like wall roughness and two main receptivity configurations can be identified: leading edge receptivity and sudden boundary layer forced adjustment receptivity. The methodological approaches used to tackle the receptivity problem can be separated into three main categories: asymptotic approach, direct numerical simulation and finite Reynolds number approach, and in this thesis the latter, based on the Orr–Sommerfeld formulation, will be adopted (see §4).

Chapter 3

Multiple–scales method

In mathematics and physics, multiple–scale analysis (also called the method of multiple scales) comprises techniques used to construct uniformly valid approximations to the solutions of perturbation problems [58]. This is done by introducing fast-scale and slow-scale variables for an independent variable, and subsequently treating these variables, fast and slow, as if they are independent. In the solution process of the perturbation problem thereafter, the resulting additional freedom introduced by the new independent variables is used to remove unwanted secular terms. The latter puts constraints on the approximate solution, which are called solvability conditions [59].

Multiple–scale method can be applied to the boundary layer where there is a slow variation of the fluid dynamic quantities along the streamwise coordinate with reference to the normal one. So, in order to deal with the analysis of the perturbation of flow field, it is useful to describe such approach. In the following sections both the homogeneous case and non-homogeneous one will be described following [2].

3.1 Homogeneous case

Let

$$\frac{d\mathbf{x}(t)}{dt} = \mathbf{A}(t)\mathbf{x}(t) \tag{3.1}$$

be the evolution equation of a generic time–dependent linear system. By fixing the coefficient of the system at a certain time $t = t_0$, i.e. setting $\mathbf{A}(t) = \mathbf{A}(t_0)$, the solution of eq. 3.1 can be expressed in terms of eigenvalues $\lambda_k(t_0)$ and eigenvectors $\mathbf{u}_k(t_0)$ of matrix $\mathbf{A}(t_0)$ as:

$$\mathbf{x}(t) = \sum_{k=1}^{N} c_k \mathbf{u}_k(t_0) e^{\lambda_k(t_0)t} \tag{3.2}$$

with N arbitrary coefficients c_k.

Let matrix $\mathbf{A}$ be slowly varying, i.e. a long time (with respect to the typical characteristic time) is required in order to appreciate a variation of the eigenvalues λ_k and eigenvectors $\mathbf{u}_k$. It can be introduced a parameter $\tilde{\epsilon}$ through the scaling $T = \tilde{\epsilon}t$, where T is a new time, so that an order–one variation of T occurs for a large variation of t and consequently of $\mathbf{A}$.

With this substitution, equations (3.1) and (3.2) become, respectively:

$$\tilde{\epsilon}\frac{d\mathbf{x}(T)}{dT} = \mathbf{A}(T)\mathbf{x}(T) \tag{3.3}$$

$$\mathbf{x}(T) = \sum_{k=1}^{N} c_k \mathbf{u}_k(T_0) e^{\lambda_k(T_0)T/\tilde{\epsilon}} \tag{3.4}$$

Let solve eq. 3.3 in the limit of $\tilde{\epsilon} \to 0$, with the hypothesis that the solution is the same of eq. 3.4, with $\mathbf{u}_k(T)$ and $\lambda_k(T)$ instead of $\mathbf{u}_k(T_0)$ and $\lambda_k(T_0)$, and that the coefficients c_k function of T and $\tilde{\epsilon}$ can be developed as series of parameter $\tilde{\epsilon}$.

A single term in eq. (3.4), in the case of a constant coefficient matrix $\mathbf{A} = \mathbf{A}(T_0)$, is

$$\mathbf{x}(T) = \mathbf{u}_k(T_0) e^{\lambda_k(T_0)T/\tilde{\epsilon}}$$

while, when the coefficient matrix $\mathbf{A}$ is slowing varying, the corresponding term can be written as

$$\mathbf{x}(T) = \mathbf{f}(T, \tilde{\epsilon}) e^{\phi(T)/\tilde{\epsilon}}$$

so that in the constant coefficient case $\mathbf{f}(T, \tilde{\epsilon})$ and $\phi(T)$ respectively reduce to $\mathbf{f}(T, \tilde{\epsilon}) = \mathbf{u}_k(T_0)$ and $\phi(T) = \lambda_k(T_0)T$. We now assume that the vector $\mathbf{f}(T, \tilde{\epsilon})$ is expandable in a power series of $\tilde{\epsilon}$ so that

$$\mathbf{f}(T, \tilde{\epsilon}) = \sum_{n=0}^{\infty} \mathbf{f}_n(T) \tilde{\epsilon}^n$$

which implies

$$\mathbf{x}(T) = \mathbf{f}(T, \tilde{\epsilon}) e^{\phi(T)/\tilde{\epsilon}} = \left(\mathbf{f}_0(T) + \tilde{\epsilon}\mathbf{f}_1(T) + \tilde{\epsilon}^2\mathbf{f}_2(T) + \cdots\right) e^{\phi(T)/\tilde{\epsilon}} \tag{3.5}$$

With this expression for the solution $\mathbf{x}(T)$, the term $\tilde{\epsilon}d\mathbf{x}/dT$ becomes

$$\begin{aligned}
\tilde{\epsilon}\frac{d\mathbf{x}(T)}{dT} &= \tilde{\epsilon}\left[\left(\frac{d\mathbf{f}_0(T)}{dT} + \tilde{\epsilon}\frac{d\mathbf{f}_1(T)}{dT} + \cdots\right) e^{\phi(T)/\tilde{\epsilon}} + \right. \\
&\quad \left. \frac{1}{\tilde{\epsilon}}\frac{d\phi(T)}{dT}(\mathbf{f}_0(T) + \tilde{\epsilon}\mathbf{f}_1(T) + \cdots) e^{\phi(T)/\tilde{\epsilon}}\right] \\
&= \left[\frac{d\phi(T)}{dT}\mathbf{f}_0(T) + \tilde{\epsilon}\left(\frac{d\phi(T)}{dT}\mathbf{f}_1(T) + \frac{d\mathbf{f}_0(T)}{dT}\right) + \mathcal{O}(\tilde{\epsilon}^2)\right] e^{\phi(T)/\tilde{\epsilon}}
\end{aligned}$$

substituting the previous derivative and the expansion (3.5) in the system (3.3), collecting terms with respect to $\tilde{\epsilon}$ order, and dividing by the exponential part, the following hierarchy of equations is found:

$$\begin{aligned}
\frac{d\phi}{dT}\mathbf{f}_0(T) &= \mathbf{A}(T)\mathbf{f}_0(T) \\
\tilde{\epsilon}\left(\frac{d\phi}{dT}\mathbf{f}_1(T) + \frac{d\mathbf{f}_0}{dT}\right) &= \tilde{\epsilon}\mathbf{A}(T)\mathbf{f}_1(T) \\
\vdots &= \vdots \\
\tilde{\epsilon}^n\left(\frac{d\phi}{dT}\mathbf{f}_n(T) + \frac{d\mathbf{f}_{n\text{-}1}}{dT}\right) &= \tilde{\epsilon}^n\mathbf{A}(T)\mathbf{f}_n(T)
\end{aligned}$$

The first equation reduces to the eigenvalue problem

$$\left[\lambda_k(T)\mathbf{I} - \mathbf{A}(T)\right]\mathbf{f}_0(T) = 0 \tag{3.6}$$

that admits a non trivial solution if

$$\lambda_k(T) = \frac{d\phi}{dT}$$

The solution is actually $\mathbf{f}_0(T) = \mathbf{u}_k(T)$, as expected, but it is defined up to a multiplicative factor since the normalization of the eigenvector $\mathbf{f}_0(T)$ can be performed in different ways. In order to express this feature, the solution at order zero is written as $\mathbf{f}_0(T) = c_k(T)\tilde{\mathbf{u}}_k(T)$ where the coefficient $c_k(T)$ is unknown and $\tilde{\mathbf{u}}_k(T)$ is normalized in a certain way. The second equation, at order $\tilde{\epsilon}$, can be written

$$\left[\lambda_k(T)\mathbf{I} - \mathbf{A}(T)\right]\mathbf{f}_1(T) = -\frac{d\mathbf{f}_0}{dT} \tag{3.7}$$

which represents a singular problem because the coefficient matrix $\dfrac{d\phi}{dT}\,\mathbf{I} - \mathbf{A}(T)$ is the same as the one at order zero, where the singularity of the matrix was required in order to obtain a non trivial solution. However, at order $\tilde{\epsilon}$ an inhomogeneous known term is present, so the solution exists if a proper "compatibility condition" is satisfied (see appendix A), which states that the dot product between the known term and the left eigenvector corresponding to the vanishing eigenvalue must be zero:

$$\tilde{\mathbf{v}}_k(T) \cdot \frac{d\mathbf{f}_0}{dT} = 0 \tag{3.8}$$

By expanding the previous equation and recalling that $\mathbf{f}_0(T) = c_k(T)\tilde{\mathbf{u}}_k(T)$, an equation for the unknown coefficient $c_k(T)$ is obtained:

$$\tilde{\mathbf{v}}_k(T) \cdot \tilde{\mathbf{u}}_k(T)\frac{dc_k}{dT} + \tilde{\mathbf{v}}_k(T) \cdot \frac{d\tilde{\mathbf{u}}_k(T)}{dT}c_k = 0 \tag{3.9}$$

It is easy to verify that eq. (3.9) is a first order homogeneous ordinary differential equation, for which a closed form solution exists. Its solution provides the coefficient $c_k(T)$ so that the product $c_k(T)\tilde{\mathbf{u}}_k(T)$ is computed. It is important to remark that the latter vector is unique, independent of the normalization, while $\tilde{\mathbf{u}}_k(T)$ was not.

Summarizing, the solution at order zero is not uniquely determined, but it is defined up to a multiplicative factor $c_k(T)$ which depends on T. $c_k(T)$ can be an arbitrary function of T and the "compatibility condition" of eq. (3.8) is used as a constraint in order to determine the unknown factor $c_k(T)$. The same compatibility problem found at order $\tilde{\epsilon}$ is present also at the next orders because the generic equation contains always the same singular matrix. In practical applications the solution is usually truncated at order zero. However, it is interesting to evaluate the error when order–$\tilde{\epsilon}$ terms are neglected. This can be done using the relation (A.5), so that the solution at order $\tilde{\epsilon}$ is written as

$$\tilde{\epsilon}\mathbf{f}_1(t) = \sum_{h\neq k} [\lambda_h(t) - \lambda_k(t)]^{-1} \left(\mathbf{v}_k^{\mathrm{T}}(t) \cdot \frac{d\mathbf{u}_k(t)}{dt}\right) \mathbf{u}_k(t)$$

where $t = T/\tilde{\epsilon}$ has been substituted and $\lambda_h(t)$ is another eigenvalue of $\mathbf{A}(t)$. From this expression, it is clear that in order for $\tilde{\epsilon}\mathbf{f}_1(T)$ to be small and negligible with respect to $\mathbf{f}_0(T)$, the derivative $d\mathbf{u}_k/dT$ must be small with respect to $\lambda_h(t) - \lambda_k(t)$. This basically implies that the multiple–scale approximation can be applied if the parameters of the system are slowly varying with respect to the characteristic frequency given by the difference between the considered eigenvalue and the other eigenvalues of the system. Therefore, multiple scales can be applied if the eigenvalues are distinct but sufficiently far, independent of how small they are.

By retaining only the order–zero term, the state vector $\mathbf{x}(T)$ is expressed as

$$\mathbf{x}(T) = c_k(T)\tilde{\mathbf{u}}_k(T)e^{\phi(T)/\tilde{\epsilon}} + \mathcal{O}(\tilde{\epsilon})$$

3.2 Non–homogeneous case

Let us consider the non–homogeneous system

$$\frac{d\mathbf{x}(t)}{dt} - \boldsymbol{A}\,(t)\,\mathbf{x}(t) = \tilde{\epsilon}\mathbf{y}(t) \tag{3.10}$$

where $\mathbf{y}$ is an order–one known term which enters at order $\tilde{\epsilon}$. Introducing the substitution $T = \tilde{\epsilon}t$, from (3.10) follows:

$$\tilde{\epsilon}\,(T)\,\frac{d\mathbf{x}(T)}{dT} - \boldsymbol{A}\,(T)\,\mathbf{x} = \tilde{\epsilon}\mathbf{y}(T) \tag{3.11}$$

As for homogeneous case:

$$\mathbf{x}(T) = \left(\mathbf{f}_0(T) + \tilde{\epsilon}\mathbf{f}_1(T) + \tilde{\epsilon}^2\mathbf{f}_2(T) + \cdots\right) e^{\frac{\phi(T)}{\tilde{\epsilon}}} \tag{3.12}$$

and substituting the expansion (3.12) in (3.11) and collecting powers of $\tilde{\epsilon}$, the following hierarchy of equations is derived:

$$\begin{aligned}
\left(\frac{d\phi}{dT}\mathbf{f}_0(T) - \boldsymbol{A}(T)\mathbf{f}_0(T)\right) e^{\frac{\phi(T)}{\tilde{\epsilon}}} &= 0 \\
\tilde{\epsilon}\left(\frac{d\phi}{dT}\mathbf{f}_1(T) + \frac{d\mathbf{f}_0}{dT} - \boldsymbol{A}\,(T)\,\mathbf{f}_1(T)\right) e^{\frac{\phi(T)}{\tilde{\epsilon}}} &= \tilde{\epsilon}\mathbf{y}(T) \\
\cdots &= \cdots \\
\tilde{\epsilon}^n\left(\frac{d\phi}{dT}\mathbf{f}_n(T) + \frac{d\mathbf{f}_{n-1}}{dT} - \boldsymbol{A}\,(T)\,\mathbf{f}_n\right) e^{\frac{\phi(T)}{\tilde{\epsilon}}} &= 0
\end{aligned} \tag{3.13}$$

At zero order, the problem reduces to the homogeneous one:

$$\left(\frac{d\phi}{dT}\boldsymbol{I} - \boldsymbol{A}(T)\right)\mathbf{f}_0(T) = 0 \tag{3.14}$$

While the first–order equation is:

$$\tilde{\epsilon}\left(\frac{d\phi}{dT}\mathbf{f}_1(T) + \frac{d\mathbf{f}_0}{dT} - \boldsymbol{A}\,(T)\,\mathbf{f}_1(T)\right) e^{\frac{\phi(T)}{\tilde{\epsilon}}} = \tilde{\epsilon}\mathbf{y}(T) \tag{3.15}$$

which can be written in the following form:

$$\left[\frac{d\phi}{dT}\boldsymbol{I} - \boldsymbol{A}(T)\right]\mathbf{f}_1(T) = -\frac{d\mathbf{f}_0}{dT} + \mathbf{y}(T)e^{-\frac{\phi(T)}{\tilde{\epsilon}}} \tag{3.16}$$

In order to solve the linear system (3.16), the solvability condition has to be satisfied, i.e.:

$$\tilde{\mathbf{v}}_k(T)\cdot\left(-\frac{d\mathbf{f}_0}{dT} + \mathbf{y}(T)e^{-\frac{\phi(T)}{\tilde{\epsilon}}}\right) = 0 \tag{3.17}$$

where the $\tilde{\mathbf{v}}_k(T)$ is the left eigenfunction of $\dfrac{d\phi}{dT}\boldsymbol{I} - \boldsymbol{A}(T)$. The condition (3.17) allows the computation of $c_k(T)$ and the unique determination of the solution $\mathbf{f}_0(T)$. Substituting $\mathbf{f}_0(T) = c_k(T)\tilde{\mathbf{u}}_k(T)$ in (3.17), the following first–order linear differential equation for $c_k(T)$ is obtained:

$$\tilde{\mathbf{v}}_k(T)\cdot\tilde{\mathbf{u}}_k(T)\frac{dc_k}{dT} + \tilde{\mathbf{v}}_k(T)\cdot\frac{d\tilde{\mathbf{u}}_k(T)}{dT}c_k = \tilde{\mathbf{v}}_k(T)\cdot\mathbf{y}(T)e^{-\frac{\phi(T)}{\tilde{\epsilon}}} \tag{3.18}$$

whose solution is well known in a closed form:

$$c_k(T_f) = \int_{T_0}^{T_f} \frac{\tilde{\mathbf{v}}_k(T)\cdot\mathbf{y}(T)}{\tilde{\mathbf{v}}_k(T)\cdot\tilde{\mathbf{u}}_k(T)} e^{-\frac{\phi(T)}{\tilde{\epsilon}}} e^{\displaystyle\int_T^{T_f} \frac{\tilde{\mathbf{v}}_k(T')\cdot\frac{d\tilde{\mathbf{u}}_k(T')}{dT'}}{\tilde{\mathbf{v}}_k(T')\cdot\tilde{\mathbf{u}}_k(T')}\,dT'}\,dT \tag{3.19}$$

or can be found numerically, by discretizing the differential equation. So the solution $\mathbf{x}$ is expressed as:

$$\mathbf{x}(T_f) = \mathbf{f}_0(T_f)e^{\frac{\phi(T_f)}{\tilde{\epsilon}}} + \mathcal{O}(\tilde{\epsilon}) = c_k(T_f)\tilde{\mathbf{u}}_k(T_f)e^{\frac{\phi(T_f)}{\tilde{\epsilon}}} + \mathcal{O}(\tilde{\epsilon}) \tag{3.20}$$

3.3 Remarks on multiple–scales

The solution (3.20) with (3.19) can be rewritten in the following compact form:

$$\mathbf{x}(T_f) = \tilde{\mathbf{u}}_k(T_f)\int_{T_0}^{T_f} \mathbf{r}(T)\cdot\mathbf{y}(T)\,dT + \mathcal{O}(\tilde{\epsilon}) \tag{3.21}$$

where $\mathbf{r}(T)$ is defined as the receptivity vector to the known source vector $\mathbf{y}(T)$. The idea is to reduce the solution to a very simple form in which it is possible to recognize a receptivity function $\mathbf{r}(T)$, that multiplied by the source term $\mathbf{y}(T)$, gives the amplitude of the final solution $\mathbf{x}(T_f)$. The receptivity vector $\mathbf{r}(T)$ represents a measure of how much the physical system is "receptive" to the source of disturbance $\mathbf{y}(T)$, or, in other words, it represents the sensitivity of the state vector $\mathbf{x}(T_f)$ to the distributed exciting source $\mathbf{y}(T)$.

In practical interesting cases, such as acoustic receptivity to wall roughness or to wall suction/blowing, the vector $\mathbf{y}(T)$ can be a simple scalar quantity, for example the wall shape $h(x)$ accounting for the roughness in the first case, or the imposed normal velocity at the wall $v_w(x)$ in the second one. This means that the dot product $\mathbf{r}(T)\cdot\mathbf{y}(T)$ between the receptivity and the source vectors can be replaced by a simple product between two constants:

$$\mathbf{x}(T_f) = \tilde{\mathbf{u}}_k(T_f)\int_{T_0}^{T_f} r(T)y(T)\,dT + \mathcal{O}(\tilde{\epsilon}) \tag{3.22}$$

obtaining, for the example of acoustic receptivity to wall roughness, a simple expression

$$\mathbf{x}(x_f) = \tilde{\mathbf{u}}_k(x_f) \int_{x_0}^{x_f} r_h(x) h(x)\, dx + \mathcal{O}(\tilde{\epsilon}) \tag{3.23}$$

where $h(x)$ is the wall shape and $r_h(x)$ is the sensitivity of the state vector $\mathbf{x}(x_f)$ to the wall roughness.

Chapter 4

Three-dimensional receptivity formulation

Let us consider the general receptivity problem which takes place in a boundary layer developing on a generic surface.

4.1 Governing equations

We consider a three–dimensional unsteady incompressible flow, governed by Navier–Stokes equations:

$$\frac{\partial u}{\partial \hat{x}} + \frac{\partial v}{\partial \hat{y}} + \frac{\partial w}{\partial \hat{z}} = 0 \tag{4.1}$$

$$\frac{\partial u}{\partial \hat{t}} + u\frac{\partial u}{\partial \hat{x}} + v\frac{\partial u}{\partial \hat{y}} + w\frac{\partial u}{\partial \hat{z}} = -\frac{\partial p}{\partial \hat{x}} + \frac{1}{R}\nabla^2 u \tag{4.2}$$

$$\frac{\partial v}{\partial \hat{t}} + u\frac{\partial v}{\partial \hat{x}} + v\frac{\partial v}{\partial \hat{y}} + w\frac{\partial v}{\partial \hat{z}} = -\frac{\partial p}{\partial \hat{y}} + \frac{1}{R}\nabla^2 v \tag{4.3}$$

$$\frac{\partial w}{\partial \hat{t}} + u\frac{\partial w}{\partial \hat{x}} + v\frac{\partial w}{\partial \hat{y}} + w\frac{\partial w}{\partial \hat{z}} = -\frac{\partial p}{\partial \hat{z}} + \frac{1}{R}\nabla^2 w \tag{4.4}$$

The equations are already non-dimensionalized by the free–stream velocity U_∞, the pressure ρU_∞^2, the characteristic length $\delta_r = \sqrt{\nu x_r / U_\infty}$ (x_r is the streamwise length) and the time δ_r / U_∞. With this parameters, the Reynolds number reads:

$$R = \frac{\delta_r U_\infty}{\nu} = \sqrt{\frac{x_r U_\infty}{\nu}} = \sqrt{Re_{x_r}} \tag{4.5}$$

Linearizing the dimensionless solution as sum of a steady quantity:

$$(\hat{U}(\hat{x},\hat{y},\hat{z}), \hat{V}(\hat{x},\hat{y},\hat{z}), \hat{W}(\hat{x},\hat{y},\hat{z}), \hat{P}(\hat{x},\hat{y},\hat{z}))$$

solution of the base flow, and an unsteady one

$$(\hat{u}(\hat{x},\hat{y},\hat{z},\hat{t}),\hat{v}(\hat{x},\hat{y},\hat{z},\hat{t}),\hat{w}(\hat{x},\hat{y},\hat{z},\hat{t}),\hat{p}(\hat{x},\hat{y},\hat{z},\hat{t}))$$

the previous set of equations becomes:

$$\frac{\partial \hat{u}}{\partial \hat{x}}+\frac{\partial \hat{v}}{\partial \hat{y}}+\frac{\partial \hat{w}}{\partial \hat{z}} = \tilde{\epsilon}\hat{S}^m \tag{4.6}$$

$$\frac{\partial \hat{u}}{\partial \hat{t}}+\hat{U}\frac{\partial \hat{u}}{\partial \hat{x}}+\hat{u}\frac{\partial \hat{U}}{\partial \hat{x}}+\hat{V}\frac{\partial \hat{u}}{\partial \hat{y}}+\hat{v}\frac{\partial \hat{U}}{\partial \hat{y}}+\hat{W}\frac{\partial \hat{u}}{\partial \hat{z}}+\hat{w}\frac{\partial \hat{U}}{\partial \hat{z}} = -\frac{\partial \hat{p}}{\partial \hat{x}}+ +\frac{1}{R}\nabla^2\hat{u}+\tilde{\epsilon}\hat{S}^x \tag{4.7}$$

$$\frac{\partial \hat{v}}{\partial \hat{t}}+\hat{U}\frac{\partial \hat{v}}{\partial \hat{x}}+\hat{u}\frac{\partial \hat{V}}{\partial \hat{x}}+\hat{V}\frac{\partial \hat{v}}{\partial \hat{y}}+\hat{v}\frac{\partial \hat{V}}{\partial \hat{y}}+\hat{W}\frac{\partial \hat{v}}{\partial \hat{z}}+\hat{w}\frac{\partial \hat{V}}{\partial \hat{z}} = -\frac{\partial \hat{p}}{\partial \hat{y}}+ +\frac{1}{R}\nabla^2\hat{v}+\tilde{\epsilon}\hat{S}^y \tag{4.8}$$

$$\frac{\partial \hat{w}}{\partial \hat{t}}+\hat{U}\frac{\partial \hat{w}}{\partial \hat{x}}+\hat{u}\frac{\partial \hat{W}}{\partial \hat{x}}+\hat{V}\frac{\partial \hat{w}}{\partial \hat{y}}+\hat{v}\frac{\partial \hat{W}}{\partial \hat{y}}+\hat{W}\frac{\partial \hat{w}}{\partial \hat{z}}+\hat{w}\frac{\partial \hat{W}}{\partial \hat{z}} = -\frac{\partial \hat{p}}{\partial \hat{z}}+ +\frac{1}{R}\nabla^2\hat{w}+\tilde{\epsilon}\hat{S}^z \tag{4.9}$$

where source terms S of order $\tilde{\epsilon}$ enter as perturbations. $\tilde{\epsilon}$ is the parameter that accounts for slow streamwise variation of the quantities, $\hat{S}^m$ is the source mass term, $\hat{S}^x$ is the x–momentum source term, $\hat{S}^y$ is the y–momentum source term and $\hat{S}^z$ is the z–momentum source term.

The boundary conditions for eqs. from (4.6) to (4.10) depend on the specific problem and can be homogeneous or non–homogeneous. In any case, the boundary conditions for the perturbations require them to be zero at the wall $(\hat{u}(\hat{x},0,\hat{z},\hat{t}),\hat{v}(\hat{x},0,\hat{z},\hat{t}),\hat{w}(\hat{x},0,\hat{z},\hat{t}))=(0,0,0)$ and to go to zero far from the wall $(\hat{u}(\hat{x},\infty,\hat{z},\hat{t}),\hat{v}(\hat{x},\infty,\hat{z},\hat{t}),\hat{w}(\hat{x},\infty,\hat{z},\hat{t}))\rightarrow(0,0,0)$. This implies that if there are non–homogeneous boundary conditions, they must enter at order $\tilde{\epsilon}$ as for the excitation source.

$$\begin{pmatrix}\hat{u}(\hat{x},0,\hat{z},\hat{t})\\ \hat{v}(\hat{x},0,\hat{z},\hat{t})\\ \hat{w}(\hat{x},0,\hat{z},\hat{t})\end{pmatrix} = \tilde{\epsilon}\begin{pmatrix}\hat{u}_{\text{wall}}(\hat{x},\hat{z},\hat{t})\\ \hat{v}_{\text{wall}}(\hat{x},\hat{z},\hat{t})\\ \hat{w}_{\text{wall}}(\hat{x},\hat{z},\hat{t})\end{pmatrix}$$
$$\begin{pmatrix}\hat{u}(\hat{x},\hat{y}\rightarrow\infty,\hat{z},\hat{t})\\ \hat{v}(\hat{x},\hat{y}\rightarrow\infty,\hat{z},\hat{t})\\ \hat{w}(\hat{x},\hat{y}\rightarrow\infty,\hat{z},\hat{t})\end{pmatrix} \rightarrow \tilde{\epsilon}\begin{pmatrix}\hat{u}_{\infty}(\hat{x},\hat{z},\hat{t})\\ \hat{v}_{\infty}(\hat{x},\hat{z},\hat{t})\\ \hat{w}_{\infty}(\hat{x},\hat{z},\hat{t})\end{pmatrix} \tag{4.10}$$

4.2 Base flow

In a stability analysis, the base flow ($\hat{U}(\hat{x},\hat{y},\hat{z})$, $\hat{V}(\hat{x},\hat{y},\hat{z})$, $\hat{W}(\hat{x},\hat{y},\hat{z})$, $\hat{P}(\hat{x},\hat{y},\hat{z})$) is always known because it is the solution around which the stability is considered. The base flow depends on the particular case which is considered in the single problem under investigation and for the boundary layer over a flat plate the base flow is given by the Blasius solution, while for more complex boundary layers, it could be obtained through CFD analysis. Usually, for the base flow, the zero–order terms are considered, but it is possible to introduce corrections of higher order as it is done for the perturbation. What is important is that the base flow, at this stage, is considered like a "known term" in the receptivity problem.

4.3 Perturbation and multiple–scales application

Once the base flow has been obtained, equations from (4.6) to (4.10) can be solved for the unknown $(\hat{u}(\hat{x},\hat{y},\hat{z},\hat{t}),\hat{v}(\hat{x},\hat{y},\hat{z},\hat{t}),\hat{w}(\hat{x},\hat{y},\hat{z}),\hat{p}(\hat{x},\hat{y},\hat{z},\hat{t}))$.

Since we want to account for the boundary layer growing, we derive the equations for the perturbation in the multiple scale framework, expanding the solution as powers of a small parameter $\tilde{\epsilon}$ which accounts for the non–parallelism of the base flow.

Starting from equations (4.6) to (4.10) we operate the following substitutions:

$$\begin{aligned} x &= \tilde{\epsilon}\hat{x} \\ y &= \hat{y} \\ z &= \tilde{\epsilon}\hat{z} \\ t &= \tilde{\epsilon}\hat{t} \\ U(x,y,z) &= \hat{U}(\hat{x},\hat{y},\hat{z}) \\ V(x,y,z) &= \frac{\hat{V}(\hat{x},\hat{y},\hat{z})}{\tilde{\epsilon}} \\ W(x,y,z) &= \hat{W}(\hat{x},\hat{y},\hat{z}) \\ P(x,y,z) &= \hat{P}(\hat{x},\hat{y},\hat{z}) \\ S(x,y,z,t) &= \hat{S}(\hat{x},\hat{y},\hat{z},\hat{t}) \end{aligned} \tag{4.11}$$

so that all the derivatives have the same order. The general quantity $q(x,y,z,t)$, which can be u,v,w,p, in the multiple-scale system can be written in the following form:

$$q(x,y,z,t) = \left(q_0(x,y,z) + \tilde{\epsilon}q_1(x,y,z) + \tilde{\epsilon}^2 q_2(x,y,z) + \cdots\right) e^{\frac{i\theta(x,z,t)}{\tilde{\epsilon}}} \tag{4.12}$$

where q_0, q_1 and q_2 are functions with a weak dependence on the streamwise coordinate, while θ is a fast–varying function. The eikonal function θ

is a non-linear partial differential equation encountered in problems of wave propagation, when the wave equation is approximated using the WKB theory [37], and represents the phase of the disturbance. The derivatives of the eikonal function, with reference to time and space:

$$\omega = -\frac{\partial\theta}{\partial t} \tag{4.13}$$

$$\alpha = \frac{\partial\theta}{\partial x} \tag{4.14}$$

$$\beta = \frac{\partial\theta}{\partial z} \tag{4.15}$$

define the frequency, the chordwise wavenumber and spanwise wavenumber, respectively.

The partial derivatives of the general quantity $q(x, y, z, t)$ are expressed as follows:

$$\begin{aligned}
\frac{\partial q}{\partial t} &= -\frac{i\omega}{\tilde{\epsilon}}\left(q_0(x,y,z) + \tilde{\epsilon}q_1(x,y,z) + \tilde{\epsilon}^2 q_2(x,y,z) + \cdots\right) e^{\frac{i\theta(x,z,t)}{\tilde{\epsilon}}} \\
\frac{\partial q}{\partial x} &= \left[\frac{i\alpha}{\tilde{\epsilon}}\left(q_0(x,y,z) + \tilde{\epsilon}q_1(x,y,z) + \tilde{\epsilon}^2 q_2(x,y,z) + \cdots\right) + \right. \\
&\quad \left.\left(\frac{\partial q_0(x,y,z)}{\partial x} + \tilde{\epsilon}\frac{\partial q_1(x,y,z)}{\partial x} + \tilde{\epsilon}^2\frac{\partial q_2(x,y,z)}{\partial x} + \cdots\right)\right] e^{\frac{i\theta(x,z,t)}{\tilde{\epsilon}}} \\
\frac{\partial q}{\partial y} &= \left(\frac{\partial q_0(x,y,z)}{\partial y} + \tilde{\epsilon}\frac{\partial q_1(x,y,z)}{\partial y} + \tilde{\epsilon}^2\frac{\partial q_2(x,y,z)}{\partial y} + \cdots\right) e^{\frac{i\theta(x,z,t)}{\tilde{\epsilon}}} \\
\frac{\partial q}{\partial z} &= \left[\frac{i\beta}{\tilde{\epsilon}}\left(q_0(x,y,z) + \tilde{\epsilon}q_1(x,y,z) + \tilde{\epsilon}^2 q_2(x,y,z) + \cdots\right) + \right. \\
&\quad \left.\left(\frac{\partial q_0(x,y,z)}{\partial z} + \tilde{\epsilon}\frac{\partial q_1(x,y,z)}{\partial z} + \tilde{\epsilon}^2\frac{\partial q_2(x,y,z)}{\partial z} + \cdots\right)\right] e^{\frac{i\theta(x,z,t)}{\tilde{\epsilon}}}
\end{aligned} \tag{4.16}$$

$$
\begin{aligned}
\frac{\partial^2 q}{\partial x^2} &= \left[-\frac{\alpha^2}{\tilde{\epsilon}^2}\left(q_0(x,y,z)+\tilde{\epsilon}q_1(x,y,z)+\tilde{\epsilon}^2 q_2(x,y,z)+\cdots\right)+\right.\\
&\quad 2\frac{i\alpha}{\tilde{\epsilon}}\left(\frac{\partial q_0(x,y,z)}{\partial x}+\tilde{\epsilon}\frac{\partial q_1(x,y,z)}{\partial x}+\tilde{\epsilon}^2\frac{\partial q_2(x,y,z)}{\partial x}+\cdots\right)+\\
&\quad \frac{i}{\tilde{\epsilon}}\frac{\partial \alpha}{\partial x}\left(q_0(x,y,z)+\tilde{\epsilon}q_1(x,y,z)+\tilde{\epsilon}^2 q_2(x,y,z)+\cdots\right)+\\
&\quad \left.\left(\frac{\partial^2 q_0(x,y,z)}{\partial x^2}+\tilde{\epsilon}\frac{\partial^2 q_1(x,y,z)}{\partial x^2}+\tilde{\epsilon}^2\frac{\partial^2 q_2(x,y,z)}{\partial x^2}+\cdots\right)\right] e^{\frac{i\theta(x,z,t)}{\tilde{\epsilon}}}\\
\frac{\partial^2 q}{\partial y^2} &= \left(\frac{\partial^2 q_0(x,y,z)}{\partial y^2}+\tilde{\epsilon}\frac{\partial^2 q_1(x,y,z)}{\partial y^2}+\tilde{\epsilon}^2\frac{\partial^2 q_2(x,y,z)}{\partial y^2}+\cdots\right) e^{\frac{i\theta(x,z,t)}{\tilde{\epsilon}}}\\
\frac{\partial^2 q}{\partial z^2} &= \left[-\frac{\beta^2}{\tilde{\epsilon}^2}\left(q_0(x,y,z)+\tilde{\epsilon}q_1(x,y,z)+\tilde{\epsilon}^2 q_2(x,y,z)+\cdots\right)+\right.\\
&\quad 2\frac{i\beta}{\tilde{\epsilon}}\left(\frac{\partial q_0(x,y,z)}{\partial z}+\tilde{\epsilon}\frac{\partial q_1(x,y,z)}{\partial z}+\tilde{\epsilon}^2\frac{\partial q_2(x,y,z)}{\partial z}+\cdots\right)+\\
&\quad \frac{i}{\tilde{\epsilon}}\frac{\partial \beta}{\partial z}\left(q_0(x,y,z)+\tilde{\epsilon}q_1(x,y,z)+\tilde{\epsilon}^2 q_2(x,y,z)+\cdots\right)+\\
&\quad \left.\left(\frac{\partial^2 q_0(x,y,z)}{\partial z^2}+\tilde{\epsilon}\frac{\partial^2 q_1(x,y,z)}{\partial z^2}+\tilde{\epsilon}^2\frac{\partial^2 q_2(x,y,z)}{\partial z^2}+\cdots\right)\right] e^{\frac{i\theta(x,z,t)}{\tilde{\epsilon}}}
\end{aligned}
\tag{4.17}
$$

Substituting the partial derivatives in the original system (4.6)-(4.10) and collecting powers of the small parameter $\tilde{\epsilon}$, a system of four equations at each order is obtained.

Zero order

At zero order, the set of equations is:

$$
\begin{aligned}
i\alpha u_0 + i\beta w_0 + \frac{\partial v_0}{\partial y} &= 0\\
\left[i\left(\alpha U+\beta W-\omega\right)+\frac{1}{R}\left(\alpha^2+\beta^2-\frac{\partial^2}{\partial y^2}\right)\right]u_0+\frac{\partial U}{\partial y}v_0+i\alpha p_0 &= 0\\
\left[i\left(\alpha U+\beta W-\omega\right)+\frac{1}{R}\left(\alpha^2+\beta^2-\frac{\partial^2}{\partial y^2}\right)\right]v_0+\frac{\partial p_0}{\partial y} &= 0\\
\left[i\left(\alpha U+\beta W-\omega\right)+\frac{1}{R}\left(\alpha^2+\beta^2-\frac{\partial^2}{\partial y^2}\right)\right]w_0+\frac{\partial W}{\partial y}v_0+i\beta p_0 &= 0
\end{aligned}
\tag{4.18}
$$

with boundary conditions:

$$\begin{array}{rcl} u_0(x,0,z) & = & 0 \\ v_0(x,0,z) & = & 0 \\ w_0(x,0,z) & = & 0 \\ & & \\ u_0(x,y\to\infty,z) & \to & 0 \\ v_0(x,y\to\infty,z) & \to & 0 \\ w_0(x,y\to\infty,z) & \to & 0 \end{array} \tag{4.19}$$

The previous system of equations and the corresponding boundary conditions can be discretized in order to solve them numerically. If we think about the discretized form, we can write the previous sets of equations and boundary conditions as

$$\boldsymbol{A}\left(\alpha,\beta,\omega,R\right)\mathbf{f}_0 = 0 \tag{4.20}$$

where $\mathbf{f}_0$ contains the unknowns at order zero evaluated at streamwise location x and at each y location. $\mathbf{f}_0$ contains $4N_y$ lines where N_y is the number of nodes in y direction:

$$\mathbf{f}_0 = \begin{pmatrix} u_0(x,y,z) \\ v_0(x,y,z) \\ w_0(x,y,z) \\ p_0(x,y,z) \end{pmatrix} \tag{4.21}$$

$\boldsymbol{A}$ is the coefficient matrix 4.22:

$$\boldsymbol{A}\left(\alpha,\beta,\omega,R\right) = \begin{pmatrix} i\alpha & \dfrac{\partial}{\partial y} & i\beta & 0 \\ \\ \mathfrak{D} & \dfrac{\partial U}{\partial y} & 0 & i\alpha \\ \\ 0 & \mathfrak{D} & 0 & \dfrac{\partial}{\partial y} \\ \\ 0 & \dfrac{\partial W}{\partial y} & \mathfrak{D} & i\beta \end{pmatrix} \tag{4.22}$$

where $\mathfrak{D} = i\left(\alpha U + \beta W - \omega\right) + \dfrac{1}{R}\left(\alpha^2 + \beta^2 - \dfrac{\partial^2}{\partial y^2}\right)$

System (4.20) is homogeneous because both equations and boundary conditions for the perturbation at zero order are homogeneous, so that it

reduces to an eigenvalue problem. The system (4.20) is formally the same as system (3.14). The only difference is that now the eigenvalue is the local wavelength α and the matrix $\boldsymbol{A}(\alpha, \beta, \omega, R)$ is a non–linear function of α. In the spatial stability problem, β, ω and R are known, while α has to be determined. In order to do that, we expand $\boldsymbol{A}(\alpha, \beta, \omega, R)$ around a known value α_0 and call $\tilde{\boldsymbol{A}}(\alpha, \beta, \omega, R)$ the new matrix:

$$\tilde{\boldsymbol{A}}(\alpha, \beta, \omega, R) = \boldsymbol{A}(\alpha_0, \beta, \omega, R) + \left.\frac{\partial \boldsymbol{A}(\alpha, \beta, \omega, R)}{\partial \alpha}\right|_{\alpha=\alpha_0} (\alpha - \alpha_0) \tag{4.23}$$

The system (4.20) can be replaced by

$$\tilde{\boldsymbol{A}}(\alpha, \beta, \omega, R)\, \mathbf{f}_0 = 0 \tag{4.24}$$

or

$$\boldsymbol{A}(\alpha_0, \beta, \omega, R)\, \mathbf{f}_0 + \boldsymbol{B}(\alpha_0, \beta, \omega, R)\, (\alpha - \alpha_0)\, \mathbf{f}_0 = 0 \tag{4.25}$$

where

$$\boldsymbol{B}(\alpha_0, \beta, \omega, R) = \left.\frac{\partial \boldsymbol{A}(\alpha, \beta, \omega, R)}{\partial \alpha}\right|_{\alpha=\alpha_0} \tag{4.26}$$

The algorithm to compute the eigenvalue is discussed in Appendix B. It is important to remark that in an eigenvalue problem a singular matrix is obtained. Another remark is that $\tilde{\boldsymbol{A}}(\alpha_0)$ singular implies $\boldsymbol{A}(\alpha_0)$ singular as well.

First order

At first order, the multiple–scales approach leads to the system of equations:

$$
\begin{aligned}
& i\alpha u_1 + \frac{\partial v_1}{\partial y} + i\beta w_1 = -\frac{\partial u_0}{\partial x} - \frac{\partial w_0}{\partial z} + S^m e^{-\frac{i\theta(x,z,t)}{\tilde{\epsilon}}} \\
& \mathfrak{D} u_1 + \frac{\partial U}{\partial y} v_1 + i\alpha p_1 = -\frac{\partial p_0}{\partial x} - \left[U - \frac{2i\alpha}{R}\right]\frac{\partial u_0}{\partial x} - \left[W - \frac{2i\beta}{R}\right]\frac{\partial u_0}{\partial z} \\
& - \left[\frac{\partial U}{\partial x} - \frac{i}{R}\frac{\partial \alpha}{\partial x} - \frac{i}{R}\frac{\partial \beta}{\partial z} + V\frac{\partial}{\partial y}\right] u_0 - \frac{\partial U}{\partial z} w_0 + S^x e^{-\frac{i\theta(x,z,t)}{\tilde{\epsilon}}} \\
& \mathfrak{D} v_1 + \frac{\partial p_1}{\partial y} = -\left[U - \frac{2i\alpha}{R}\right]\frac{\partial v_0}{\partial x} - \left[W - \frac{2i\beta}{R}\right]\frac{\partial v_0}{\partial z} \\
& - \left[\frac{\partial V}{\partial y} - \frac{i}{R}\frac{\partial \alpha}{\partial x} - \frac{i}{R}\frac{\partial \beta}{\partial z} + V\frac{\partial}{\partial y}\right] v_0 + S^y e^{-\frac{i\theta(x,z,t)}{\tilde{\epsilon}}} \\
& \frac{\partial W}{\partial y} v_1 + \mathfrak{D} w_1 + i\beta p_1 = -\frac{\partial p_0}{\partial z} - \left[U - \frac{2i\alpha}{R}\right]\frac{\partial w_0}{\partial x} - \left[W - \frac{2i\beta}{R}\right]\frac{\partial w_0}{\partial z} \\
& - \left[\frac{\partial W}{\partial z} - \frac{i}{R}\frac{\partial \alpha}{\partial x} - \frac{i}{R}\frac{\partial \beta}{\partial z} + V\frac{\partial}{\partial y}\right] w_0 - \frac{\partial W}{\partial x} u_0 + S^z e^{-\frac{i\theta(x,z,t)}{\tilde{\epsilon}}}
\end{aligned}
\tag{4.27}
$$

with boundary conditions:

$$
\begin{aligned}
u_1(x,0,z) &= u_{\text{wall}}(x,z,\omega) e^{-\frac{i\theta(x,z,t)}{\tilde{\epsilon}}} \\
v_1(x,0,z) &= v_{\text{wall}}(x,z,\omega) e^{-\frac{i\theta(x,z,t)}{\tilde{\epsilon}}} \\
w_1(x,0,z) &= w_{\text{wall}}(x,z,\omega) e^{-\frac{i\theta(x,z,t)}{\tilde{\epsilon}}} \\
u_1(x, y\to\infty, z) &\to u_\infty(x,z,\omega) e^{-\frac{i\theta(x,z,t)}{\tilde{\epsilon}}} \\
v_1(x, y\to\infty, z) &\to v_\infty(x,z,\omega) e^{-\frac{i\theta(x,z,t)}{\tilde{\epsilon}}} \\
w_1(x, y\to\infty, z) &\to w_\infty(x,z,\omega) e^{-\frac{i\theta(x,z,t)}{\tilde{\epsilon}}}
\end{aligned}
\tag{4.28}
$$

Again, if we think about the discretized form of the previous sets of equations and corresponding boundary conditions, they can be written in following compact way:

$$
\boldsymbol{A}\mathbf{f}_1 = -\boldsymbol{H}\frac{d\mathbf{f}_0}{dx} - \boldsymbol{G}\frac{d\mathbf{f}_0}{dz} - \boldsymbol{C}\mathbf{f}_0 + \mathbf{y} e^{-\frac{i\theta(x,z,t)}{\tilde{\epsilon}}} \tag{4.29}
$$

The number of lines in each vector or matrix is always $4N_y$ where N_y is the number of nodes in y direction. The matrix $\boldsymbol{A}$ is the same as order zero

and defined by eq (4.22), $\mathbf{f}_0$ is defined by eq (4.21), and

$$\mathbf{f}_1 = \begin{pmatrix} u_1(x,y) \\ v_1(x,y) \\ w_1(x,y) \\ p_1(x,y) \end{pmatrix} \tag{4.30}$$

$$\boldsymbol{H} = \begin{pmatrix} 1 & 0 & 0 & 0 \\ \left[U - \dfrac{2i\alpha}{R}\right] & 0 & 0 & 1 \\ 0 & \left[U - \dfrac{2i\alpha}{R}\right] & 0 & 0 \\ 0 & 0 & \left[U - \dfrac{2i\alpha}{R}\right] & 0 \end{pmatrix} \tag{4.31}$$

$$\boldsymbol{G} = \begin{pmatrix} 0 & 0 & 1 & 0 \\ \left[W - \dfrac{2i\beta}{R}\right] & 0 & 0 & 1 \\ 0 & \left[W - \dfrac{2i\beta}{R}\right] & 0 & 0 \\ 0 & 0 & \left[W - \dfrac{2i\beta}{R}\right] & 1 \end{pmatrix} \tag{4.32}$$

$$\boldsymbol{C} = \begin{pmatrix} 0 & 0 & 0 & \\ \left[\dfrac{\partial U}{\partial x} + \mathfrak{G}\right] & 0 & \dfrac{\partial U}{\partial z} & 0 \\ 0 & \left[\dfrac{\partial V}{\partial y} + \mathfrak{G}\right] & 0 & 0 \\ \dfrac{\partial W}{\partial x} & 0 & \left[\dfrac{\partial W}{\partial z} + \mathfrak{G}\right] & 0 \end{pmatrix} \tag{4.33}$$

$$\mathbf{y} = \begin{pmatrix} \mathbf{f}_{\text{wall}}(x,z,\omega) \\ \mathbf{s}(x,y,z,\omega) \\ \mathbf{f}_{\infty}(x,z,\omega) \end{pmatrix} \tag{4.34}$$

with $\mathfrak{G} = V\dfrac{\partial}{\partial y} - \dfrac{i}{R}\left(\dfrac{\partial \alpha}{\partial x} + \dfrac{\partial \beta}{\partial z}\right)$. In the source term $\mathbf{y}$ we have included the sources coming from the equations $\mathbf{s}$ and the boundary conditions $\mathbf{f}_{\text{wall}}$ and $\mathbf{f}_{\infty}$, where

$$\mathbf{s} = \begin{pmatrix} S^m(x,y,z,\omega) \\ S^x(x,y,z,\omega) \\ S^y(x,y,z,\omega) \\ S^z(x,y,z,\omega) \end{pmatrix} \tag{4.35}$$

$$\mathbf{f}_{\text{wall}} = \begin{pmatrix} u_{\text{wall}}(x,z,\omega) \\ v_{\text{wall}}(x,z,\omega) \\ w_{\text{wall}}(x,z,\omega) \\ p_{\text{wall}}(x,z,\omega) \end{pmatrix}; \quad \mathbf{f}_{\infty} = \begin{pmatrix} u_{\infty}(x,z,\omega) \\ v_{\infty}(x,z,\omega) \\ w_{\infty}(x,z,\omega) \\ p_{\infty}(x,z,\omega) \end{pmatrix} \tag{4.36}$$

Since the system defined by eq (4.29) is no more homogeneous and the coefficient matrix $\boldsymbol{A}$ is singular because it has been imposed at order zero, the solvability condition (3.17) is required:

$$\mathbf{y}_0^* \cdot \left(-\boldsymbol{H}\frac{d\mathbf{f}_0}{dx} - \boldsymbol{G}\frac{d\mathbf{f}_0}{dz} - \boldsymbol{C}\mathbf{f}_0 + \mathbf{y}e^{-\frac{i\theta(x,z,t)}{\epsilon}}\right) = 0 \tag{4.37}$$

where $\mathbf{y}_0^*$ is the left–eigenvector of the eigenvalue problem (the adjoint of the solution).

Observing that the eigenvector $\mathbf{f}_0$ is not unique since it has been obtained by an eigenvalue problem, so that instead of $\mathbf{f}_0$ we can substitute $c\mathbf{f}_0$, eq (4.37) reads

$$\mathbf{y}_0^* \cdot \left(-c\boldsymbol{H}\frac{d\mathbf{f}_0}{dx} - \boldsymbol{H}\mathbf{f}_0\frac{dc}{dx} - c\boldsymbol{C}\mathbf{f}_0 + \mathbf{y}e^{-\frac{i\theta(x,z,t)}{\epsilon}}\right) = 0 \tag{4.38}$$

or

$$\left[\mathbf{y}_0^* \cdot (\boldsymbol{H}\mathbf{f}_0)\right]\frac{dc}{dx} + \left[\mathbf{y}_0^* \cdot \left(\boldsymbol{H}\frac{d\mathbf{f}_0}{dx} + \boldsymbol{C}\mathbf{f}_0\right)\right]c = \mathbf{y}_0^* \cdot \mathbf{y}e^{-\frac{i\theta}{\epsilon}} \tag{4.39}$$

where $\boldsymbol{H}$, $\boldsymbol{C}$, $\mathbf{f}_0$, $\mathbf{y}_0^*$, $\mathbf{y}$ and c are all functions of the streamwise coordinate x. Substituting

$$a_1 = \mathbf{y}_0^* \cdot (\boldsymbol{H}\mathbf{f}_0) \tag{4.40}$$

$$a_2 = \mathbf{y}_0^* \cdot \left(\boldsymbol{H}\frac{d\mathbf{f}_0}{dx} + \boldsymbol{G}\frac{d\mathbf{f}_0}{dz} + \boldsymbol{C}\mathbf{f}_0\right) \tag{4.41}$$

eq. (4.39) can be written in the compact form:

$$\frac{dc}{dx} + \frac{a_2}{a_1}c = \frac{\mathbf{y}_0^* \cdot \mathbf{y}}{a_1}e^{-\frac{i\theta}{\epsilon}} \tag{4.42}$$

The conclusion, from the first–order analysis, is that an equation for c has been obtained in order to make $c\mathbf{f}_0$ univocally defined even if $\mathbf{f}_0$, coming from zero–order analysis, was not unique.

4.4 Receptivity analysis

The solvability condition (4.42) can be integrated in a closed form, obtaining:

$$c(x_f, z, t) = \int_{x_0}^{x_f} \frac{\mathbf{y}_0^*(x) \cdot \mathbf{y}(x)}{a_1(x)} e^{-\frac{i\theta(x,z,t)}{\tilde{\epsilon}}} e^{-\int_x^{x_f} \frac{a_2(x')}{a_1(x')}\, dx'}\, dx \tag{4.43}$$

which yields

$$\mathbf{f}(x_f) = \left[\int_{x_0}^{x_f} \frac{\mathbf{y}_0^*(x) \cdot \mathbf{y}(x)}{a_1(x)} e^{-\frac{i\theta(x,z,t)}{\tilde{\epsilon}}} e^{-\int_x^{x_f} \frac{a_2(x')}{a_1(x')}\, dx'}\, dx \right] \mathbf{f}_0(x_f) e^{\frac{i\theta(x_f,z,t)}{\tilde{\epsilon}}} + \mathcal{O}(\tilde{\epsilon}) \tag{4.44}$$

It is worth observing that if $\mathbf{y}(x)$ behaves like $e^{\frac{i\theta(x,z,t)}{\tilde{\epsilon}}}$, the integral in eq. (4.44) is non–zero which means that $\mathbf{y}(x)$ produces a considerable effect.

Observing that

$$\theta(x, z, t) = \int_{x_0}^{x} \alpha(x')\, dx' - \int_{t_0}^{t} \omega(t')\, dt' \tag{4.45}$$

which, in the case of spatial instabilities at fixed frequency, since α varies with x and ω is constant, reduces to

$$\theta(x, z, t) = \int_{x_0}^{x} \alpha(x')\, dx' - \omega t \tag{4.46}$$

and substituting in eq. (4.44), $\mathbf{f}(x_f)$ reads:

$$\left[\int_{x_0}^{x_f} \frac{\mathbf{y}_0^*(x) \cdot \mathbf{y}(x)}{a_1(x)} e^{-\frac{i\int_{x_0}^{x} \alpha(x')\, dx'}{\tilde{\epsilon}}} e^{\frac{i\int_{x_0}^{x_f} \alpha(x')\, dx'}{\tilde{\epsilon}}} e^{-\int_x^{x_f} \frac{a_2(x')}{a_1(x')}\, dx'}\, dx \right] \mathbf{f}_0(x_f) + \mathcal{O}(\tilde{\epsilon}) \tag{4.47}$$

or simply:

$$\mathbf{f}(x_f) = \left[\int_{x_0}^{x_f} \frac{\mathbf{y}_0^*(x) \cdot \mathbf{y}(x)}{a_1(x)} e^{-\int_x^{x_f} \left(\frac{a_2(x')}{a_1(x')} - \frac{i\alpha(x')}{\tilde{\epsilon}} \right) dx'}\, dx \right] \mathbf{f}_0(x_f) + \mathcal{O}(\tilde{\epsilon}) \tag{4.48}$$

and finally

$$\mathbf{f}(x_f) = \left[\int_{x_0}^{x_f} \frac{\mathbf{y}_0^*(x) \cdot \mathbf{y}(x)}{a_1(x)} e^{-\int_x^{x_f} a(x')\,dx'} dx \right] \mathbf{f}_0(x_f) + \mathcal{O}(\tilde{\epsilon}) \tag{4.49}$$

where

$$a(x') = \frac{a_2(x')}{a_1(x')} - \frac{i\alpha(x')}{\tilde{\epsilon}} \tag{4.50}$$

The solution (4.49) can be rewritten in the following compact form:

$$\mathbf{f}(x_f) = \mathbf{f}_0(x_f) \int_{x_0}^{x_f} \mathbf{r}(x) \cdot \mathbf{y}(x)\,dx + \mathcal{O}(\tilde{\epsilon}) \tag{4.51}$$

where

$$\mathbf{r}(x) = \frac{\mathbf{y}_0^*(x)}{a_1(x)} e^{-\int_x^{x_f} a(x')\,dx'} \tag{4.52}$$

We know that $\mathbf{f}_0(x_f)$ has been obtained by solving an eigenvalue problem, which means that it is not unique. Nevertheless, the solution (4.44) and (4.51) are unique because the solvability condition provides the constraint in order to resolve the uncertainty.

The final vector $\mathbf{f}(x_f)$ written in the form (4.51) shows a sensitivity to the known vector $\mathbf{y}(x)$ via $\mathbf{r}(x)$. This means that we can define $\mathbf{r}(x)$ as the receptivity vector to the known source vector $\mathbf{y}(x)$.

The known vector $\mathbf{y}(x)$ can contain source terms coming from the continuity or the momentum equations and from non–homogeneous boundary conditions.

It is important to note that the receptivity vector $\mathbf{r}(x)$ can be expressed as

$$\mathbf{r}(x) = a_3(x)\mathbf{y}_0^*(x) \tag{4.53}$$

where

$$a_3(x) = \frac{1}{a_1(x)} e^{-\int_x^{x_f} a(x')\,dx'} \tag{4.54}$$

which means that, apart from a constant $a_3(x)$, the receptivity is simply the adjoint solution or the left–eigenvector of the direct problem.

Chapter 5

Results

In the present section, results obtained from the application of the code are discussed. The first analyses are aimed to validate the stability code on the ASU test case, while the second test case refers to the computations of the receptivity function to a bump on a Falkner-Skan-Cooke boundary layer.

5.1 ASU Test Case

This case comes from experiments performed by Bill Saric and coworkers [60]. It is chosen as reference as it minimizes presence of attachment-line, TS or Görtler instabilities and encourages growth of crossflow disturbances. The ASU(67)-0315 is installed in the low-turbulence Klebanoff-Saric Wind Tunnel at Texas A&M University. It has a 1.83 m chord and a pressure minimum at 71% chord. Naphthalene flow visualization, used to determine transition location, and detailed velocity profile scans using hotwire anemometry are provided. RANS computations have been performed [61] in order to obtain a pressure distribution which agrees well with the experimental data from the ASU(67)-0315 tests. Different RANS computations at $M = 0.04$ and a chord-Reynolds-number 2.4 10^6 have been performed for the wing mounted in the wind tunnel using the infinite-swept wing approximation. In these computations the flow over the airfoil has been assumed to be either fully turbulent or transitional. The wind tunnel walls have either been approximated by slip boundary conditions or no-slip boundary conditions with turbulent boundary layer. The transition was triggered at $x/c = 70\%$ on the upper surface and at $x/c = 10\%$ on lower surface of the wing.

Stability analyses on the ASU(67)-0315 are performed for steady and unsteady modes. The spanwise wavelength is fixed at $\beta = 400\ 1/m$, while frequency ranges from 0 Hz to 200 Hz. The results at $\mathcal{O}(0)$, in terms of

growth rate α and N factor curves, are compared with the data supplied by FOI and shown from figure 5.1 to figure 5.5. As it can be seen, the results are in good agreement for all the frequencies.

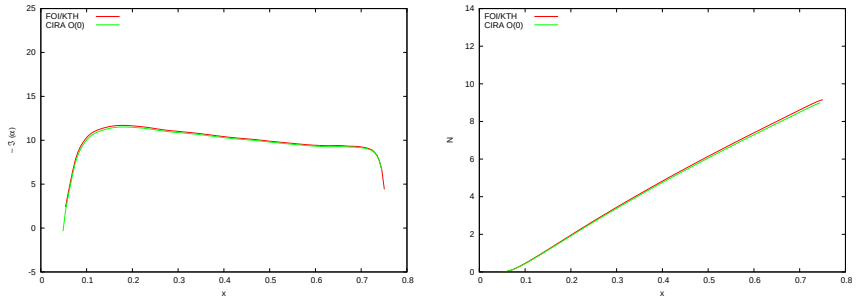

Figure 5.1: ASU test case, comparisons with FOI data at $F = 0\ Hz$

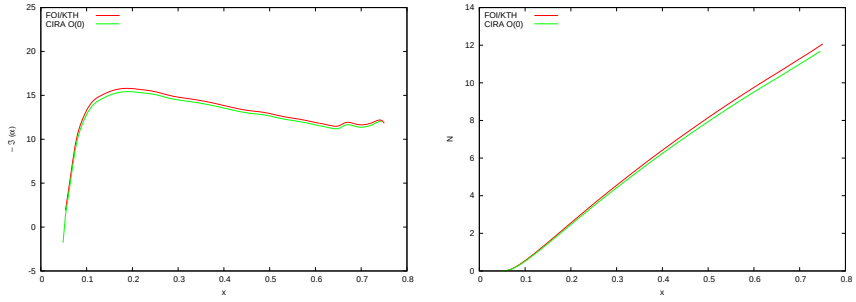

Figure 5.2: ASU test case, comparisons with FOI data at $F = 50\ Hz$

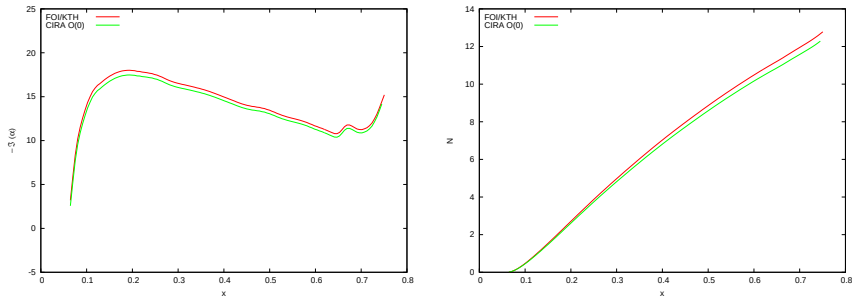

Figure 5.3: ASU test case, comparisons with FOI data at $F = 100\ Hz$

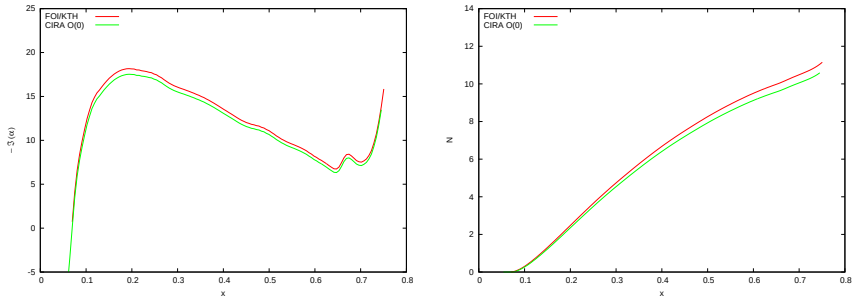

Figure 5.4: ASU test case, comparisons with FOI data at $F = 150\ Hz$

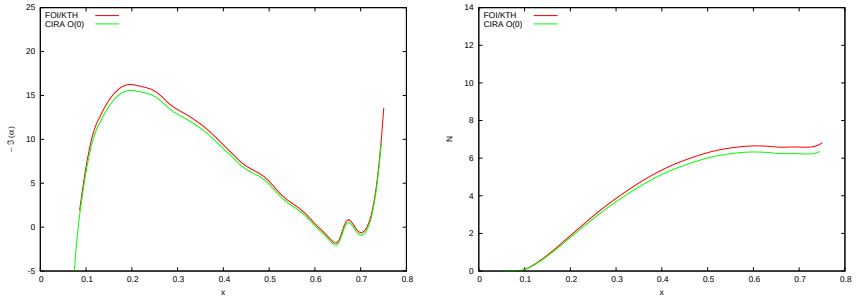

Figure 5.5: ASU test case, comparisons with FOI data at $F = 200\ Hz$

The results at $\mathcal{O}(0)$ and $\mathcal{O}(1)$, obtained by the developed stability code, are compared in order to show the effect of the first order correction. The computations refer to the same frequencies and spanwise wavelength as before and are shown from figure 5.6 to figure 5.10.

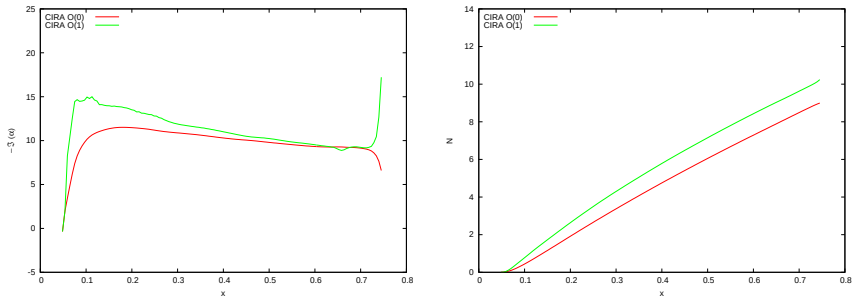

Figure 5.6: ASU test case, comparisons for $\mathcal{O}(0)$ and $\mathcal{O}(1)$ at $F = 0\ Hz$

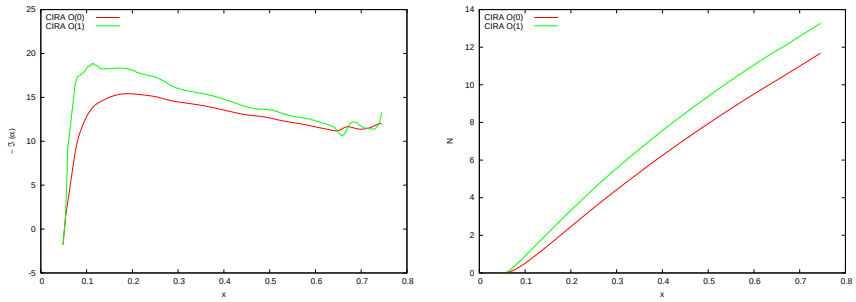

Figure 5.7: ASU test case, comparisons for $\mathcal{O}(0)$ and $\mathcal{O}(1)$ at $F = 50\ Hz$

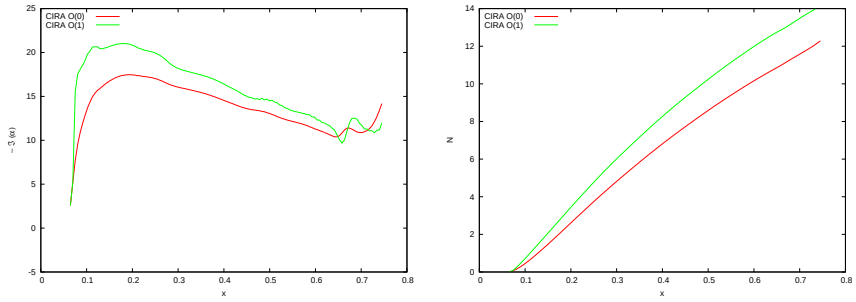

Figure 5.8: ASU test case, comparisons for $\mathcal{O}(0)$ and $\mathcal{O}(1)$ at $F = 100\ Hz$

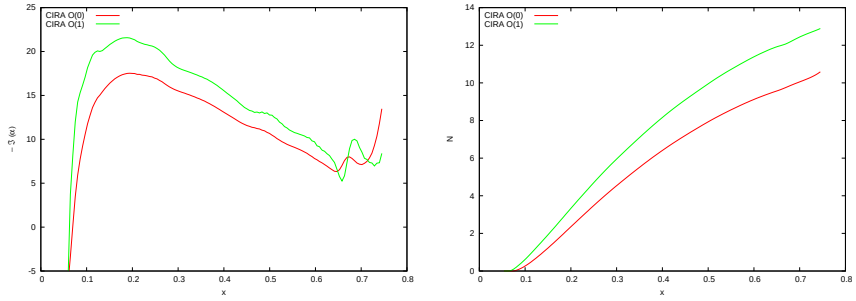

Figure 5.9: ASU test case, comparisons for $\mathcal{O}(0)$ and $\mathcal{O}(1)$ at $F = 150\ Hz$

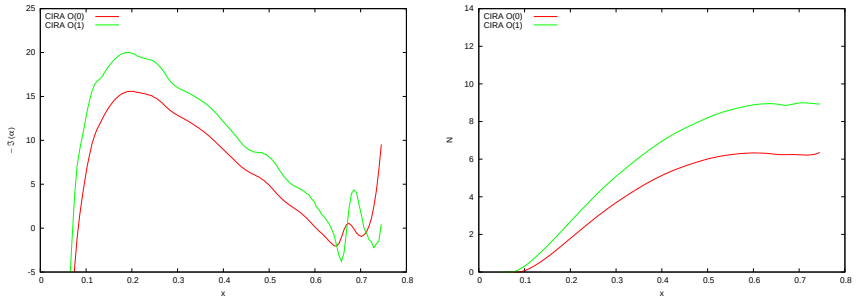

Figure 5.10: ASU test case, comparisons for $\mathcal{O}(0)$ and $\mathcal{O}(1)$ at $F = 200\ Hz$

5.2 Falkner-Skan-Cooke Test Case

For the receptivity analysis, a boundary-layer flow over a swept flat plate is considered. The mean flow is obtained by solving the Navier-Stokes equations with Falkner-Skan-Cooke (FSC) velocity profiles [62, 63] as the initial condition. This configuration often serves as a prototype for swept-wing boundary-layer flow, including many of its characteristics such as chordwise pressure gradient, streamline curvature and crossflow, while leading edge and surface curvature are not taken into account. The flow configuration corresponds to the direct numerical simulations performed by Schrader et al. [64] of a FSC boundary layer with a Hartree parameter of $\beta_H = 0.333$. All the quantities are non-dimensionalized with reference to δ^* and U_e at $x = 167$.

The stability analysis is relative to the stationary mode ($F = 0\ Hz$) and a spanwise wavelength $\beta = 0.19\ 1/m$. In figure 5.11 the growth rate and N curve are compared with the available data, while in figure 5.12 the results at $\mathcal{O}(0)$ and $\mathcal{O}(1)$ are compared.

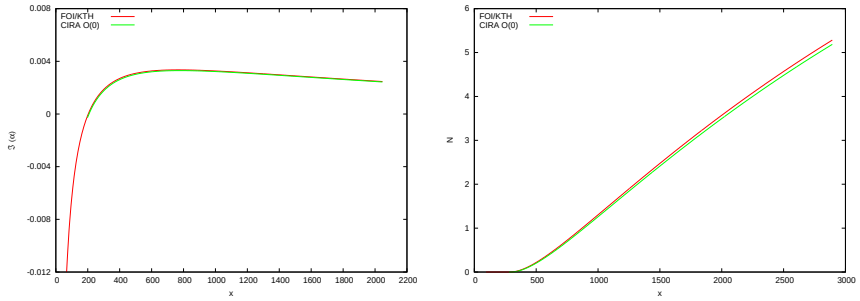

Figure 5.11: Falkner-Skan-Cooke test case, comparisons with FOI data

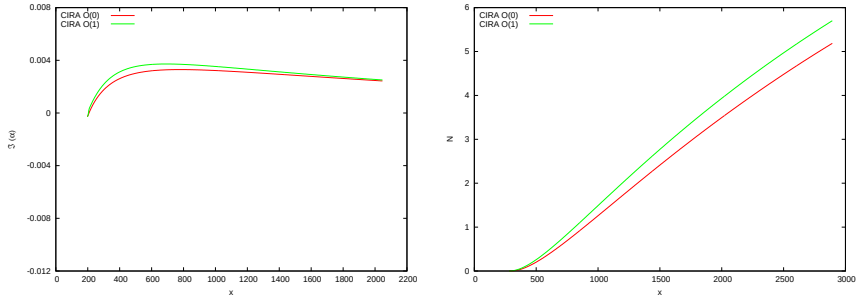

Figure 5.12: Falkner-Skan-Cooke test case, comparisons for $\mathcal{O}(0)$ and $\mathcal{O}(1)$

5.3 Receptivity analysis

The receptivity function is computed for the Falkner-Skan-Cooke boundary layer. The function is computed with reference to the roughness element at different chordwise locations. The considered element is a bump whose shape is described by the following equation:

$$h_x(x) = \left[S\left(\frac{x - h_{start}}{h_{rise}}\right) - S\left(\frac{x - h_{end}}{h_{fall}} + 1\right)\right]$$

$$S(\xi) = \begin{cases} 0 & \xi \leq 0 \\ 1/(1 + e^{1/(\xi-1)+1/\xi}) & 0 < \xi < 1 \\ 1 & \xi \geq 1 \end{cases}$$

In figure 5.13 the shape of the bump is shown.

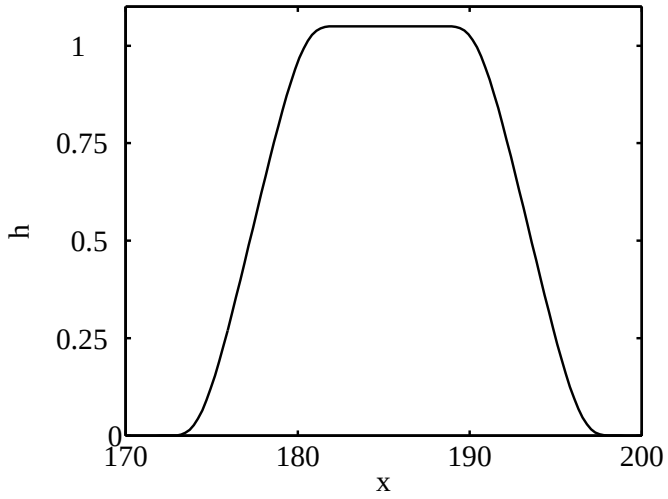

Figure 5.13: Shape of the bump

The values h_{start}, h_{rise}, h_{end} and h_{fall} are constant for a given location. In order to introduce the disturbance related to the presence of the bump as a wall–disturbance to superimpose on the base flow, a Taylor series is applied:

$$\mathbf{u}(x, h(x), z) = 0 \approx \mathbf{u}(x, 0, z) + \left.\frac{\partial \mathbf{V}_b}{\partial y}\right|_{y=0} h(x)$$
$$\mathbf{u}(x, 0, z) = -\left.\frac{\partial \mathbf{V}_b}{\partial y}\right|_{y=0} h(x) \tag{5.1}$$

By using the expansion, it is not necessary to modify the geometry of the test case, but the disturbance enters in the flow as a velocity.

Computations were performed placing the bump in different locations, in order to observe the effect on the base flow. In figure 5.14, the bump (solid line) and the equivalent disturbance (dashed line) are shown for the chordwise position $x_r = 305$. Note that the bump height is scaled by a factor 0.018. In figure 5.15 three bumps are shown at different chordwise stations, in particular at $x_r = 305$, $x_r = 628$ and $x_r = 962$ in order to compare the relative perturbations on the base flow.

As it can be seen, even though the shape is the same, the disturbance is different as it depends on the value at the wall of the y-derivative of the base flow velocity, eq. 5.1.

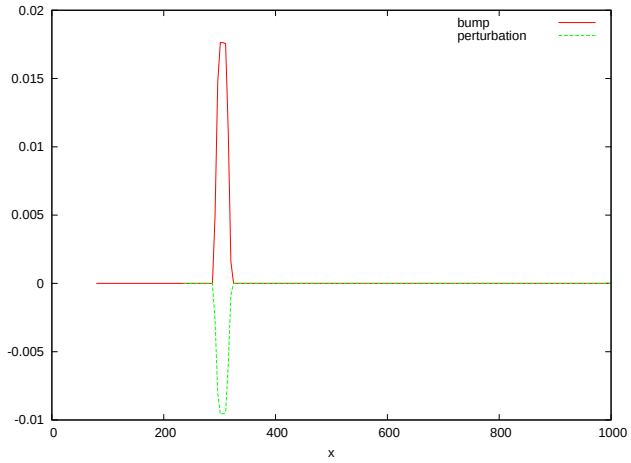

Figure 5.14: Bump shape and relative disturbance at $x_r = 305$

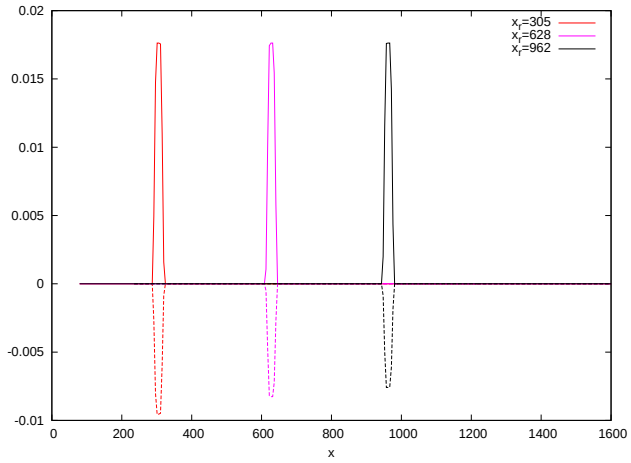

Figure 5.15: Comparison of the disturbances at $x_r = 305$, $x_r = 628$ and $x_r = 962$

Recalling eq. 4.54, the constant $a_3(x)$, whose expression is reported below, is computed and shown in figure 5.16.

$$a_3(x) = \frac{1}{a_1(x)} e^{-\int_x^{x_f} a(x')\,dx'}$$

As it depends only on the stability analysis and not on the disturbance element, it is unique for the test case considered once fixed frequency F and spanwise wavenumber β.

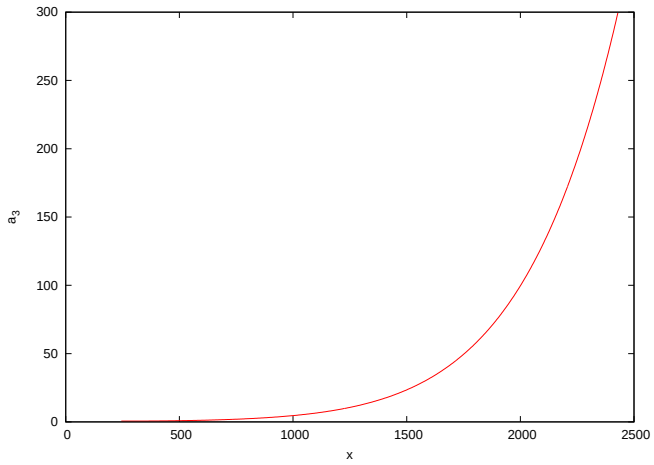

Figure 5.16: Coefficient a_3 for receptivity vector

Once the coefficient a_3 is computed, and consequently the receptivity vector $\mathbf{r}$ (eq. 4.53) , the computation of

$$c = \int_{x_0}^{x_f} \mathbf{r}(x) \cdot \mathbf{y}(x) dx$$

is straightforward. From figure 5.17 to 5.25, the value of the receptivity constant c (solid line) is shown as function of the chordwise coordinate for different roughness positions. In the same figures, the disturbance is superimposed (dashed line). The first roughness location is $x_r = 305$ while the first neutral point is $x = 297$.

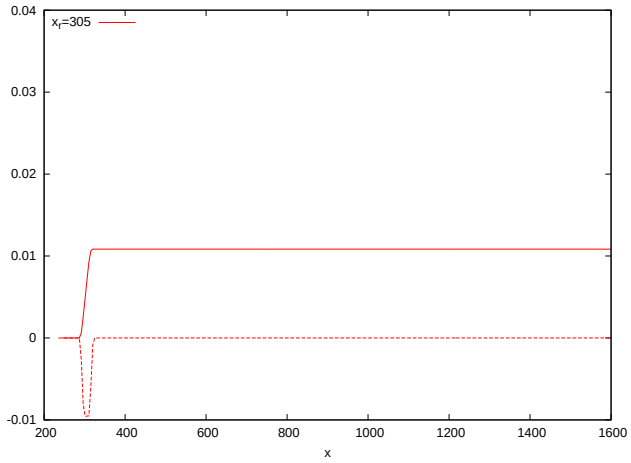

Figure 5.17: Receptivity coefficient for roughness at $x_r = 305$

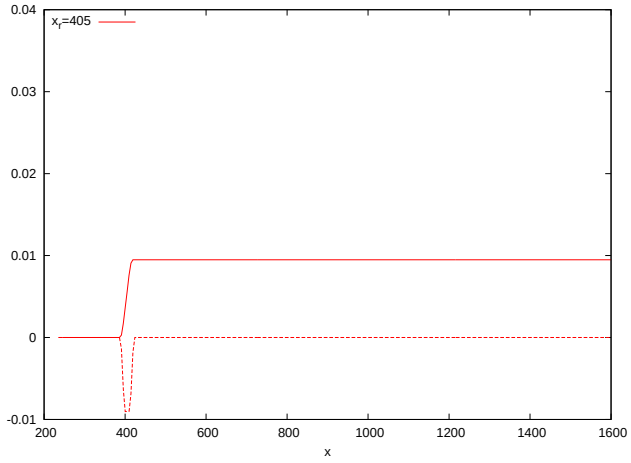

Figure 5.18: Receptivity coefficient for roughness at $x_r = 405$

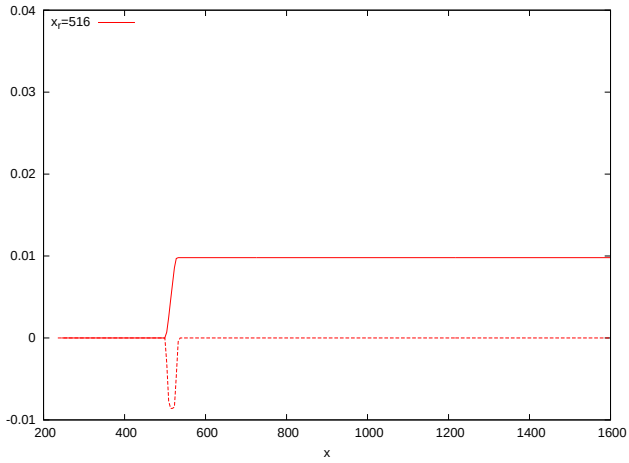

Figure 5.19: Receptivity coefficient for roughness at $x_r = 516$

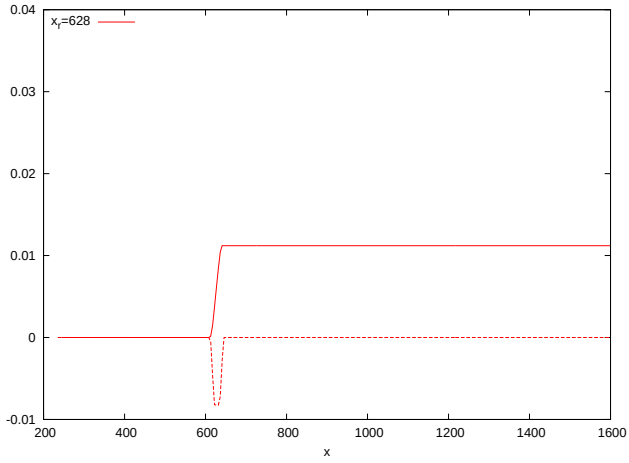

Figure 5.20: Receptivity coefficient for roughness at $x_r = 628$

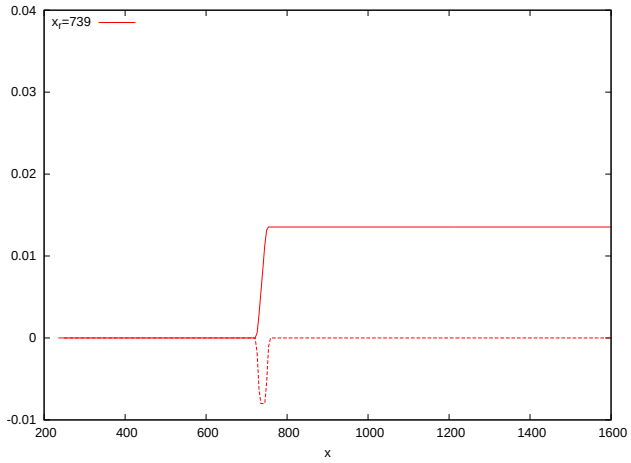

Figure 5.21: Receptivity coefficient for roughness at $x_r = 739$

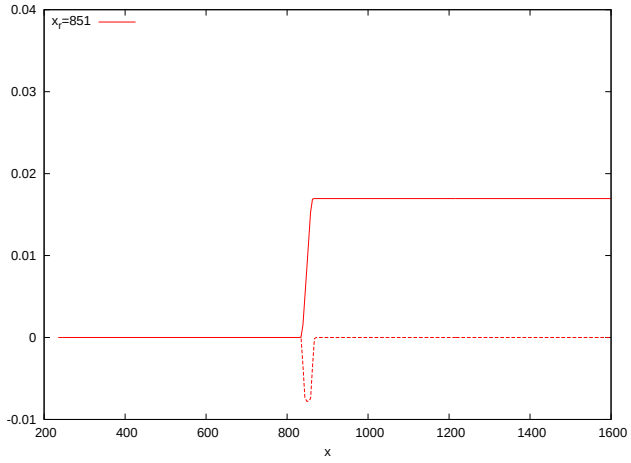

Figure 5.22: Receptivity coefficient for roughness at $x_r = 851$

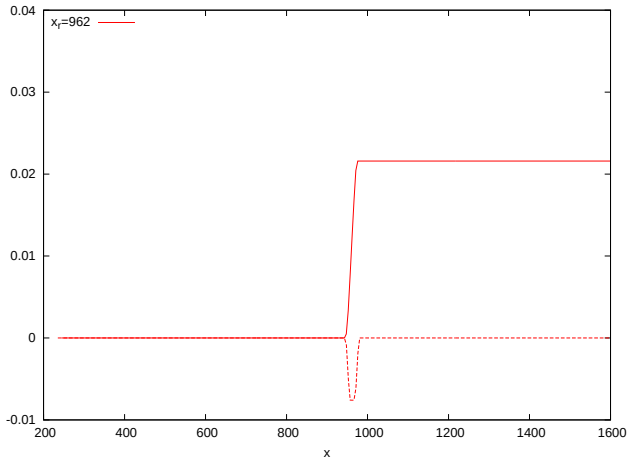

Figure 5.23: Receptivity coefficient for roughness at $x_r = 962$

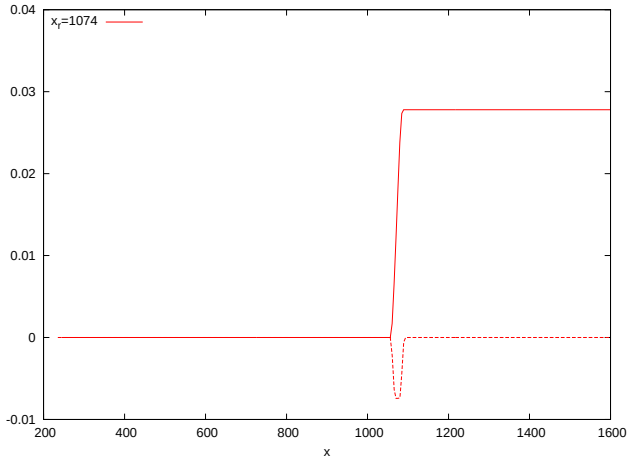

Figure 5.24: Receptivity coefficient for roughness at $x_r = 1074$

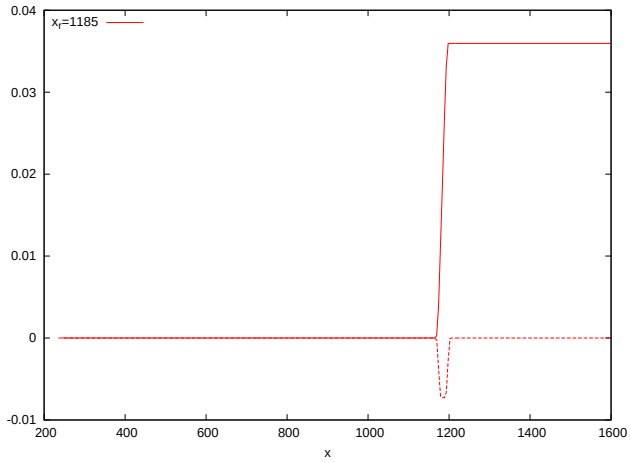

Figure 5.25: Receptivity coefficient for roughness at $x_r = 1185$

In figure 5.26 the value of c is shown as function of the roughness location x_r. It is worth noting that the receptivity coefficient c presents a minimum,

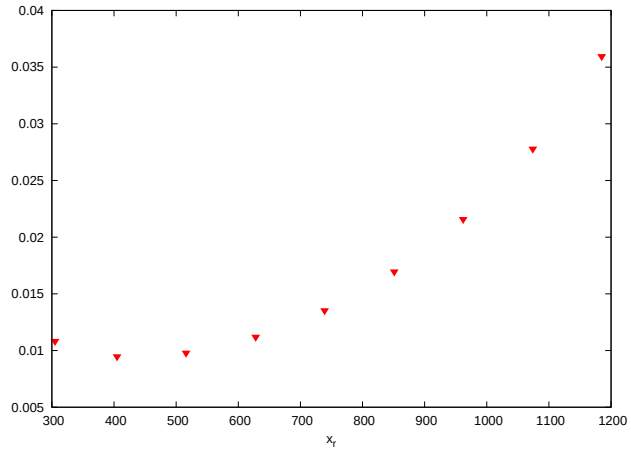

Figure 5.26: Receptivity coefficient at different chordwise locations

for this simulation at $x_r = 405$, which corresponds to the second station analyzed. Two main conclusions can be achieved. The first is that the same bump introduces a different disturbance in function of the applied location. The second is that the function is not monotonic and the minimum does not

necessarily coincide with the roughness location nearest to the first neutral point.

Chapter 6

Receptivity to free-stream disturbances

The aim of this chapter is the formulation of a theory for the prediction of boundary-layer receptivity arising from the interaction of free-stream disturbances with local or distributed surface inhomogeneities. The attention will be focused on the generation of TS waves by the interaction of surface roughness with an acoustic- or vortical-wave induced perturbation. The aim is to express the amplitude of the resulting TS wave downstream of the interaction zone in the simple form:

$$|A(x_f)| = \left| \int_{x_0}^{x_f} r(x)\, y(x)\, dx \right| \tag{6.1}$$

Recalling eq. 4.52, the generic function $y(x)$ represents a known forcing term and the function $r(x)$ is the receptivity of $A(x_f)$ with respect to $y(x)$. Within this formulation it is clear that the receptivity function $r(x)$ represents the sensitivity of the solution to the specific forcing term and plays the role of a Green's function.

As an example, consider the interaction of an acoustic wave with a surface bump of shape $y = \delta h(x)$, where δ is the typical length-scale of the bump and $h(x)$ is a shape function of $\mathcal{O}(1)$. In this case the function $r(x)$ will depend on the characteristics of the impinging disturbance and linearly on its amplitude ϵ if weak enough. Thus $r(x) = \epsilon r_h(x)$ and the resulting TS amplitude can be expressed as

$$A(x_f) = \left| \epsilon\delta \int_{x_0}^{x_f} r_h(x) h(x) dx \right| . \tag{6.2}$$

6.1 Problem formulation and governing equations

We will focus our attention on an incompressible two-dimensional boundary layer over a flat plate. The set of equations can be written in a compact form through the notation

$$\mathbf{L}\left[\mathbf{q}\right] + \mathbf{N}\left[\mathbf{q},\mathbf{q}\right] = \mathbf{0}\,, \tag{6.3}$$

where

$$\mathbf{L} = \begin{bmatrix} \dfrac{\partial}{\partial x} & \dfrac{\partial}{\partial y} & 0 \\ \dfrac{\partial}{\partial t} - \dfrac{1}{Re}\left(\dfrac{\partial^2}{\partial x^2} + \dfrac{\partial^2}{\partial y^2}\right) & 0 & \dfrac{\partial}{\partial x} \\ 0 & \dfrac{\partial}{\partial t} - \dfrac{1}{Re}\left(\dfrac{\partial^2}{\partial x^2} + \dfrac{\partial^2}{\partial y^2}\right) & \dfrac{\partial}{\partial y} \end{bmatrix} \tag{6.4}$$

$$\mathbf{N}\left[\mathbf{q}_1,\mathbf{q}_2\right] = \begin{bmatrix} 0 \\ \dfrac{\partial U_1 U_2}{\partial x} + \dfrac{1}{2}\dfrac{\partial U_1 V_2 + U_2 V_1}{\partial y} \\ \dfrac{\partial V_1 V_2}{\partial y} + \dfrac{1}{2}\dfrac{\partial U_1 V_2 + U_2 V_1}{\partial x} \end{bmatrix} \tag{6.5}$$

and $\mathbf{q}(x,y,t) = [u(x,y,t), v(x,y,t), p(x,y,t)]$ with boundary conditions at wall

$$\begin{cases} \hat{U} = 0 \\ \hat{V} = \epsilon \hat{v}_{wall}(x,y,t) \end{cases} \quad \text{at} \quad y = \delta h(x) \tag{6.6}$$

and in the free-stream

$$\begin{cases} \hat{U} \to 1 + \epsilon \hat{u}_\infty(x,y,t) \\ \hat{V} = \epsilon \hat{v}_\infty(x,y,t) \\ \hat{P} = 1 + \epsilon \hat{p}_\infty(x,y,t) \end{cases} \quad \text{as } y \to \infty \tag{6.7}$$

In the previous conditions, an unsteady perturbation, with a typical velocity scale $u_\infty << U_\infty$ and frequency ω_ϵ, is superimposed on the mean flow. The receptivity mechanism is assumed to occur for the presence of surface roughness distribution of shape $y^* = \ell^* h(x)$, where ℓ^* is a typical length-scale of the roughness height, much shorter than the boundary layer thickness δ^*

In eqs. 6.6 and 6.7, $\hat{u}_\infty(x,y,t)$, $\hat{v}_\infty(x,y,t)$ and $\hat{p}_\infty(x,y,t)$ are the non-dimensional far-field velocities and pressure of the unsteady perturbation, while $\hat{v}_{wall}(x,y,t)$ is a possible unsteady suction velocity, $\delta = \ell^*/\delta^*_{x_r} << 1$ and $\epsilon = u_\infty/U_\infty << 1$. The function $h(x)$ is considered to be $\mathcal{O}(1)$ with respect to δ and the functions $\hat{u}_\infty(x,y,t)$, $\hat{v}_\infty(x,y,t)$ and $\hat{v}_{wall}(x,y,t)$ are both assumed to be $\mathcal{O}(1)$ with respect to ϵ.

Since we have considered both the unsteady and the roughness induced perturbation to be small, solution of NS equations with the previous boundary conditions can be found in the form of an asymptotic series in the small parameters ϵ and δ

$$\begin{aligned}\hat{\mathbf{q}}(x,y,t) &= \mathbf{Q}(x,y) + \epsilon\mathbf{q}_\epsilon(x,y)e^{i\omega_\epsilon t} + \delta\mathbf{q}_\delta(x,y) \\ &+ \epsilon^2\mathbf{q}_{\epsilon^2}(x,y)e^{i2\omega_\epsilon t} + \epsilon\delta\mathbf{q}_{\epsilon\delta}(x,y)e^{i\omega_\epsilon t} + \delta^2\mathbf{q}_{\delta^2}(x,y) + \dots\end{aligned} \tag{6.8}$$

The first term in the expansion is the steady base flow in the absence of any kind of perturbation and can be approximated by

$$\mathbf{Q}(x,y) = \mathbf{Q}_B(\varepsilon x, y) + O(\varepsilon) \qquad \text{with} \quad \varepsilon = 1/Re << 1 \tag{6.9}$$

under the assumption $Re >> 1$, where $\mathbf{Q}_B(\varepsilon x, y)$ is the Blasius profile. The second term in the expansion represents a non stationary wave of amplitude ϵ and non-dimensional frequency ω_ϵ which models an acoustic- or vortical-induced perturbation. The third term is a stationary standing wave and accounts for the mean-flow distortion induced by the steady surface roughness distribution. All the other terms in the expansion are caused by the nonlinear interaction between the base flow and the steady and unsteady disturbances. Only the $\mathcal{O}(\epsilon\delta)$ term has the correct time-spatial characteristics typical of the TS instability wave among the nonlinear interaction. Thus, only that term will be considered, neglecting all the other second order contributions. Substituting eqs. 6.8 and 6.9 in the Navier–Stokes equations and collecting coefficient of powers in ϵ and δ yields
$\mathcal{O}(\epsilon)$

$$\mathbf{L}_0\mathbf{q}_\epsilon(x,y)e^{i\omega_\epsilon t} = \mathbf{0} \tag{6.10a}$$

$$\begin{cases} u_\epsilon(x,y)e^{i\omega_\epsilon t} \to u_{\epsilon\infty}(x,y)e^{i\omega_\epsilon t} \\ v_\epsilon(x,y)e^{i\omega_\epsilon t} \to v_{\epsilon\infty}(x,y)e^{i\omega_\epsilon t} \\ p_\epsilon(x,y)e^{i\omega_\epsilon t} \to p_{\epsilon\infty}(x,y)e^{i\omega_\epsilon t} \end{cases} \qquad \text{as } y \to \infty \tag{6.10b}$$

$$\begin{cases} u_\epsilon(x,y) = 0 \\ v_\epsilon(x,y)e^{i\omega_\epsilon t} = v_{\epsilon\ wall}(x,y)e^{i\omega_\epsilon t} \end{cases} \qquad \text{at } y = 0 \qquad (x > 0) \tag{6.10c}$$

$\mathcal{O}(\delta)$

$$\mathbf{L}_0\mathbf{q}_\delta(x,y) = \mathbf{0} \tag{6.11a}$$

$$\begin{cases} u_\delta(x,y) \to 0 \\ v_\delta(x,y) \to 0 \\ p_\delta(x,y) \to 0 \end{cases} \qquad \text{as } y \to \infty \tag{6.11b}$$

$$\begin{cases} u_\delta(x,y) = -\dfrac{\partial U_B}{\partial y} h(x) \\ v_\delta(x,y) = 0 \end{cases} \qquad \text{at } y = 0 \quad (x > 0) \tag{6.11c}$$

$\mathcal{O}(\epsilon\delta)$

$$\mathbf{L}_0\mathbf{q}_{\epsilon\delta}(x,y)e^{i\omega_\epsilon t} = \mathbf{S}\left[\mathbf{q}_\delta; \mathbf{q}_\epsilon\right] e^{i\omega_\epsilon t} \tag{6.12a}$$

$$\begin{cases} u_{\epsilon\delta}(x,y)e^{i\omega_\epsilon t} \to 0 \\ v_{\epsilon\delta}(x,y)e^{i\omega_\epsilon t} \to 0 \\ p_{\epsilon\delta}(x,y)e^{i\omega_\epsilon t} \to 0 \end{cases} \qquad \text{as } y \to \infty \tag{6.12b}$$

$$\begin{cases} u_{\epsilon\delta}(x,y)e^{i\omega_\epsilon t} = -\dfrac{\partial u_\epsilon}{\partial y} h(x) e^{i\omega_\epsilon t} \\ v_{\epsilon\delta}(x,y)e^{i\omega_\epsilon t} = -\dfrac{\partial v_\epsilon}{\partial y} h(x) e^{i\omega_\epsilon t} \end{cases} \qquad \text{at } y = 0 \qquad (x > 0) \tag{6.12c}$$

where $\mathbf{S}[\mathbf{q_1}, \mathbf{q_2}] \equiv -2\mathbf{N}[\mathbf{q_1}, \mathbf{q_2}]$ and $\mathbf{L}_0$ is defined as $\mathbf{L}_0\mathbf{q} \equiv \mathbf{L}(\mathbf{q}) + 2\mathbf{N}(\mathbf{Q}, \mathbf{q})$. Since it is assumed that $\delta << 1$, the boundary conditions at $y = \delta\, h(x)$ are moved to $y = 0$, by making use of a Taylor series expansion about $\mathbf{q}(x, 0, t)$:

$$\mathbf{q}(x, \delta\, h(x)) = \mathbf{q}(x, 0) + \frac{\partial \mathbf{q}}{\partial y}(x, 0)\delta\, h(x) + \mathcal{O}(\delta^2) \tag{6.13}$$

The linearization is valid only if the typical height of the surface roughness is much smaller than the typical lengthscale over which the surface shape changes in the streamwise direction.

For sake of simplicity the multiple scale approach is not demonstrated here, but follows the development in [65]. The formula for the amplitude of the TS wave at any station $x > x_2$, where x_2 represents the end of the roughness element, is

$$A = \int_{x_1}^{x_2} \frac{a_3(x)}{a_1(\varepsilon x)}\, e^{\,i \int_{x_0}^{x} \kappa_{\epsilon\delta}(\varepsilon x')\, dx'} \, dx + \mathcal{O}(\varepsilon) \tag{6.14}$$

where $\kappa_{\epsilon\delta}(X)$ is given by

$$\kappa_{\epsilon\delta}(X) = \alpha_{\epsilon\delta}(X) - i\varepsilon\frac{a_2(X)}{a_1(X)} \tag{6.15}$$

and a_1, a_2 and a_3 are defined respectively as

$$a_1(X) = \int_0^\infty \mathbf{v}_{\epsilon\delta}(X,y)\cdot\left[\mathbf{H}\,\frac{d\mathbf{u}_{\epsilon\delta,0}(X,y)}{dX} + \mathbf{C}\,\mathbf{u}_{\epsilon\delta,0}(X,y)\right]dy \tag{6.16a}$$

$$a_2(X) = \int_0^\infty \mathbf{v}_{\epsilon\delta}(X,y)\cdot\left[\mathbf{H}\,\mathbf{u}_{\epsilon\delta,0}(X,y)\right]dy \tag{6.16b}$$

$$a_3(x) = \int_0^\infty \mathbf{v}_{\epsilon\delta}(X,y)\cdot\mathbf{S}(x,y)\,dy \;+\; \mathbf{u}_{\epsilon\delta}(x,0)\cdot\tilde{\mathscr{S}}(X) \tag{6.16c}$$

where $\mathbf{H}$ and $\mathbf{C}$ are the operators defined in §4 and A is the amplitude of the excited wave. Note that while a_1 and a_2 are functions of X, a_3 is not slowly varying but depends on the fast variable x. Furthermore a_3 contains two different terms: the first one derives from the forcing of equation 6.12a, while the second accounts for the forcing in the wall boundary conditions 6.12c. The vector $\tilde{\mathscr{S}}(X)$, which is usually referred to as adjoint stress, is explicitly found to be

$$\tilde{\mathscr{S}}(X) = \begin{bmatrix} 0 \\ \dfrac{1}{Re}\,\dfrac{\partial u^\dagger_{\epsilon\delta}}{\partial y}\Big|_{y=0} \\ p^\dagger_{\epsilon\delta}(X,0) \end{bmatrix} \tag{6.17}$$

The forcing term $\mathbf{S}(x,y)$ in its explicit form is given by

$$\mathbf{S}(x,y) \equiv -2\mathbf{N}(\mathbf{q}_\epsilon,\mathbf{q}_\delta) = -\begin{bmatrix} 0 \\ \dfrac{\partial u_\epsilon}{\partial x}u_\delta + u_\epsilon\dfrac{\partial u_\delta}{\partial x} + v_\epsilon\dfrac{\partial u_\delta}{\partial y} + v_\delta\dfrac{\partial u_\epsilon}{\partial y} \\ \dfrac{\partial v_\epsilon}{\partial x}u_\delta + u_\epsilon\dfrac{\partial v_\delta}{\partial x} + v_\epsilon\dfrac{\partial v_\delta}{\partial y} + v_\delta\dfrac{\partial v_\epsilon}{\partial y} \end{bmatrix} \tag{6.18}$$

The dependence of the integrand in eq. 6.14 on the arbitrary initial position X_0 can be eliminated by introducing the position $X_N = \varepsilon x_N$ of the

neutral point, i.e. the position where the function

$$\kappa_{\epsilon\delta}(X) = \alpha_{\epsilon\delta}(X) - i\varepsilon\frac{a_2(X)}{a_1(X)} \tag{6.19}$$

crosses the imaginary axis, i.e. where $\Im(\kappa(X_N)) = 0$. The solution of the receptivity problem can be re-written as

$$\mathbf{q}_{\varepsilon\delta}(X,y) = A_T\ \mathbf{u}_{\epsilon\delta\ ,0}(X,y)\ \mathrm{e}^{-\frac{i}{\varepsilon}\int_{X_N}^{X}\kappa_{\epsilon\delta}(X)dX'} + \mathcal{O}(\varepsilon) \tag{6.20}$$

where we have re-defined the total amplitude A_T as

$$A_T = \int_{x_1}^{x_2}\frac{a_{\,3}(x)}{a_1(\varepsilon x)}\mathrm{e}^{i\int_{x_N}^{x}\kappa_{\epsilon\delta}(\varepsilon x')dx'}dx \tag{6.21}$$

This solution can now be used to evaluate the effects of the streamwise growth of the boundary layer for different kinds of external disturbances. In order to obtain quantitative results we must now evaluate the coefficient a_1, a_2 and a_3 which depends on the solution of the $\mathcal{O}(\epsilon)$ and $\mathcal{O}(\delta)$ problem.

6.2 The unsteady perturbation

We consider unsteady perturbations which can be locally approximated in the far field by planar waves:

$$\mathbf{q}_\epsilon \sim \mathbf{u}_\epsilon(\varepsilon x, y, \varepsilon)e^{-i\phi_\epsilon(X)/\varepsilon}\ = \mathbf{u}_\epsilon(\varepsilon x, y, \varepsilon)e^{-i\int\alpha_\epsilon\,dx} \tag{6.22}$$

where $\phi_\epsilon(X)$ is a known function. A local solution of eq. 6.10 can be found by imposing the multiple scale expansion

$$\mathbf{q}_\epsilon(X,y) = e^{-i\phi_\epsilon(X)/\varepsilon}\mathbf{u}_\epsilon\ (X,y,\varepsilon)\ = e^{-i\phi_\epsilon(X)/\varepsilon}\sum_n \mathbf{u}_{\epsilon\ ,n}(X,y)\,\varepsilon^n \tag{6.23}$$

which substituted in eq. 6.10 gives rise to a series of problems for the determination of the leading order solution and its corrections:

$\mathcal{O}(\varepsilon^0)$

$$\mathbf{A}(\alpha_\epsilon, \omega_\epsilon, Re)\,\mathbf{u}_{\epsilon,0}(X,y) = \mathbf{0} \tag{6.24a}$$

$$\begin{cases} u_{\epsilon,0}(X,y) \to u_{\epsilon,0\,\infty}(X,y) \\ v_{\epsilon,0}(X,y) \to v_{\epsilon,0\,\infty}(X,y) \\ p_{\epsilon,0}(X,y) \to p_{\epsilon,0\,\infty}(X,y) \end{cases} \quad \text{as} \quad y \to \infty \tag{6.24b}$$

$$\begin{cases} u_{\epsilon,0}(X,y) = 0 \\ v_{\epsilon,0}(X,y) = v_{\epsilon,0\,wall}(X,y) \end{cases} \quad \text{at } y = 0 \tag{6.24c}$$

$\mathcal{O}(\varepsilon^1)$

$$\mathbf{A}(\alpha_\epsilon, \omega_\epsilon, Re)\mathbf{u}_{\epsilon,1}(X,y) = -\mathbf{H}(\alpha_\epsilon, Re)\frac{d\mathbf{u}_{\epsilon,0}}{dX} - \mathbf{C}(\alpha_\epsilon, Re)\mathbf{u}_{\epsilon,0} \tag{6.25a}$$

$$\begin{cases} u_{\epsilon,1}(X,y) \to 0 \\ v_{\epsilon,1}(X,y) \to 0 \\ p_{\epsilon,1}(X,y) \to 0 \end{cases} \quad \text{as} \quad y \to \infty \tag{6.25b}$$

$$\begin{cases} u_{\epsilon,1}(X,y) = 0 \\ v_{\epsilon,1}(X,y) = 0 \end{cases} \quad \text{at } y = 0 \tag{6.25c}$$

where

$$\alpha_\epsilon = \frac{d\phi_\epsilon}{dX} \tag{6.26}$$

is the wave-number of the unsteady perturbation and $\mathbf{A}, \mathbf{H}, \mathbf{C}$ are the operators defined in §4. We now specify two different kinds of perturbations which will be used to evaluate the amplitude of the TS wave generated by their interaction with the surface roughness.

6.2.1 Sound wave

Here we consider the response of the boundary layer to a time harmonic pulsation of frequency ω_ε such that $\alpha_\varepsilon = 0$, $u_{\epsilon\infty}(x,y) = 1$, $v_{\epsilon\infty}(x,y) = 0$ and $v_{\epsilon\,wall}(x,y) = 0$ in eq. 6.24. In the low Mach number limit this represents an acoustic wave propagating parallel to the plate direction. No diffraction effects are originated at the leading edge of the plate and the multiple scale expansion results in this particular case are uniformly valid in the y direction. At order ε, we get the following equations describing the acoustic signature inside the boundary layer:

$$\frac{\partial v_{\epsilon,0}}{\partial y} = 0 \tag{6.27a}$$

$$i\omega_\epsilon u_{\epsilon,0} - \frac{1}{Re}\frac{\partial^2 u_{\epsilon,0}}{\partial y^2} + \frac{\partial U_B}{\partial y} v_{\epsilon,0} = 0 \tag{6.27b}$$

$$i\omega_\epsilon v_{\epsilon,0} - \frac{1}{Re}\frac{\partial^2 v_{\epsilon,0}}{\partial y^2} + \frac{\partial p_{\epsilon,0}}{\partial y} = 0 \tag{6.27c}$$

with boundary conditions

$$\begin{aligned} &u_{\epsilon,0} \to 1 \quad \text{for } y \to \infty \\ &p_{\epsilon,0} \to 0 \quad \text{for } y \to \infty \\ &u_{\epsilon,0} = 0 \quad \text{at } y = 0 \\ &v_{\epsilon,0} = 0 \quad \text{at } y = 0\,. \end{aligned} \tag{6.28}$$

The problem is easily solved and the solution corresponds to the well-known Stokes shear wave

$$\begin{aligned} u_{\epsilon,0} &= 1 - \mathrm{e}^{-\sqrt{i\omega_\epsilon Re}\, y} \\ v_{\epsilon,0} &= 0 \\ p_{\epsilon,0} &= 0 \end{aligned} \tag{6.29}$$

Figure 6.1 shows the modulus and the argument of the solution (6.29) at the neutral location for an impinging perturbation of frequency $F = 38 \times 10^{-6}$.

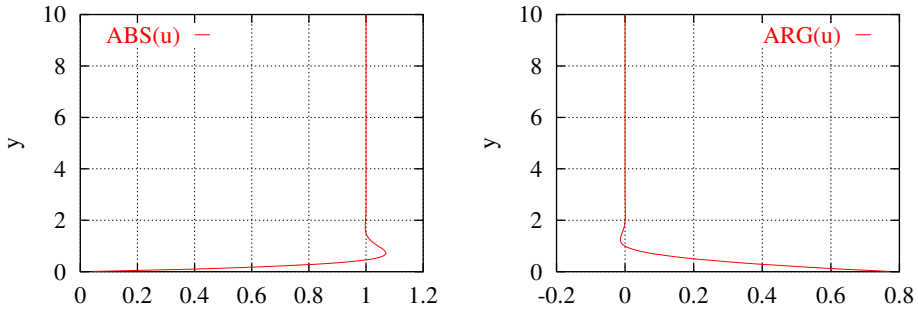

Figure 6.1: Stokes wave at the neutral position for $F = 38\ 10^{-6}$

Using the multiple scale approach we can also include non-parallel correction terms from the next-order equation. At $\mathcal{O}(\varepsilon^1)$, in fact, we have

$$\frac{\partial v_{\epsilon,1}}{\partial y} = 0 \tag{6.30a}$$

$$i\omega_\epsilon u_{\epsilon,1} - \frac{1}{Re}\frac{\partial^2 u_{\epsilon,1}}{\partial y^2} = -u_{\epsilon,0}\frac{\partial U_B}{\partial X} - V_B\frac{\partial u_{\epsilon,0}}{\partial y} \tag{6.30b}$$

$$i\omega_\epsilon v_{\epsilon,1} - \frac{1}{Re}\frac{\partial^2 v_{\epsilon,1}}{\partial y^2} + \frac{\partial p_{\epsilon,1}}{\partial y} = 0 \tag{6.30c}$$

with boundary conditions

$$\begin{aligned} &u_{\epsilon,1} \to 0 \text{ for } y \to \infty \\ &p_{\epsilon,1} \to 0 \text{ for } y \to \infty \\ &u_{\epsilon,1} = 0 \text{ at } y = 0 \\ &v_{\epsilon,1} = 0 \text{ at } y = 0 \end{aligned} \tag{6.31}$$

where U_B, V_B are the velocity components of the Blasius solution. The leading order solution appears as a forcing term in the right hand side of the equations. In the present case, for typical values of the Reynolds number Re and frequency parameter F used for the receptivity calculations, $|u_{\epsilon,1}|_{\max} \simeq 0.01\ |u_{\epsilon,0}|$. Thus non-parallel corrections are quite small and can be effectively neglected.

6.2.2 Vortical wave

For a vortical wave the gust is convected by the free-stream and therefore $\alpha_\epsilon \sim \omega_\epsilon$. Assuming the perturbation to be bounded at ∞, i.e.

$$\frac{\partial \psi}{\partial y} = u(y) \sim e^{-i\gamma_\epsilon y} \text{ as } y \to \infty \tag{6.32}$$

where γ is real and positive, we get the dispersion relation

$$\alpha_\varepsilon^2 + iRe_\delta\,(\omega_\varepsilon - \alpha_\varepsilon) = -\gamma_\epsilon^2\ , \tag{6.33}$$

which relates the vertical and the streamwise wave number of the perturbation. If $\gamma_\epsilon = 0$ and the vortical signature is attenuated in the streamwise direction, the value of α_ϵ to be used in the Orr-Sommerfeld operator is given by

$$\alpha_\epsilon = \frac{iRe - i\sqrt{Re^2 + 4i\omega_\epsilon Re}}{2}\ . \tag{6.34}$$

The boundary conditions become

$$\begin{cases} u_{\epsilon,0}(X,y) \to -\alpha_\epsilon Z_1 e^{-\alpha_\epsilon y} + Z_4 \\ v_{\epsilon,0}(X,y) \to -i\alpha_\epsilon \left(Z_1 e^{-\alpha_\epsilon y} + Z_3 + Z_4 y\right) \quad \text{as } y \to \infty \\ p_{\epsilon,0} = 0 \end{cases} \tag{6.35a}$$

$$\begin{cases} u_{\epsilon,0}(X,y) = 0 \\ v_{\epsilon,0}(X,y) = 0 \end{cases} \qquad \text{at } y = 0 \tag{6.35b}$$

where Z_1 and Z_3 are constant to be determined and Z_4 is fixed and assumed here to be 1. Figure 6.2 shows the modulus and the argument of the solution at the neutral location for the frequency $F = 38 \times 10^{-6}$. Numerical tests on the second-order problem 6.25 have confirmed that for typical values of the frequency parameter and Reynolds number non-parallel corrections are quite small for the Blasius boundary layer and can be therefore effectively neglected in the present context.

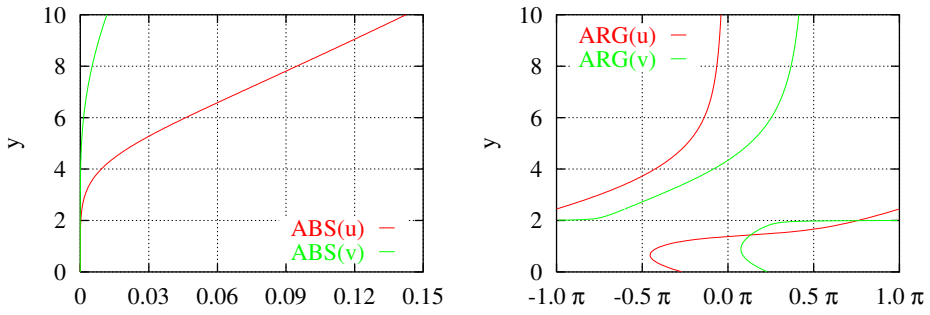

Figure 6.2: Vortical wave components at the neutral position for $F = 38\ 10^{-6}$

6.3 The steady perturbation

The equations describing the steady perturbation to the base flow induced by the surface roughness are given by 6.11. The formula for the final amplitude can be rewritten as

$$A_T = \int_{x_1}^{x_2} \frac{< \mathbf{v}_{\epsilon\delta} \, , \, \mathbf{S}(\mathbf{q}_\epsilon, \mathbf{q}_\delta) > + \mathbf{u}_{\epsilon\delta}(x,0) \cdot \tilde{\mathscr{S}}(X)}{< \mathbf{v}_{\epsilon\delta} \ , \ \mathbf{H}\mathbf{q}_{\epsilon\delta,0} >} \, e^{\, i \int_{x_N}^{x} \kappa_{\epsilon\delta}(\varepsilon x') dx'} \, dX \tag{6.36}$$

where the unsteady perturbation is assumed to have the local wave form

$$\mathbf{q}_\epsilon = \mathbf{u}_{\varepsilon,0}(\varepsilon x, y) e^{-\frac{i}{\varepsilon}\int_{X_N}^{X} \alpha_\epsilon dX} \tag{6.37}$$

and where, using the boundary conditions in 6.12c, we can replace $\mathbf{u}_{\epsilon\delta}(x,0)$ with $-\left.\frac{d\mathbf{q}_\epsilon}{dy}\right|_{y=0} h(x)$. The leading-order approximation is obtained by considering only the Fourier component of $\mathbf{q}_\delta$ which satisfies the resonance condition

$$\alpha_\delta = \kappa - \alpha_\varepsilon \tag{6.38}$$

Since the base flow is slowly evolving, the Green's function for the $\mathcal{O}(\delta)$ problem is a slowly-varying function of the streamwise coordinate x, and consequently we can write locally the broad-band response of the boundary layer as

$$\begin{aligned} \mathbf{q}_\delta(x,y) &= \iint \mathbf{u}_\delta\,(X,y,\varepsilon,\alpha_\delta) e^{i\alpha_\delta(x-x_0)} h(x_0) dx_0\, d\alpha_\delta \\ &= \sum_n \varepsilon^n \iint \mathbf{u}_{\delta,n}(X,y,\alpha)\, e^{i\alpha_\delta(x-x_0)} h(x_0) d\alpha_\delta dx_0 \end{aligned} \tag{6.39}$$

where $\mathbf{u}_\delta\,(X,y,\varepsilon,\alpha)$ represents the local Fourier transform of the solution. So, considering only the resonating term, eq. 6.39 is approximated as:

$$\begin{aligned} \mathbf{q}_\delta(x,y) &\sim \sum_n \varepsilon^n \mathbf{u}_{\delta,n}(X,y,\alpha_\delta) \iint e^{i\alpha_\delta(x-x_0)} h(x_0)\, d\alpha_\delta\, dx_0 \\ &= \mathbf{u}_{\delta,0}(X,y,\alpha_\delta) \int \delta(x-x_0) h(x_0) dx_0 + \mathcal{O}(\varepsilon) \\ &= \mathbf{u}_{\delta,0}(X,y,\alpha_\delta)\, h(x) \end{aligned} \tag{6.40}$$

where $\mathbf{u}_{\delta,0}(X,y,\alpha_\delta)$ is now a solution of

$$\mathbf{A}(\alpha_\delta, 0, Re)\, \mathbf{u}_{\delta,0} = \mathbf{0} \tag{6.41}$$

with wall boundary conditions given by

$$\begin{cases} u_{\delta,0} = -\dfrac{\partial U_B}{\partial y} \\ v_{\delta,0} = 0 \end{cases} \qquad \text{at} \quad y = 0 \tag{6.42}$$

The free-stream conditions for eq. 6.41 must be imposed so that the solution of eq. 6.41 must decay as $y \to \infty$, to the resonant value α_δ determined by eq. 6.38. Figure 6.3 shows the typical shape of the steady boundary layer response components used to evaluate the receptivity in case of an impinging vortical wave at $F = 38 \times 10^{-6}$.

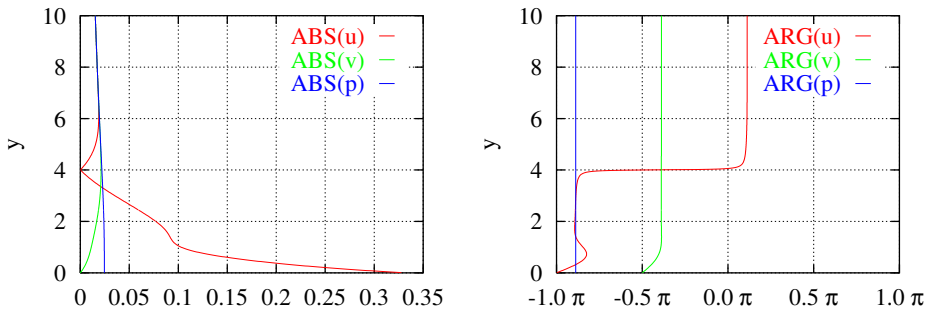

Figure 6.3: Resonant Fourier mode at the neutral point for $F = 38\ 10^{-6}$

6.4 Final TS wave amplitude

Having expressed both the solution of the $\mathcal{O}(\epsilon)$ and $\mathcal{O}(\delta)$ problems with a local wave-form approximation, the final solution for the excited TS wave becomes

$$\mathbf{q}_{\epsilon\delta}(X,y) = A_T\ \mathbf{u}_{\epsilon\delta\ ,0}(X,y)\ e^{-\frac{i}{\varepsilon}\int_{X_N}^{X}\kappa_{\epsilon\delta}(X')\,dX'} + \mathcal{O}(\varepsilon) \tag{6.43}$$

where A_T simplifies at order ε to

$$A_T \approx \int_{x_1}^{x_2} \Lambda(x)\, e^{i\int_{x_N}^{x}\alpha_\delta(\varepsilon x')\,dx'} h(x)\,dx \tag{6.44}$$

The function

$$\Lambda\,(x) = \frac{< \mathbf{v}_{\epsilon\delta}\ ,\ \bar{\mathbf{S}}(\mathbf{u}_{\epsilon,0},\mathbf{u}_{\delta,0}) > - \left.\dfrac{d\mathbf{u}_{\epsilon,0}}{dy}\right|_{y=0} \cdot \tilde{\mathscr{F}}(X)}{< \mathbf{v}_{\epsilon\delta}\ ,\ \mathbf{H}\mathbf{q}_{\epsilon\delta,0} >} \tag{6.45}$$

is a local efficiency function which returns the amplitude of a TS wave generated by a point-wise roughness element of unit strength. The vector

term $\bar{\mathbf{S}}(\mathbf{u}_{\epsilon,0}, \mathbf{u}_{\delta,0})$ is, up to the factor $h(x)$, the leading-order approximation of the forcing $\mathbf{S}$ and is explicitly given by

$$\bar{\mathbf{S}}(\mathbf{u}_{\epsilon,0}, \mathbf{u}_{\delta,0}, \alpha_\epsilon, \alpha_\delta) = -\begin{bmatrix} 0 \\ -i\alpha_\epsilon u_{\epsilon,0} u_{\delta,0} - i\alpha_\delta u_{\epsilon,0} u_{\delta,0} + v_{\epsilon,0}\dfrac{\partial u_{\delta,0}}{\partial y} + v_{\delta,0}\dfrac{\partial u_{\epsilon,0}}{\partial y} \\ -i\alpha_\epsilon v_{\epsilon,0} u_{\delta,0} - i\alpha_\delta u_{\epsilon,0} v_{\delta,0} + v_{\epsilon,0}\dfrac{\partial v_{\delta,0}}{\partial y} + v_{\delta,0}\dfrac{\partial v_{\epsilon,0}}{\partial y} \end{bmatrix} \tag{6.46}$$

Equation 6.44 is the same of 6.1 by setting

$$r_h(x) = \Lambda(x)\, e^{\frac{i}{\varepsilon}\int_{X_N}^{X} \alpha_\delta(X)dX} \tag{6.47}$$

where α_δ satisfies eq. 6.38. In cases in which the roughness is localized, rewriting eq. 6.44 in term of x_r and considering that the inhomogeneity has compact support, the coefficient becomes

$$A_T = e^{-\int_{x_r}^{x} i\alpha_\delta dx} \int_{-\infty}^{\infty} \Lambda(x)\, e^{\int_{x_r}^{x} i\alpha_\delta dx} h(x)dx \tag{6.48}$$

In particular at $x = x_r$ the first exponential reduce to 1

$$A_T = \int_{-\infty}^{\infty} \Lambda(x)\, e^{\int_{x_r}^{x} i\alpha_\delta dx} h(x)dx \tag{6.49}$$

If we now assume the flow to be locally parallel then $\alpha_\delta = \alpha_{TS} - \alpha_\epsilon$. As $\Lambda(x)$ and α_δ change only of a small quantity over the roughness element, we can assume them to be constant and equal to their value at $x = x_r$ ($\Lambda(x_r)$ and α_{δ_r}). Thus

$$A_T = \Lambda(x_r) \int_{-\infty}^{\infty} e^{i\alpha_{\delta_r} x} h(x)dx = \Lambda(x_r) H(\alpha_{\delta_r}) \,, \tag{6.50}$$

where $H(\alpha_{\delta_r})$ is the Fourier transform of the wall-shape evaluated at the resonating wavenumber α_{δ_r}.

6.5 Numerical results

We now report some numerical results obtained using the previously described theory. The mean flow profile is assumed to be the Blasius boundary layer.

Note that expression 6.44 gives the value of the coupling coefficient using an nondimensionalization based on a fixed δ_r^*. Taking as reference length the local boundary-layer thickness the coupling coefficient reads:

$$A_T \approx \int_{Re_1}^{Re_2} r_x(Re)\, h(Re)\, dRe \tag{6.51}$$

with

$$r_x(Re) = 2\Lambda_x(Re) e^{\,i \int_{Re_N}^{Re} 2\,\alpha_\delta \, dRe'} \tag{6.52}$$

and

$$\Lambda_x(Re) = \Lambda_{\delta_r}(x) \left(\frac{Re_{\delta_x}}{Re_{\delta_r}} \right)^2 \tag{6.53}$$

In the previous equations Re_1 and Re_2 stand respectively for the Reynolds numbers of the locations x_1 and x_2 which delimit the support of the roughness shape function $h(x)$.
In figure 6.4 the modulus of the efficiency function Λ_x and of the Green's function r_x relative to the interaction of the wall-roughness with the Stokes wave (6.29) for different values of the frequency parameter F are plotted.

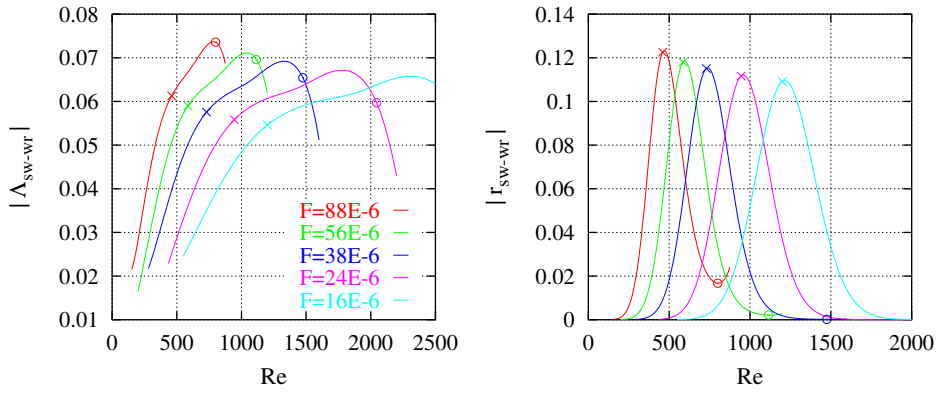

Figure 6.4: Efficiency and Green function for the acoustic wave case

Both functions are normalized on the local boundary-layer thickness δ_x^*. Crosses and circles indicate respectively the branch I and II locations. The efficiency function retains its typical shape for the whole range of frequencies investigated, shifting upward as F is decreased. The Green's function $r_x(x)$ shows a typical bell shape, which attains its maximum in a region close to branch I, decaying exponentially as we move away from that location. The magnitude and the bandwidth of the Green's function change only slowly with the frequency, the first one increasing and the second one decreasing as F is lowered. Comparing these results with those relative to the vorticity-roughness interaction, shown in figure 6.5, we immediately realize that acoustic perturbations are much more efficient TS wave generators than vortical gusts: the modulus of the Green's function, in fact, is now almost two orders of magnitude smaller than in the previous case.

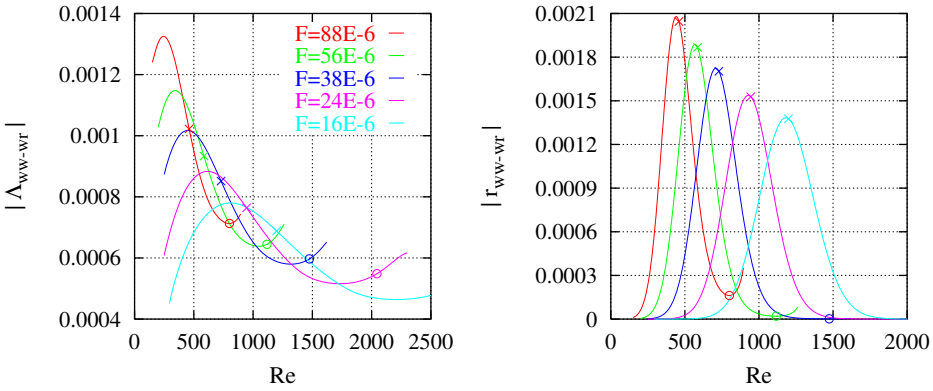

Figure 6.5: Efficiency and Green function for the vortical wave case

In figure 6.6 we plot the N factor

$$N = \int_{x_N}^{x} \alpha^{(i)} + \varepsilon \Delta\alpha^{(i)} dx = \int_{x_N}^{x} \kappa^{(i)} dx \tag{6.54}$$

based on the non-parallel growth rate $\kappa^{(i)}$ for different values of the frequency parameter F.

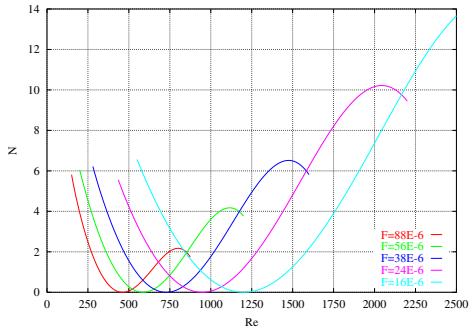

Figure 6.6: N factor for different values of F

In figure 6.7 we evaluate the non-parallel effects at a fixed frequency $F = 38 \times 10^{-6}$, comparing the Green's functions obtained using the previously developed theory and those derived by the classical parallel flow assumption. In the same picture we also plot the N factor for the parallel and non-parallel case. As we can see the slow variation of the mean flow profile produces in this case only a small change in the value of r_x and N. Thus, we can claim that for a Blasius boundary layer profile non-parallel effects are definitely weak and could be ignored in a transition prediction analysis. Anyway, tests currently in progress at CIRA have shown that in real wing configurations the corrections can be quite large and must be considered for an effective transition prediction.

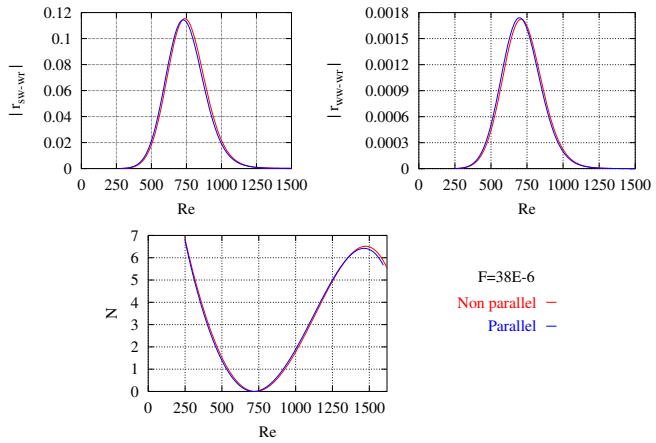

Figure 6.7: Parallel vs non-parallel results for $F = 38 \times 10^{-6}$

Chapter 7

Conclusions

In this thesis, the problem of the transition from laminar to turbulent flow in an incompressible boundary layer has been considered. Fluid dynamics instabilities have been analyzed and, in particular, attention has been payed to the receptivity process of wall disturbances.

In order to solve the receptivity problem a multiple–scale approach has been introduced in non–homogeneous formulation. A receptivity function is obtained which relates the amplitude of the unstable wave to the external disturbances. Non–parallel effects are also taken into account. From the numerical point of view, the multiple–scale method is not computationally expensive, does not have numerical stability problems and can be applied to any base flow, obtained from computations or experimental data. For all these reasons, the receptivity analysis using multiple scales can be efficiently included in an industrial code for transition prediction.

Two test cases have been analyzed and the results compared with the ones available from FOI . The first, relative to ASU test case performed by Saric et al., has been selected in order to validate the numerical tool. Stability analyses have been performed at different frequencies and the results compared to the ones obtained by the FOI. At zero–order the agreement between the curves proved good. The first–order correction has been also plotted. The second test case, relative to a Falkner–Skan–Cooke flow, has been selected for the wall–roughness receptivity analysis. The roughness element is a bump, whose location has been shifted in order to compute the receptivity coefficient as function of chordwise abscissa. The chosen locations start from the first neutral point, $x = 297$, onward and the simulation shows that the receptivity coefficient function is not monotonic. The minimum does not correspond to the first roughness location ($x_r = 305$), but is reached in the second analyzed station ($x_r = 405$).

Receptivity related to the interaction of free-stream disturbances with local or distributed surface inhomogeneities has also been analyzed. The

attention was focused on the generation of TS waves by the interaction of surface roughness with an acoustic- or vortical-wave induced perturbation. The formulation for such analyses is performed in two-dimensional flowfield and a Blasius boundary layer on a flat plate is considered.

The comparison of the efficiency function and the Green's function shows that the acoustic perturbations are much more efficient TS wave generators than vortical gusts. In fact, the modulus of the Green's function is almost two orders of magnitude higher for acoustic wave than for vortical disturbance. The evaluation of the non-parallel effects, compared to parallel one, shows that they are weak and could be ignored in a transition prediction analysis, in the particular case of Blasius profile.

Appendix A

Basic matrix properties

Let us consider a complex square matrix $\mathbf{A}$. The eigenvalue problem

$$\mathbf{A}\mathbf{u} = \lambda\mathbf{u}$$

furnishes n generally complex values λ_i (the eigenvalues) and, if all the eigenvalues are distinct, the eigenvector $\mathbf{u}_i$ which are defined up to a constant and can be arbitrarily normalized. Under these hypotheses, the eigenvectors $\mathbf{u}_i$ are linearly independent so that the matrix

$$\mathbf{U} = (\mathbf{u}_1 \cdots \mathbf{u}_n)$$

is invertible. The problem

$$\mathbf{v}^{\mathrm{T}}\mathbf{A} = \lambda\mathbf{v}^{\mathrm{T}}$$

gives the eigenvalues λ_i and the left eigenvector $\mathbf{v}_i$, defined up to a constant too. One possibility is to normalize $\mathbf{v}_i$ in such a way that

$$\mathbf{v}_i^{\mathrm{T}}\mathbf{u}_i = 1$$

If all the eigenvalues λ_i are distinct the left eigenvectors $\mathbf{v}_i$ are linearly independent and the matrix

$$\mathbf{V} = \begin{pmatrix} \mathbf{v}_1^{\mathrm{T}} \\ \vdots \\ \mathbf{v}_n^{\mathrm{T}} \end{pmatrix}$$

is non singular and therefore invertible.

It can be proved that, if $\mathbf{v}_i^{\mathrm{T}}\mathbf{u}_i = 1$, then $\mathbf{V}\mathbf{U} = \mathbf{I}$. From the right– and left–eigenvalue problems

$$\begin{aligned} \mathbf{A}\mathbf{u}_i &= \lambda_i\mathbf{u}_i \\ \mathbf{v}_j^{\mathrm{T}}\mathbf{A} &= \lambda_j\mathbf{v}_j^{\mathrm{T}} \end{aligned} \tag{A.1}$$

left multiplying the first expression by $\mathbf{v}_j^{\mathrm{T}}$ one gets

$$\mathbf{v}_j^{\mathrm{T}}\mathbf{A}\mathbf{u}_i = \lambda_i \mathbf{v}_j^{\mathrm{T}}\mathbf{u}_i$$

but since $\mathbf{v}_j^{\mathrm{T}}\mathbf{A} = \lambda_j \mathbf{v}_j^{\mathrm{T}}$:

$$\lambda_j \mathbf{v}_j^{\mathrm{T}}\mathbf{u}_i = \lambda_i \mathbf{v}_j^{\mathrm{T}}\mathbf{u}_i \implies (\lambda_j - \lambda_i)\mathbf{v}_j^{\mathrm{T}}\mathbf{u}_i = 0$$

$\lambda_j \neq \lambda_i$ implies

$$\mathbf{v}_j^{\mathrm{T}}\mathbf{u}_i = 0$$

This result, together with the normalization $\mathbf{v}_i^{\mathrm{T}}\mathbf{u}_i = 1$ leads to

$$\mathbf{V}\mathbf{U} = \mathbf{I}$$

which is what we wanted to prove and furnishes $\mathbf{U} = \mathbf{V}^{-1}$ so that $\mathbf{U}\mathbf{V} = \mathbf{V}^{-1}\mathbf{V} = \mathbf{I}$ and therefore

$$\mathbf{V}\mathbf{U} = \mathbf{U}\mathbf{V} = \mathbf{I}$$

We now prove a more useful property which allows the decomposition of a matrix in the form:

$$\mathbf{A} = \sum_{k=1}^{n} \lambda_k \mathbf{u}_k \mathbf{v}_k^{\mathrm{T}}$$

The equations (A.1) can be written in a matrix form as

$$\begin{aligned} \mathbf{A}\mathbf{U} &= \mathbf{\Lambda}\mathbf{U} \\ \mathbf{V}\mathbf{A} &= \mathbf{\Lambda}\mathbf{V} \end{aligned} \tag{A.2}$$

where $\mathbf{\Lambda} = \mathrm{diag}(\lambda_1, \ldots, \lambda_n)$. Left multiplying the second equation by $\mathbf{U}$ and remembering that $\mathbf{U}\mathbf{V} = \mathbf{I}$:

$$\mathbf{U}\mathbf{V}\mathbf{A} = \mathbf{U}\mathbf{\Lambda}\mathbf{V} \implies \mathbf{I}\mathbf{A} = \mathbf{U}\mathbf{\Lambda}\mathbf{V} \implies \mathbf{A} = \mathbf{U}\mathbf{\Lambda}\mathbf{V} \tag{A.3}$$

The matrix $\mathbf{U}\mathbf{\Lambda}\mathbf{V}$ is obviously

$$\mathbf{U}\mathbf{\Lambda}\mathbf{V} = (\mathbf{u}_1 \cdots \mathbf{u}_n) \begin{pmatrix} \lambda_1 & 0 & 0 \\ 0 & \ddots & 0 \\ 0 & 0 & \lambda_n \end{pmatrix} \begin{pmatrix} \mathbf{v}_1^{\mathrm{T}} \\ \vdots \\ \mathbf{v}_n^{\mathrm{T}} \end{pmatrix}$$

$$= (\mathbf{u}_1 \cdots \mathbf{u}_n) \begin{pmatrix} \lambda_1 \mathbf{v}_1^{\mathrm{T}} \\ \vdots \\ \lambda_n \mathbf{v}_n^{\mathrm{T}} \end{pmatrix}$$

Indicating with

$$\begin{array}{rcl} \mathbf{u}_1 & = & \begin{pmatrix} u_1^1 & u_2^1 \cdots u_{n-1}^1 & u_n^1 \end{pmatrix} \\ \mathbf{u}_2 & = & \begin{pmatrix} u_1^2 & u_2^2 \cdots u_{n-1}^2 & u_n^2 \end{pmatrix} \\ \vdots & = & \vdots \\ \mathbf{v}_1^{\mathrm{T}} & = & \begin{pmatrix} v_1^1 & v_2^1 \cdots v_{n-1}^1 & v_n^1 \end{pmatrix} \\ \mathbf{v}_2^{\mathrm{T}} & = & \begin{pmatrix} v_1^2 & v_2^2 \cdots v_{n-1}^2 & v_n^2 \end{pmatrix} \\ \vdots & = & \vdots \end{array}$$

the general ij–th term of the matrix $\mathbf{U\Lambda V}$ is:

$$(\mathbf{U\Lambda V})_{ij} = \sum_{k=1}^{n} u_i^k \lambda_k v_j^k = \sum_{k=1}^{n} \lambda_k \bar{a}_{ij}^k$$

Basically, the matrix $\mathbf{U\Lambda V}$ has been decomposed in the sum of n matrices $\lambda_k \bar{a}_{ij}^k$ where $\bar{a}_{ij}^k = u_i^k v_j^k$ so that

$$[\bar{a}_{ij}^k] = [u_i^k v_j^k] = \mathbf{u}_k \mathbf{v}_k^{\mathrm{T}}$$

Finally, $\mathbf{A} = \mathbf{U\Lambda V}$ implies

$$\mathbf{A} = \sum_{k=1}^{n} \lambda_k \mathbf{u}_k \mathbf{v}_k^{\mathrm{T}}$$

which is what we wanted to prove.

A couple of other interesting properties can be derived for singular matrices or for matrices with an eigenvalue that goes to zero as a function of a parameter. Referring to the general linear system

$$\mathbf{Ax} = \mathbf{b}$$

if all the eigenvalues λ_i are distinct, the right eigenvalues form a basis so that the solution can be expressed as

$$\mathbf{x} = \mathbf{Uh}$$

and

$$\mathbf{AUh} = \mathbf{b}$$

left multiplying by $\mathbf{V}$

$$\mathbf{VAUh} = \mathbf{Vb}$$

and noticing that from the left–eigenvalue problem $\mathbf{VA} = \mathbf{\Lambda V}$

$$\mathbf{VAU} = \mathbf{\Lambda VU} = \mathbf{\Lambda I} = \mathbf{\Lambda}$$

the original linear system reduces to

$$\mathbf{\Lambda h} = \mathbf{V b}$$

or

$$\lambda_i \mathbf{h} = \mathbf{v}_i^{\mathrm{T}} \mathbf{b}$$

If the initial matrix $\mathbf{A}$ is singular, all the eigenvalues are distinct and $\lambda_i = 0$, the only possibility for the solution $\mathbf{h}$, and therefore $\mathbf{x}$, to exist is

$$\mathbf{v}_i^{\mathrm{T}} \mathbf{b} = 0 \tag{A.4}$$

Expression (A.4) is usually called "compatibility condition" for linear systems with a singular matrix and is another way to express the Rouché–Capelli theorem.

Finally, the last interesting feature regards system with an eigenvalue going to zero as a function of a parameter. In this case, from the previous developments, the linear system $\mathbf{Ax} = \mathbf{b}$ can be reduced to $\mathbf{\Lambda h} = \mathbf{V b}$ with $\mathbf{x} = \mathbf{U h}$. The solution is therefore

$$\mathbf{x} = \mathbf{U \Lambda}^{-1} \mathbf{V b}$$

Since

$$\mathbf{\Lambda}^{-1} = \mathrm{diag}(\lambda_1^{-1}, \cdots, \lambda_n^{-1})$$

when $\lambda_i \to 0$ the greatest contribution in $\mathbf{\Lambda}^{-1}$ is simply the term λ_i^{-1} so that

$$\mathbf{x} \to \frac{1}{\lambda_i} \mathbf{u}_i (\mathbf{v}_i^{\mathrm{T}} \mathbf{b}) \text{ for } \lambda_i \to 0 \tag{A.5}$$

This expression leads to the conclusion that the RHS of a linear system with an eigenvalue going to zero as a function of a parameter produces a contribution of order λ_i^{-1} and, moreover, the solution $\mathbf{x}$ behaves like the corresponding right eigenvector $\mathbf{u}_i$.

Appendix B

Numerical method

In order to solve the eigenvalue problem, the relative differential problems have to be discretized and the boundary conditions included in the right way.

B.1 Discretization

The discretization is necessary in order to solve the differential problems. The second–order finite difference operators were applied and a staggering of the pressure has been introduced. This means that velocity components are computed in the nodal point i, while the pressure is computed for the point $i + 1/2$ as shown in figure B.1.

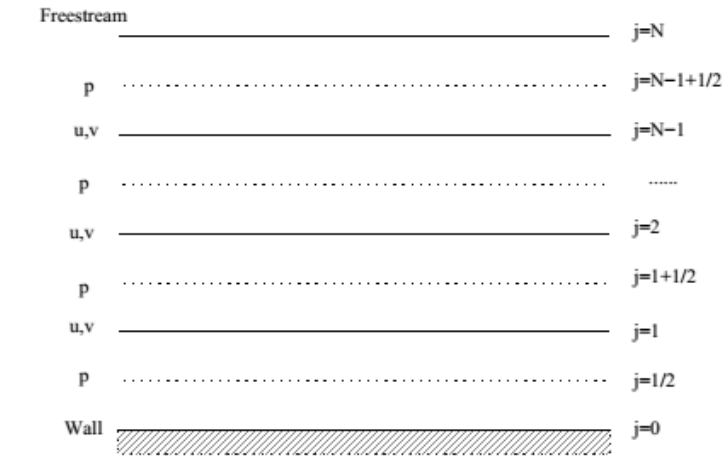

Figure B.1: Staggered grid

B.2 Boundary conditions

The boundary conditions are included in the coefficient matrix (4.22), imposing that perturbations go to zero at the wall and vanish at infinity. In fact, the Orr–Sommerfeld equation for $y \to \infty$ reduces to a constant coefficient ordinary differential equation which can be easily solved finding that there are four possible exponential solution:

$$q(y) = \sum_{n=1}^{4} c_n e^{-p_n y} \tag{B.1}$$

where

$$p_1 = \alpha \tag{B.2}$$
$$p_2 = -\alpha \tag{B.3}$$
$$p_3 = \sqrt{\alpha^2 + iR\,(\omega - \alpha U)} \tag{B.4}$$
$$p_4 = -\sqrt{\alpha^2 + iR\,(\omega - \alpha U)} \tag{B.5}$$

Since the disturbance $q(y)$ vanishes at infinity ($q(y) \to 0$ as $y \to \infty$), p_2 and p_4 imply $c_2 = c_4 = 0$. It can be demonstrated that the inviscid root p_1 has a slower decay than the viscous root p_3, which means that it is sufficient to impose that the perturbation at infinity behaves like $e^{-\alpha y}$:

$$q(y) \to c e^{-\alpha y} \text{ as } y \to \infty \tag{B.6}$$

So we can impose the disturbance to behave like $e^{-\alpha y}$ in a y position far from the wall but not so far as required for imposing it to be zero. This implies that in the coefficient matrix the perturbation in the last point $q(y_{N_y})$ is imposed to behave like the exponential starting from the previous point:

$$q(y_{N_y}) = q(y_{N_y-1}) e^{-\alpha \left(y_{N_y} - y_{N_y-1}\right)} \tag{B.7}$$

B.3 Eigenvalue–finding algorithm

The eigenvalue–finding algorithm is based on the inverse–iteration algorithm which is based on the direct–iteration algorithm. The idea of the direct–iteration algorithm is that it is easy to find the eigenvalue of maximum modulus of a matrix $\boldsymbol{A}$ using:

$$\mathbf{x}_n \simeq \boldsymbol{A}\mathbf{x}_{n-1} = \boldsymbol{A}^n \mathbf{x}_0 \tag{B.8}$$

since $\boldsymbol{A} = \mathbf{v}_M \lambda_M \mathbf{u}_M$, where λ_M is the eigenvalue of maximum modulus and $\mathbf{v}_M$ and $\mathbf{u}_M$ respectively the left and right eigenvector associated to λ_M, we can write

$$\mathbf{x}_n \simeq \boldsymbol{A}^n \mathbf{x}_0 = \mathbf{v}_M \cdot \mathbf{x}_0 \lambda_M^n \mathbf{u}_M \tag{B.9}$$

so that the eigenvalue of maximum modulus is easily obtained by:

$$\lambda_M = \frac{\mathbf{v}_M \cdot \mathbf{x}_0 \lambda_M^n \mathbf{u}_M \cdot \mathbf{p}}{\mathbf{v}_M \cdot \mathbf{x}_0 \lambda_M^{n-1} \mathbf{u}_M \cdot \mathbf{p}} x_n \simeq \frac{\mathbf{x}_n \cdot \mathbf{p}}{\mathbf{x}_{n-1} \cdot \mathbf{p}} \tag{B.10}$$

where $\mathbf{p}$ is a projecting vector which can be simply $\mathbf{p} = \mathbf{x}_{n-1}$ in order to be sure not to have division by zero.

The direct–iteration algorithm can be summarized in the following steps:

1. guess value for $\mathbf{x}_0$

↓

2. $\mathbf{x}_n \leftarrow \boldsymbol{A}\mathbf{x}_{n-1}$

↓

3. $(\lambda_M)_n \leftarrow \dfrac{\mathbf{x}_n \cdot \mathbf{p}}{\mathbf{x}_{n-1} \cdot \mathbf{p}}$
where $\mathbf{p}$ could be $\mathbf{p} = \mathbf{x}_{n-1}$

↓

4. normalization of $\mathbf{x}_n$

↓

5. if $|(\lambda_M)_n - (\lambda_M)_{n-1}|$ is small enough end,
otherwise $\mathbf{x}_{n-1} \leftarrow \mathbf{x}_n$ and go to 2.

This algorithm has two drawbacks: it allows the calculation of only the eigenvalue of maximum modulus and only if it is real.

The inverse–iteration algorithm, which is based on a modification of the previous one, requires a lower number of iteration and works also in the complex case. The idea of the inverse–iteration algorithm is based on the consideration that the eigenvalues of $\boldsymbol{B} = f(\boldsymbol{A})$ are $f(\lambda_k)$ where λ_k are the

eigenvalues of $\boldsymbol{A}$: if we are looking for λ and we know a guess value λ_{guess} for it, so that $(\lambda - \lambda_{\text{guess}})$ is small, $(\lambda - \lambda_{\text{guess}})^{-1}$ will be the eigenvalue of maximum modulus of the matrix $(\boldsymbol{A} - \lambda_{\text{guess}}\boldsymbol{I})^{-1}$ since $(\lambda_k - \lambda_{\text{guess}})^{-1}$ are its eigenvalues.

This means that we can substitute $(\boldsymbol{A} - \lambda_{\text{guess}}\boldsymbol{I})^{-1}$ instead of $\boldsymbol{A}$ in the direct iterative algorithm, obtaining:

1. guess value for λ_0 and $\mathbf{x}_0$

↓

2. $\mathbf{x}_n \leftarrow (\boldsymbol{A} - \lambda_{n-1}\boldsymbol{I})^{-1}\,\mathbf{x}_{n-1}$

↓

3. $(\lambda)_n \leftarrow (\lambda)_{n-1} + \dfrac{\mathbf{x}_n \cdot \mathbf{p}}{\mathbf{x}_{n-1} \cdot \mathbf{p}}$
where $\mathbf{p}$ could be $\mathbf{p} = \mathbf{x}_{n-1}$ or $\mathbf{p} = \mathbf{x}_n^*$
with $\mathbf{x}_n^*$ complex conjugated of $\mathbf{x}_n$

↓

4. normalization of $\mathbf{x}_n$

↓

5. if $|(\lambda)_n - (\lambda)_{n-1}|$ is small enough end,
otherwise $(\lambda)_{n-1} \leftarrow (\lambda)_n$, $\mathbf{x}_{n-1} \leftarrow \mathbf{x}_n$ and go to 2.

It can be demonstrated that this algorithm works if the guess values are close to the right ones, that the convergence is quadratic and that it works also for the complex case. On the other hand, it requires the inversion of a matrix at point (2.), which could be computationally hard, but since the matrix is usually a band–matrix, the inversion algorithm is very fast.

The problem we have to solve (4.20) is:

$$\boldsymbol{A}(\lambda)\mathbf{x} = 0 \tag{B.11}$$

where $\boldsymbol{A}(\lambda)$ is a non–linear function of λ. In order to solve the eigenvalue

problem (B.11), the matrix $\boldsymbol{A}$ is linearized around a guess value λ_0:

$$\tilde{\boldsymbol{A}}(\lambda) = \boldsymbol{A}(\lambda_0) + \left.\frac{\partial \boldsymbol{A}(\lambda)}{\partial \lambda}\right|_{\lambda=\lambda_0} (\lambda - \lambda_0) \tag{B.12}$$

so that the system (B.11) is replaced by

$$\left[\boldsymbol{A}(\lambda_0) + \boldsymbol{B}(\lambda_0)\,(\lambda - \lambda_0)\right]\mathbf{x} = 0 \tag{B.13}$$

where

$$\boldsymbol{B}(\lambda_0) = \left.\frac{\partial \boldsymbol{A}(\lambda)}{\partial \lambda}\right|_{\lambda=\lambda_0} \tag{B.14}$$

the inverse–iteration algorithm in this case becomes:

1. guess value for λ_0, $\mathbf{x}_0$ and $\mathbf{x}_0^*$

↓

2. $\mathbf{x}_n \leftarrow \left[\boldsymbol{A}(\lambda_0)\right]^{-1}\left[\boldsymbol{B}(\lambda_0)\right]\mathbf{x}_{n-1}$ and
$\mathbf{x}_n^* \leftarrow \left[\boldsymbol{B}(\lambda_0)\right]^T\left[\boldsymbol{A}^T(\lambda_0)\right]^{-1}\mathbf{x}_{n-1}^*$

↓

3. $(\lambda)_n \leftarrow (\lambda)_{n-1} - \dfrac{\mathbf{x}_n^*\boldsymbol{A}(\lambda_0)\mathbf{x}_n}{\mathbf{x}_n^*\boldsymbol{B}(\lambda_0)\mathbf{x}_n}$
where $\mathbf{x}_n^*\boldsymbol{A}(\lambda_0)\mathbf{x}_n = \mathbf{x}_n^*\boldsymbol{B}(\lambda_0)\mathbf{x}_{n-1} = \mathbf{x}_{n-1}^*\boldsymbol{B}(\lambda_0)\mathbf{x}_n$

↓

4. normalization of $\mathbf{x}_n$ and $\mathbf{x}_n^*$

↓

5. if $|(\lambda)_n - (\lambda)_{n-1}|$ is small enough end, otherwise
$(\lambda)_{n-1} \leftarrow (\lambda)_n$, $\mathbf{x}_{n-1} \leftarrow \mathbf{x}_n$, $\mathbf{x}_{n-1}^* \leftarrow \mathbf{x}_n^*$ and go to 2.

This last algorithm is more efficient than the standard inverse iteration one, yields the left eigenvector (or adjoint) and when marching in x direction can use previous step as guess.

Bibliography

[1] J. L. Van Ingen. A suggested semi–empirical method for the calculation of the boundary layer transition region. Technical Report VTH-74, University of Technology, Delft, 1956.

[2] S. Zuccher. *Receptivity and Control of Flow Instabilities in a Boundary Layer*. PhD thesis, University of Milan - Aerospace Engineer Department, 2001.

[3] L. Prandtl. Über flüssigkeitsbewegung bei sehr kleiner reibung. pages 484–491, Teubner, Leipzig, 1905. Third International Congress of Mathematicians, Heidelberg, 1904.

[4] O. Reynolds. An experimental investigation of the circumstances which determine whether the motion of water shall be direct or sinuous, and of the law of resistance in parallel channels. *Royal Society of London*, 174:935–982, 1883.

[5] H. von Helmholtz. Über discontinuirliche flüssigkeitsbewegungen. *Monatsberichte der Königlichen Preussische Akademie der Wissenschaften zu Berlin*, 23:215–228, 1868.

[6] Lord Kelvin. On the vibrations of a columnar vortex. *Philosophical Magazine*, 10:155–168, 1880.

[7] Lord Kelvin. On the stability of steady and of periodic fluid motion. *Philosophical Magazine*, 23:459–464, 1887.

[8] Lord Rayleigh. On the instability of jets. *London Mathematical Society*, 10:4–13, 1879.

[9] Lord Rayleigh. On the stability, or instability, of certain fluid motions. *London Mathematical Society*, 11:57–70, 1880.

[10] W. Orr. The stability or instability of the steady motions of a perfect liquid and of a viscous liquid. *Royal Irish Academy*, 27:9–68 and 69–138, 1907.

[11] A. Sommerfeld. Ein beitrag zur hydrodynamischen erklaerung der turbulenten fluessigkeitsbewegungen. In *4th International Congress of Mathematicians*, volume 3, pages 116–124, Rome, 1908.

[12] W. Tollmien. Über die entstehung der turbulenz. *Nachrichten von der Gesellschaft der Wissenschaften zu Göttingen, Mathematisch-Physikalische Klasse*, pages 21–44, 1929.

[13] H. Schlichting. Zur entstehung der turbulenz bei der plattenströmung. *Nachrichten von der Gesellschaft der Wissenschaften zu Göttingen, Mathematisch-Physikalische Klasse*, pages 181–208, 1933.

[14] H. B. Squire. On the stability of three-dimensional disturbance of viscous fluid between parallel walls. *Royal Society of London*, 142:621–628, 1933.

[15] G. I. Taylor. Stability of a viscous liquid contained between two rotating cylinders. *Philosophical Transactions of the Royal Society of London. Series A, Containing Papers of a Mathematical or Physical Character*, 223(605-615):289–343, 1923.

[16] L. Lees and C. C. Lin. Investigation of the stability of the laminar boundary layer in a compressible flow. Technical Report 1115, NACA, 1946.

[17] G. B. Schubauer and H. K. Skramstad. Laminar boundary layer oscillations and transition on a flat plate. *Journal of Research of the National Bureau of Standards*, 38:251–292, 1947.

[18] L. H. Thomas. The stability of plane poiseuille flow. *Phys. Rev.*, 91:780–783, Aug 1953.

[19] R. E. Kaplan. *The stability of laminar incompressible boundary layers in the presence of compliant boundaries*. PhD thesis, Massachusetts Institute of Technology, 1964.

[20] A. M. O. Smith and N. Gamberoni. *Transition, pressure gradient and stability theory*. Douglas Aircraft Company, 1956.

[21] S. A. Orszag. Accurate solution of the orr–sommerfeld stability equation. *Journal of Fluid Mechanics*, 50:689–703, 11 1971.

[22] L. M. Mack. Boundary-layer stability theory. Technical report, Jet Propulsion Laboratory, Pasadena, CA., 1969.

[23] V. I. Lysenko and A. A. Maslov. The effect of cooling on the supersonic boundary layer stability and transition. In V.V. Kozlov, editor, *Laminar-Turbulent Transition*, International Union of Theoretical and Applied Mechanics, pages 495–502. Springer Berlin Heidelberg, 1985.

[24] L. M. Mack. A numerical study of the temporal eigenvalue spectrum of the blasius boundary layer. *Journal of Fluid Mechanics*, 73:497–520, 2 1976.

[25] C. E. Grosch and H. Salwen. The continuous spectrum of the orr-sommerfeld equation. part 1: The spectrum and the eigenfunctions. *Journal of Fluid Mechanics*, 87:33–54, 1978.

[26] C. E. Grosch and H. Salwen. The continuous spectrum of the orr-sommerfeld equation. part 2: Eigenfunction expansion. *Journal of Fluid Mechanics*, 104:445–465, 1981.

[27] W. S. Saric and A. H. Nayfeh. Nonparallel stability of boundary-layer flows. *Physics of Fluids*, 18:945–950, August 1975.

[28] P. S. Klebanoff. Effect of freestream turbulence on the laminar boundary layer. *Bull. Am. Phys. Soc.*, 10:1323, August 1971.

[29] J. T. Stuart. On finite amplitude oscillations in laminar mixing layers. *Journal of Fluid Mechanics*, 29:417–440, 1967.

[30] L. M. Maseev. Occurrence of three-dimensional perturbations in a boundary layer. *Fluid Dynamics*, 3(6):23–24, 1968.

[31] K. Stewartson. On the flow near the trailing edge of a flat plate ii. *Mathematika*, 16:106–121, 6 1969.

[32] V. Ya. Neiland. Theory of laminar boundary layer separation in supersonic flow. *Fluid Dynamics*, 4(4):33–35, 1969.

[33] A. F. Messiter. Boundary-layer flow near the trailing edge of a flat plate. *SIAM J. Appl. Math.*, 18(6):241–257, 1970.

[34] L. Kleiser and T. A. Zang. Numerical simulation of transition in wall-bounded shear flows. *Annual Review of Fluid Mechanics*, 23(1):495–537, 1991.

[35] H. Fasel, H. Meitz, and C. Bachman. DNS and LES for investigating transition and transition control. *AIAA Paper*, 97-1820, 1997.

[36] F. P. Bertolotti, Th. Herbert, and P. R. Spalart. Linear and nonlinear stability of the blasius boundary layer. *Journal of Fluid Mechanics*, 242:441–474, 9 1992.

[37] B-J. Grea. *Application of complex ray theory to the analysis and control of flow instability in boundary layers.* PhD thesis, 2005.

[38] H. Schlichting. *Boundary layer theory.* McGraw-Hill series in mechanical engineering. McGraw-Hill, 1960.

[39] F. White. *Viscous Fluid Flow.* McGraw-Hill series in mechanical engineering. McGraw-Hill Education, 2005.

[40] P. G. Drazin and W. H. Reid. *Hydrodynamic Stability.* Cambridge Mathematical Library. Cambridge University Press, 2004.

[41] P. J. Schmid and D. S. Henningson. *Stability and Transition in Shear Flows.* Number v. 142 in Applied Mathematical Sciences. Springer-Verlag, 2001.

[42] J. Lighthill. *Waves in Fluids.* Cambridge Mathematical Library. Cambridge University Press, 2001.

[43] John D. Anderson. *Hypersonic and high-temperature gas dynamics.* AIAA education series. American Institute of Aeronautics and Astronautics, 2006.

[44] R. S. Donelli, D. Guida, and A. Schettino. Stima preliminare della transizione per le traiettorie hft e srt del velivolo usv. Technical report, CIRA.

[45] M. D. Jackson and D. L. Baker. Passive nosetip technology (PANT) program. volume III. surface roughness effects, part 1. experimental data. Interim Report SAMSO-TR-74-86, Vol. III, Pt. I, U.S. Air Force, Jan. 1974. (Available from DTIC as AD B001 120.).

[46] A. D. Anderson. Passive nosetip technology (PANT) program. volume III. surface roughness effects, part 3. boundary layer transition correlation and analysis. Interim Report SAMSO-TR-74-86, Vol. III, Pt. I, U.S. Air Force, Jan. 1974. (Available from DTIC as AD B001 120.).

[47] R. S. Donelli, J. Perraud, D. Fletcher, A. Schettino, and S. Paris. Design of a laminar-turbulent transition flight experiment. In *International Space Planes and Hypersonic Systems and Technologies Conferences*, pages –. American Institute of Aeronautics and Astronautics, May 2005.

[48] P. Paris, L. Cerignat, A. Garzon, and D. G. Fletcher. Roughness induced transition for flight experiments. In *4th International Symposium Atmospheric Reentry Vehicles & Systems*, Arcachon, France, March 2005.

[49] R. G. Batt and H. L. Legner. A review of roughness-induced nosetip transition. *AIAA Journal*, 21(1):7–22, January 1983.

[50] D. C. Reda. Correlation of nosetip boundary-layer transition data measured in ballistics-range experiments. *AIAA Journal*, 19(3):329–339, March 1981.

[51] J. Perraud. Natural and roughness induced transition on the expert vehicle - pl 4/5,. Technical Report RT 2/12092 DMAE, ONERA, June 2007.

[52] E. Reshotko and A. Tumin. Role of transient growth in roughness-induced transition. *AIAA Journal*, 42(4):766–770, April 2004.

[53] J. Müir. Experimental investigation of the effects of nose bluntness, free-stream unit reynolds number, and angle of attack on cone boundary layer transition at a mach number of 6. In *Meeting Paper Archive*, pages –. American Institute of Aeronautics and Astronautics, January 1963.

[54] L. M. Mack. Boundary layer stability theory, special course on stability and transition of laminar flow. Technical Report 709, AGARD Report, 1984.

[55] F. Capizzano, P. Catalano, C. Marongiu, and P. Vitagliano. U-rans modelling of turbulent flows controlled by synthetic jets. In *Fluid Dynamics and Co-located Conferences*, pages –. American Institute of Aeronautics and Astronautics, June 2005.

[56] A. Marino, P. Catalano, C. Marongiu, P. Peschke, C. Hollestein, and R. Donelli. Effect of high-voltage pulsed dbd plasma on the aerodynamic performances in subsonic and transonic conditions. In *43th*

AIAA Fluid Dynamics Conference, pages 2703–2752, San Diego, June 2013. American Institute of Aeronautics and Astronautics.

[57] M. V. Morkovin. Bypass-transition research: Issues and philosophy. In D.E. Ashpis, T.B. Gatski, and R. Hirsh, editors, *Instabilities and Turbulence in Engineering Flows*, volume 16 of *Fluid Mechanics and Its Applications*, pages 3–30. Springer Netherlands, 1993.

[58] C.M. Bender and S.A. Orszag. *Advanced Mathematical Methods for Scientists and Engineers I: Asymptotic Methods and Perturbation Theory*. Advanced Mathematical Methods for Scientists and Engineers. Springer, 1999.

[59] J. K. Kevorkian and J. D. Cole. *Multiple Scale and Singular Perturbation Methods*. Applied Mathematical Sciences. Springer London, Limited, 2011.

[60] L. Hunt and W. Saric. Boundary-layer receptivity of three-dimensional roughness arrays on a swept-wing. In *Fluid Dynamics and Co-located Conferences*, pages –. American Institute of Aeronautics and Astronautics, June 2011.

[61] J. Pralits and A. Hanifi. Description of test cases. Technical memo TM 3.1 GA No. ACPO-GA-2010-265094, FOI, 2010.

[62] V.M. Falkneb and S.W. Skan. LXXXV. solutions of the boundary-layer equations. *Philosophical Magazine Series 7*, 12(80):865–896, 1931.

[63] J. C. Cooke. The boundary layer of a class of infinite yawed cylinders. *Mathematical Proceedings of the Cambridge Philosophical Society*, 46:645–648, 10 1950.

[64] L. U. Schrader, L. Brandt, and D. S. Henningson. Receptivity mechanisms in three-dimensional boundary-layer flows. *Journal of Fluid Mechanics*, 618:209–241, 2009.

[65] F. Giannetti. *Boundary Layer Receptivity*. PhD thesis, University of Cambridge, Fitzwilliam College, May 2002.